Cellular and Circuit Dynamics Underlying Circadian Timekeeping

Cellular and circuit dynamics underlying circadian timekeeping

A dissertation presented

by

Bryan Joohyun Song

to

The Division of Medical Sciences

in partial fulfillment of the requirements

for the degree of

Doctor of Philosophy

in the subject of

Neurobiology

Harvard University

Cambridge, Massachusetts

February 2020

Dissertation Advisor: Dr. Dragana Rogulja Bryan Joohyun Song

Cellular and circuit dynamics underlying circadian timekeeping

Abstract

Circadian clocks internally represent the passage of each day, and organize physiology and behavior to align with changing external conditions. The central organizers of circadian rhythms are molecular oscillators that enable individual cells to track time autonomously. Clock neuron networks also represent the passage of time, with distinct ensembles active at different times of day. While the general organization of molecular oscillators has been solved, it remains unclear how clock neurons populations transition reliably and accurately between network activity states.

To address this gap in knowledge, we used *Drosophila melanogaster* to search for cellular and circuit mechanisms that account for differences between daytime and nighttime behavioral states. Flies undergo an internal switch in how light is contextualized: a light pulse during the night evokes a startle-like response (increased locomotor activity), but the same stimulus during the day causes locomotor quiescence. Genetic perturbance of molecular oscillators revealed that circadian clocks differentially modify behavioral responsiveness to light during daytime vs. nighttime. Optogenetic silencing experiments further showed distinct roles for two clock neuron subpopulations: LNvs contextualize light during the day, while DN1as do so during the night. Anatomical and functional investigation revealed that LNvs and DN1as form a mutually inhibitory microcircuit. Structural plasticity occurs at the presynaptic terminals of both populations, which is poised to redistribute activity between LNv and DN1a subpopulations. Rho1 pathway manipulations that interfere with remodeling also prevent

transitions between light-responsive states. Together these results support a model where structural plasticity shifts the balance of activity between specialized subpopulations.

In summary, this work provides new evidence that a representation of ~24 hours is functionally distributed across clock neuron subpopulations. Further our results imply that internal time representations might be updated by daily changes to neurite morphology. The cellular and circuit motifs we identify may be generally useful to explain how behavioral states can pendulate over long timescales.

Table of Contents

List of Figures

List of Supplementary Tables and Videos

Contributions

This thesis was written by Bryan Song with guidance from Dragana Rogulja. Major sections from this thesis, including all of **Chapter 2** and **Chapter 3** are adapted from the following submitted manuscript: Song, B.J., Sharp, S. and Rogulja, D. Daily axonal remodeling in a circadian microcircuit organizes transitions between behavioral states. Bryan Song and Dragana Rogulja wrote the manuscript. Bryan Song performed all experiments and analyses. Slater Sharp and Tara Kane assisted with experiments. Other contributions are acknowledged in Methods sections.

Acknowledgements

This work would have not been possible without the guidance and support of my advisor Dragana Rogulja. She is an abundantly enthusiastic and caring mentor. I am deeply grateful to have learned from her, and worked closely with her over the past several years. My time here was made more productive and cheerful by current and former labmates; especially (but not limited to) Stephen Zhang, Zhihua Liu, Iris Titos Vivancos, Yosef Kaplan Dor, Alex Vaccaro, Keishi Nambara, Hannah Somhegyi, and Michelle Frank. I was lucky to have exceptional experimental support from Slater Sharp, Tara Kane, Ofra Dor Kaplan and Victoria Clendaniel. Thank you to Michael Crickmore and Stephen Thornquist for the invaluable feedback and for challenging me to be a better scientist.

Thank you to PIN and the HMS Neurobiology community for this incredible experience. I am indebted to Rachel Wilson, David Ginty, Rosalind Segal, and Karen Harmin for pivotal professional advice. Thank you to Leslie Griffith, Thomas Schwarz, and Jonathan Lipton for giving feedback on my thesis. I am especially grateful to my DAC: Charles Weitz, Michael Do and Matt Pecot for the many years of excellent guidance. Matt, your optimism, determination and enthusiasm inspires me to improve. Thank you for the great conversations and your encouragement. You will be missed.

Thank you to my family, and especially my parents, for always supporting my odd interests. Thank you Joanna Jankowsky for taking a chance on me, and for continued mentorship. Thank you to my classmates, especially Ivan Santiago and Elizabeth Lamkin Cebul, who have been endless sources of humor, advice and encouragement. Last but foremost, thank you to Ellura Pepito for the love, support, and understanding. You made every day of this PhD

better, especially when you assisted with experiments, presentations and writing. I hope and expect to find continued success in this collaboration.

For my parents and Ellura

Chapter 1: Introduction

Most organisms follow regular daily schedules, allowing behavioral and physiological preparations for essential biological functions such as sleeping and feeding. To facilitate this, our bodies create internal representations of time. Biological cycles lasting ~24 hours, e.g. circadian rhythms, give appropriate timing to many physiological outputs. Circadian rhythms are directed by molecular oscillators within relatively small populations of specialized clock neurons. The utility of circadian clocks is evidenced by their conservation: they are present in most organisms, including bacteria, flies and humans (Vitaterna et al., 2001).

Because environmental conditions, such as light and temperature, vary dramatically from daytime to nighttime, animals benefit from specializing within a temporal niche. For example, diurnal animals have visual systems best adapted for daylight, and are inactive at night. The ability to predict upcoming changes in the environment allows for preparatory biological and behavioral processes that might take many hours. For example, the ability to anticipate nightfall can allow organisms to seek shelter before the sun goes down.

The circadian clock evolved around predictable and consistent schedules of luminance, but ubiquitous artificial lighting places new demands on a system that has been relatively unchallenged across evolutionary history. Misalignment between internal rhythms and the external world can have profound consequences on health and cognition. The feeling of jetlag demonstrates the acute physical and mental burden of when internal clocks are at odds with the external world (Wright et al., 2012). Chronic misalignment, such as in the case of night-shift workers, causes increased rates of cancer (Bedrosian et al., 2016; Patel, 2006; Schernhammer et al., 2001; Schernhammer et al., 2003). As society is becoming increasingly operational across 24-hour periods, it is vital to understand interactions between internal circadian clocks and external environments.

Because of its short generational time and availability of powerful genetic tools, *Drosophila melanogaster* has emerged as a valuable model for circadian research. In addition, the fly brain is a relatively compact system, permitting tractable dissection of neural substrates of behavior. While circadian genes are widely expressed in *Drosophila* and human tissue, the *Drosophila* circadian clock seems to be controlled by only ~150 clock cells (Kaneko and Hall, 2000). The small number of circadian cells permits systems-level analysis of the interactions between clusters of circadian neurons (Chatterjee et al., 2018; Liang et al., 2017; Shafer et al., 2008; Yao et al., 2012), as well as the molecules within them.

Molecular clocks

General organization

Circadian time is tracked cell-autonomously through molecular oscillations of core circadian clock proteins; these oscillations are organized by environmental cues like the natural cycles of light and darkness, and rely on biochemical events to create a remarkably accurate representation of the daily passage of time (Bhadra et al., 2017; Hardin, 2011). The first circadian gene, *period* (*per*), was discovered in flies. In the 1970s, *per* was discovered by Ron Konopka and Seymour Benzer in a screen for mutants with abnormal eclosion rhythms (Konopka and Benzer, 1971). Subsequent studies have shown that PER is a core component of the circadian clock in many species, including humans (Sun et al., 1997; Tei et al., 1997). Decades of research on period lead to identification of PER-interacting proteins that dictate rhythmic behavior. Acting in unison, these factors compose a molecular program that follows a 24-hour cycle. In brief, the logic of circadian clocks is that transcription factors create their own inhibitors, resulting in fluctuations of circadian protein levels over a ~24 hour cycle (**Figure 1.1,** (Hardin, 2011)). This cycle is called

the transcription-translation feedback loop (TTFL). Not only are most of these genes conserved across species, but the general organization of the TTFL is also highly conserved (Song and Rogulja, 2017).

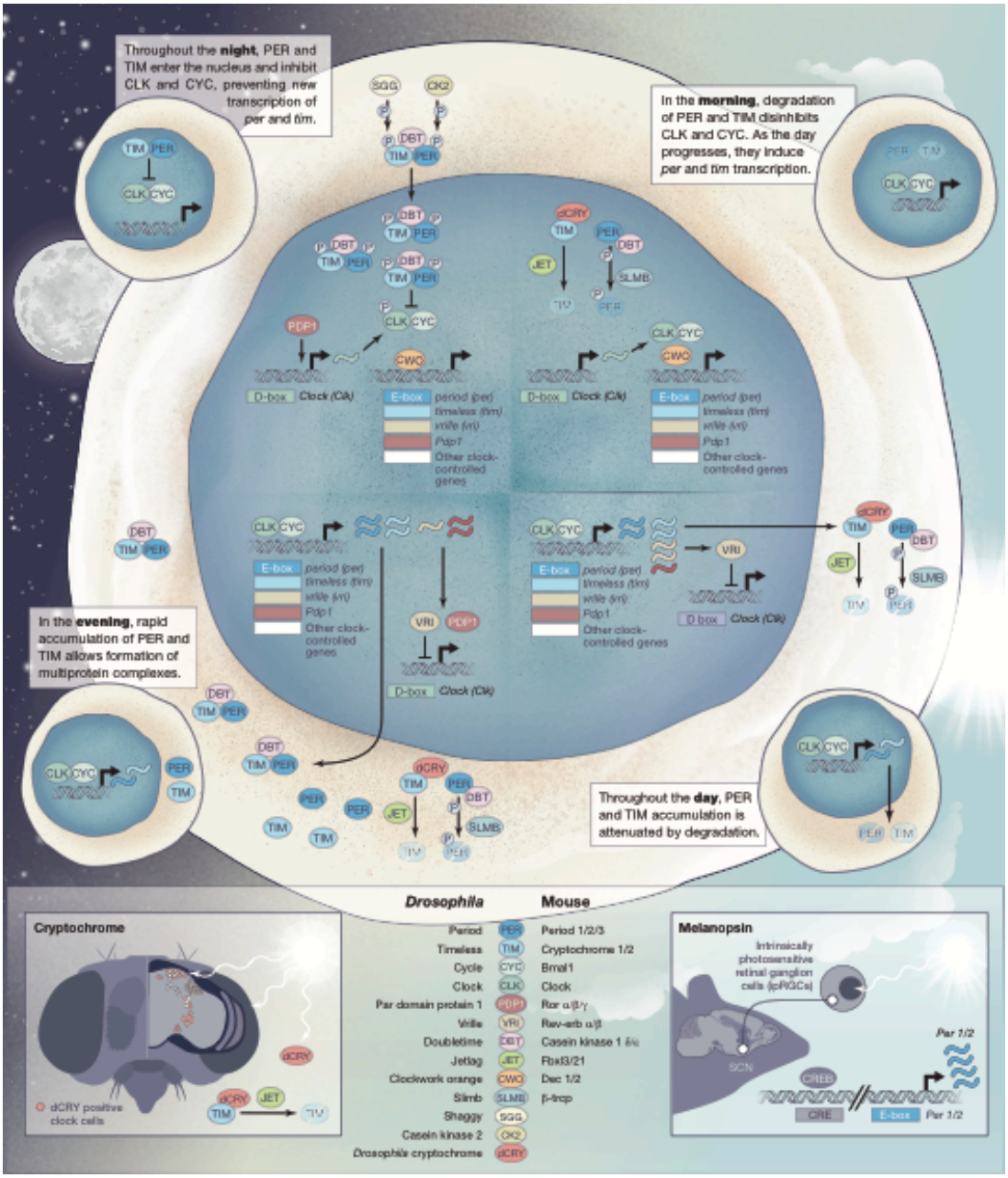

Figure 1.1. Schematic of the molecular clock. Bottom, light input pathways into the clock and common roles of invertebrates and mammalian circadian factors. This figure is reprinted from Song, B.J., and Rogulja, D. (2017). SnapShot: Circadian Clock. Cell *171*, 1468-1468 e1461, with permission from Elsevier.

Core TTFL proteins in Drosophila

Two overlapping processes, positive regulation and negative regulation, cause levels of circadian proteins to oscillate. The positive arm of the loop includes mechanisms that increase circadian protein levels, and includes transcriptional expression of clock genes. In the morning, the transcription factors Clock (CLK, (Allada et al., 1998)) and Cycle (CYC, (Rutila et al., 1998)) bind E-box genetic sequences as heterodimers (Hao et al., 1997). E-box sequences are in the promoter region of genes whose transcription is regulated by circadian cycles (Hao et al., 1997). CLK and CYC promote expression of other circadian factors (Darlington et al., 1998), Period (PER, (Bargiello and Young, 1984; Konopka and Benzer, 1971; Reddy et al., 1984; Zehring et al., 1984)) and Timeless (TIM, (Sehgal et al., 1994)); their levels accumulate gradually in the cytoplasm throughout the day. PER and TIM are targeted by kinases, Doubletime (DBT, also known as Casein Kinase 1, (Kloss et al., 1998; Price et al., 1998)) and Shaggy (SGG,(Martinek et al., 2001)) respectively. PER is stabilized by binding to TIM, allowing for its gradual accumulation (Price et al., 1995). Phosphorylation of PER and TIM slows the kinetics of accumulation throughout the day, by causing degradation via SCF ubiquitin ligases (Ko et al., 2002) or by regulation of translation (Chiu et al., 2008) .

The negative arm of the loop includes mechanisms that inhibit clock gene expression. In the evening, cytoplasmic PER and TIM are at their highest levels. At sufficiently high levels, PER and TIM form protein complexes with DBT, and PER is phosphorylated by Casein Kinase 2 (Akten et al., 2003; Lin et al., 2002) and TIM is phosphorylated by SGG; these modifications signal for the complexes to translocated into the nucleus (Akten et al., 2003; Lin et al., 2002; Martinek et al., 2001). PER-TIM-DBT causes phosphorylation of CLK and consequential dissociation of CLK-CYC from E-Box domains (Yu et al., 2009). Inhibition of CLK-CYC

transcription prevents further expression of PER and TIM (Lee et al., 1998, 1999). As levels of PER-TIM inhibitors decline, CLK-CYC can become active, allowing the cycle to begin anew.

A secondary loop with its own positive and negative arms helps regulate the core TTFL. Vrille (VRI, (Blau and Young, 1999)) and PAR-domain protein 1 (PDP1, (Cyran et al., 2003)) are both factors that are transcribed by circadian clock machinery, but at different times (Cyran et al., 2003). Vrille and PDP1 inhibit or promote the transcription of CLK, respectively. The oscillating transcription of *clk* that reaches peak levels of expression in the morning (Bae et al., 1998), has been proposed to help turnover CLK that has been hyperphosphorylated (and thus inactivated) throughout the nighttime (Yu et al., 2006).

Environmental inputs into the clock

*C*ircadian rhythms are exquisitely sensitive to environmental conditions, especially temperature (Sehadova et al., 2009) and luminance (Hunter-Ensor et al., 1996; Myers et al., 1996; Zeng et al., 1996). Entrainment refers to repeated exposure to environmental conditions (typically at least ~2 daily cycles) that will instruct the internal clock's schedule (Chiu et al., 2010). Stimuli that can reset or entrain the clock are called zeitgebers (German for "time-giver", (Dubowy and Sehgal, 2017)). Strong zeitgebers include cues that are associated with daytime, such as heat and bright light. Light is the most commonly studied zeitgeber; however other environmental considerations, such as meals (Patton and Mistlberger, 2013), mechanical stimulation (Simoni et al., 2014), and social interactions (Aschoff et al., 1971), can also instruct the clock.

In mammals, light enters circadian pathways through the visual system. Intrinsically photosensive retinal ganglion cells are specialized light detectors in the retina that send efferents to the suprachiasmatic nucleus (SCN), the anatomical cluster in mammalian brains where clock

neurons reside (Do, 2019). In flies, light input into the circadian clock is more complex. Light also passes through the visual system to instruct clock neurons (Yoshii et al., 2016). However, many clock neurons cell-autonomously express light sensitive proteins such as Cryptochrome (CRY, (Emery et al., 1998; Stanewsky et al., 1998)) or Rhodopsin 7 (Ni et al., 2017). The thin cuticle of the fly allows light to penetrate into the brain and instruct clock neurons directly (Yoshii et al., 2016).

Molecular consequences of zeitgebers

Roughly a third of the *Drosophila* circadian cells express the photosensitive circadian protein CRY (Benito et al., 2008; Yoshii et al., 2008), which in flies interacts with and degrades the core clock components in a light-dependent manner (Emery et al., 1998; Stanewsky et al., 1998). This mechanism has two important roles in a light-dark cycles. In the morning, light activates the photosensitive protein Cryptochrome (CRY) that binds TIM and promotes its degradation through the action of the E3 ligase JETLAG (Hardin, 2011; Koh et al., 2006). Without the presence of its binding partner TIM, PER is phosphorylated by Double-Time kinase (DBT), which in turn degrades PER (Kloss et al., 2001; Price et al., 1998). Without PER-TIM nuclear complexes transcriptional inhibition is released and the clock is reset. By this mechanism, the kinetics of accumulation are greatly inhibited by light: CRY prevents the nuclear translocation of PER and TIM during the daytime by keeping TIM levels low. This same light-responsive mechanism is important for entrainment to new timezones (Emery et al., 1998; Stanewsky et al., 1998).

Though CRY is highly influential in setting and regulating the pace of molecular oscillations in light cycles, it is dispensable for the maintenance of timekeeping (Stanewsky et al.,

1998). Even in constant darkness (where CRY is not activated but circadian rhythms persist), PER and TIM do not undergo premature translocation in the evening, and PER/TIM levels still decline in the morning (Shafer et al., 2002). CRY has notable functions outside of setting the pace of the clock: CRY is important for adjusting to new light schedules. i.e. adjusting to jetlag. In addition, CRY's effect on resetting the clock is the reason why nighttime light is so disruptive: even brief exposure to nighttime light will delay sleep onset and also modifying the pace of rhythms in subsequent days (Stanewsky et al., 1998).

The TTFL is malleable, as evidenced by its ability to flexibly adapt to new conditions. It is also remarkably robust to seasonal changes in light and temperature. All molecular processes are somewhat slowed or accelerated by cool and warm temperatures respectively. But the TTFL operates accurately across a wide range of temperatures (Sawyer et al., 1997). Similarly, the clock operates accurately across seasonal changes in light schedules – such as shorter days in the winter (Stoleru et al., 2007). This stability is thought to arise from regulation of the TTFL (Narasimamurthy and Virshup, 2017), as well as by interactions between clock neuron clusters (Zhang et al., 2010a).

Clock control of gene expression

In addition to regulating its own timing, TTFL transcription factors also directly regulate rhythmic expression of thousands of genes that mediate circadian outputs (Zhang et al., 2014). The output of this cell-autonomous genetic program manifests as secreted factors or electrical transmissions that non-autonomously synchronize, regulate or strengthen the rhythms of cells elsewhere in the body (Mohawk et al., 2012). With current techniques it was estimated in mice that almost half of the genes are rhythmically transcribed somewhere in the body, and that 5-20%

of transcripts oscillate within a given tissue (Zhang et al., 2014). Clocks can therefore regulate virtually all biological processes (Takahashi, 2017; Takahashi et al., 2008).

Clock control of neuronal activity

One class of rhythmically expressed genes within clock neurons includes regulators of membrane conductance (Buhl et al., 2016; Flourakis et al., 2015; Fogle et al., 2015; Hastings et al., 2018; Hodge and Stanewsky, 2008; Lear et al., 2005; Liu et al., 2014; Meredith et al., 2006). Circadian regulation of clock neuron activity occurs both cell-autonomously and non-autonomously. Autonomous regulation of sodium leak conductances by NCA localization factor 1 (Nlf-1) at least partially accounts for activity rhythms in some clock neurons (Flourakis et al., 2015). Nlf-1 is rhythmically expressed by the clock, and binds sodium leak channels and transports them between endoplasmic reticulum and cell membranes, resulting in antiphase daily oscillations in sodium and potassium currents (Flourakis et al., 2015). WAKE is another factor that is rhythmically expressed by the clock; WAKE acts both autonomously and non-autonomously to affect the activity of clock neurons (Liu et al., 2014; Tabuchi et al., 2018). WAKE transports K_{ca} channels, and Na^+/K^+ transporters that autonomously effect clock neuron activity rhythms (Tabuchi et al., 2018). WAKE also dampens clock neuron activity through non cell-autonomous interactions, such as by rhythmically transporting $GABA_A$ receptors to the membranes of wake-promoting clock neurons in the evening (Liu et al., 2014), thus increasing the inhibitory influence of upstream partners in a rhythmic fashion.

In flies and mice, clock neurons display dramatic electrical activity rhythms (Cao and Nitabach, 2008; Cao et al., 2013; Colwell, 2011; Flourakis et al., 2015; Itri et al., 2005; Kunst et al., 2014; Pennartz et al., 2002; Sheeba et al., 2008b; Tabuchi et al., 2018). Clock neurons can

have surprisingly specific tuning curves (Enoki et al., 2012; Liang et al., 2016; Schaap et al., 2003). Chronic electrical recordings of individual neurons in the SCN revealed their temporal tuning profiles: clock neurons have different windows of increased activity that last ~5 hours every day (Schaap et al., 2003; Welsh et al., 2010). Properly timing the activity of clock neurons is vital, as these neurons control behavioral outputs like sleep, or physiological outputs like metabolism (Takahashi et al., 2008). Below I discuss the organization of circadian clock network, and emergent circuit activity patterns that may explain neuronal timekeeping.

Clock neuron networks

Clock neuron subpopulations

Circadian oscillators are present in most tissues (Mohawk et al., 2012; Takahashi et al., 2008). A relatively small number of neurons in the brain (Mohawk et al., 2012) are thought to be central coordinators of the peripheral oscillators elsewhere in the body (Dubowy and Sehgal, 2017; Herculano-Houzel et al., 2006; Welsh et al., 2010; Zheng et al., 2018)). The fly brain has approximately 100,000 neurons (Zheng et al., 2018), and only ~150 contain robust cell-intrinsic molecular oscillators ((Dubowy and Sehgal, 2017), **Figure 1.2**). There is substantial cellular diversity within the mammalian and fly circadian networks. In the *Drosophila* brain, the ~150 clock neurons are organized into at least 9 anatomically and molecularly distinct clusters (Helfrich-Forster et al., 2007). Four subpopulations that have characterized roles in sleep and arousal include the small lateral ventral neurons (s-LNvs, (Grima et al., 2004; Stoleru et al., 2004)), large lateral ventral neurons (l-LNvs, (Sheeba et al., 2008a)), posterior dorsal neurons 1 (DN1ps, (Cavanaugh et al., 2014; Guo et al., 2016; Kunst et al., 2014; Zhang et al., 2010a; Zhang et al., 2010b)), and lateral dorsal neurons (LNds, (Grima et al., 2004; Guo et al., 2017; Stoleru et al., 2004)). The

dorsal neurons 2 (DN2s) have an established role in temperature preference (Kaneko et al., 2012). Four subpopulations that are comparatively poorly understood include the 5th PDF-negative small lateral ventral neurons (5th PDF- s-LNVs (Rieger et al., 2006)), dorsal neurons 3 (Diaz et al., 2019), lateral posterior neurons (LPNs, (Ni et al., 2019)), and the anterior dorsal neurons 1 (DN1a (Fujiwara et al., 2018)). In the next sections, I expand upon the LNv and DN1a subpopulations that feature prominently in my work, and discuss a circuit model that lays the groundwork for my findings.

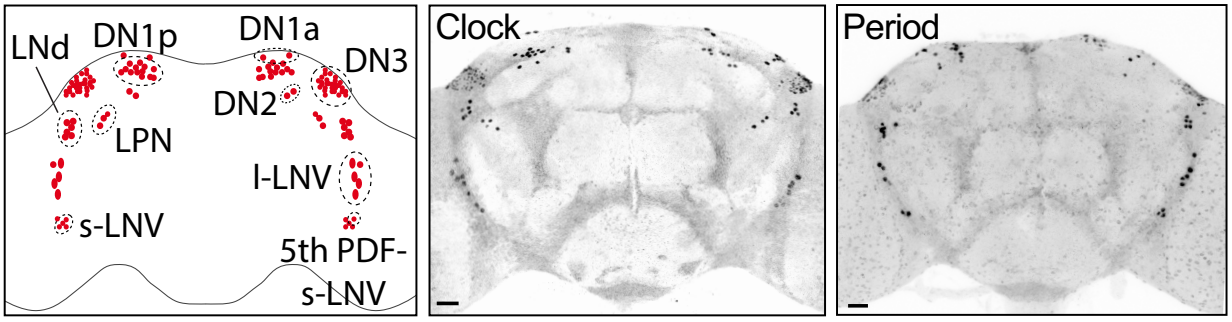

Figure 1.2. Schematic of clock neuron subpopulations in the *Drosophila* central brain. Middle, representative expression pattern of a control brain stained with antibody against the circadian transcription factor Clock. Right, representative expression pattern of a control brain stained with antibody against the circadian protein Period. This sample was obtained 1 hour after lights on, when Period levels are high. Scale bars: 20 μm.

Lateral ventral neurons (LNVs)

Of the ~9 subpopulations of circadian clock neurons in Drosophila, perhaps the best characterized, and arguably the most influential, include the lateral ventral neurons (LNvs). The LNVs themselves are composed of three subpopulations, one with large cell bodies that cluster in the dorsolateral protocerebrum (large lateral ventral neurons, l-LNvs, and another has small

cell bodies that cluster in the ventral accessory medulla (small lateral ventral neurons, s-LNvs). The third subpopulation, the 5th PDF- s-LNvs, are anatomically similar to other s-LNvs, but differ in function and neuropeptide content (Rieger et al., 2006). This work will focus primarily on the small and large s-LNvs.

Though morphologically and functionally distinct, s-LNvs and l-LNvs both express a specifically-expressed neuropeptide, pigment dispersing factor (PDF), that is found only in two other neurons in the *Drosophila* nervous system (Renn et al., 1999; Shafer and Taghert, 2009). PDF has an important organizing role in the circadian clock network. The PDF receptor (PDFR) is a G-protein coupled receptor expressed in ~50% of circadian clock neurons (Im and Taghert, 2010). Most clock neurons subpopulations, aside from l-LNvs, contain neurons that respond to PDF with cAMP signaling (Shafer et al., 2008). Within subpopulations, however, some neurons can be unresponsive to PDF (Yao and Shafer, 2014). PDF appears to have an outsized organizing role in the circadian clock network. Without PDF signaling, molecular clocks between cells become desynchronized or weakened (Lin et al., 2004; Yoshii et al., 2009; Zhang et al., 2010a) and clock neurons lose their activity tunings (Liang et al., 2016). Clock-controlled locomotor behaviors also differ in the absence of PDF signaling; rhythmicity in constant darkness gradually disappears. In light dark cycles, the clock-controlled locomotor activity peak in the morning disappears, while the evening peak occurs earlier, in the absence of PDF (Renn et al., 1999). PDF also participates in entraining to new light conditions. LNv activity can degrade timeless in downstream neurons (Guo et al., 2014). In addition PDFR can initiate a cAMP signaling cascade that stabilizes PER (Li et al. 2014, Zheng et al. 2014).

l-LNvs are thought to drive light-mediated arousal, as stimulation of these cells drive wakefulness in the nighttime (Shang et al., 2008; Sheeba et al., 2008a). l-LNvs have extensive

arborizations throughout the optic lobe (visual system of the fly), and also send commissural projections to the contralateral hemisphere. l-LNVs also influence the circadian network by synapsing onto s-LNV pacemakers (Klose et al., 2016; Oh et al., 2014). Due to their large cell bodies, l-LNvs are the subpopulation that are most easily accessed for electrophysiology (Flourakis and Allada, 2015). Most insights about clock regulation of physiology therefore comes from l-LNvs. Because s-LNvs are smaller, and lie deep within the brain, only few groups have successfully recorded from these cells (Cao and Nitabach, 2008; Choi and Nitabach, 2013; Li et al., 2018).

s-LNvs appear to have an outsized role in the circadian clock network of flies, as they are necessary for the maintenance of rhythms in constant darkness (Grima et al., 2004; Stoleru et al., 2004). s-LNvs are thought to be a central oscillator, because their activity can influence the phase of the clock in downstream cells. s-LNvs send projections to the dorsal protocerebrum, where the neurites of many other clock neuron subpopulations reside. Molecular manipulations that speed up or slow down the clock within s-LNvs autonomously, such as by overexpressing PER-phosphorylating kinases correspondingly changes the pace of the clock within other subpopulations (Stoleru et al., 2005; Yao et al., 2016; Yao and Shafer, 2014). Notably, not all cells are affected, suggesting that other subpopulations and neuropeptides, such as LNds and short neuropeptide F, also play a timekeeping role (Yao and Shafer, 2014).

Structural plasticity of s-LNv axons

In addition to daily electrophysiological fluctuations, s-LNvs undergo presynaptic modifications that change their output every day. In 2000, it was first observed that PDF neuropeptide levels in LNvs have daily fluctuations: their levels are highest in the morning and

lower in the evening (Park et al., 2000). In 2008, it was observed that s-LNv presynaptic terminals undergo daily rhythms in axonal fasciculation ((Fernandez et al., 2008), **Figure 1.3**). s-LNv axons in the dorsal protocerebrum are spread out (defasciculated) during the day, and bundled up (fasciculated) at night. Since then, several other groups have replicated these findings (Fujiwara et al., 2018; Gunawardhana and Hardin, 2017; Petsakou et al., 2015; Sivachenko et al., 2013), but the function of this daily axonal remodeling remains unclear (Muraro et al., 2013). s-LNv structural plasticity can modify connections to downstream circadian targets (Gorostiza et al., 2014), and genetic perturbation of plasticity can attenuate the strength (power) of locomotor rhythms (Petsakou et al., 2015). However, the functional significance of structural plasticity is controversial, as genetic manipulations that eliminate dorsal s-LNv terminals, or their rhythms, do not perturb behavioral rhythmicity (Agrawal and Hardin, 2016; Kula et al., 2006; Prakash et al., 2017), like s-LNv ablation would (Stoleru et al., 2004).

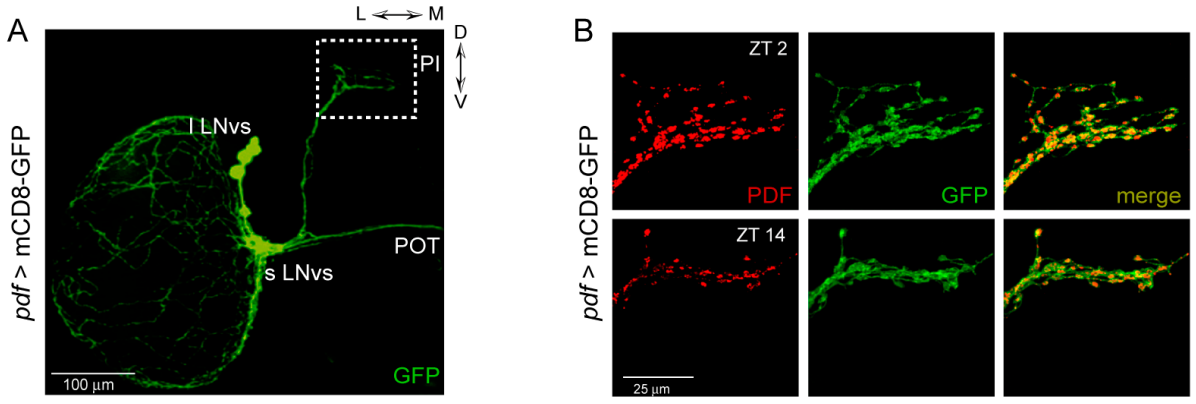

Figure 1.3. s-LNv dorsal axon daily plasticity. This figure is reprinted from Fernandez, M.P., Berni, J., and Ceriani, M.F. (2008). Circadian remodeling of neuronal circuits involved in rhythmic behavior. PLoS Biol *6*, e69, available from PLOS under a Creative Commons Atribution license. Captions are my own. **(A)** Dorsal proteocrebrum-extending small LNv axons

Figure 1.3 (continued). where daily structural plasticity occurs. **(B)** Daily patterns of presynaptic structural remodeling. Top row (ZT 2) shows axon configurations in the morning, two hours after lights-on. Bottom row (ZT 14) shows axon configurations in the evening, two hours after lights-off.

Some of the pathways regulating structural plasticity are known. Notably, electrical activity can induce fasciculation. Activity-dependent fasciulation/defasciulation rhythms are thought to be controlled by circadian regulation transcription factor Myocyte Enhancer Factor 2 (MEF2); although it has been argued that Mef2 is not a daily regulator of structural plasticity, but instead acts during development. Circadian regulation of Rho1 GTPase and guanine nucleotide exchange factor (GEF) Pura has been shown to regulate the polymerization/depolymerization rhythms that underlies neurite remodeling.

Structural plasticity is a mechanism of neuronal modification that is poorly understood. After salient experiences, neurons strengthen or weaken relevant connections through synaptic mechanisms (Citri and Malenka, 2008). This can be due to presynaptic modification, such as intracellular signaling programs that causes transmitter release probability to increase (Citri and Malenka, 2008; Zucker and Regehr, 2002). This can also be due to postsynaptic mechanisms, such as receptor trafficking (Collingridge et al., 2004; Sheng and Kim, 2002; Song and Huganir, 2002). Another form of plasticity occurs with morphological changes to spines, which are relatively small (~0.05-1 μm) protrusions that extend roughly perpendicularly from main neurite branches (Harris and Kater, 1994). Spines can enlarge, emerge, or disappear after salient experience (Yuste and Bonhoeffer, 2001). In contrast to these mechanisms, structural plasticity is unlikely to appear in introductory texts. Even classic examples of structural plasticity are not widely recognized: these examples include the daily remodeling of photoreceptor terminals in

the human retina and daily axonal swelling the fly visual system (Pyza and Gorska-Andrzejak, 2008; Pyza and Meinertzhagen, 1995; Weber et al., 2009). In Zebrafish, hypocretin/orexin neurons that regulate sleep and wakefulness undergo dramatic cycling of synapse number; which the authors showed to be under circadian regulation (Appelbaum et al., 2010). More recent discoveries of structural plasticity in behavior-regulating neurons will be discussed in **Chapter 4**.

Anterior dorsal neurons 1 (DN1as)

The DN1as are an underrepresented subpopulation in studies of the adult *Drosophila* clock network. In developing larvae, DN1a neurons are one of the four circadian subpopulations that is present (Kaneko et al., 1997). Alongside the larval s-LNvs, DN1as appear to be a major oscillators. LNvs and DN1as communicate between each other with PDF and glutamate respectively. The two subpopulations appear to be active at different times (Collins et al., 2012) which is important for behavioral and molecular rhythms. The glutamate gated chloride channel (GluCl) and metabotropic glutamate receptor (mGluR) are important for DN1a->LNv regulation of molecular and behavioral rhythms respectively (Collins et al., 2012; Collins et al., 2014). Intriguingly, glutamate is still expressed in adult DN1as, and the metabotropic glutamate receptor is expressed in adult s-LNvs (Hamasaka et al., 2007).

In addition to glutamate, adult DN1as also express the neuropeptide CCHamide1 (CCHa1, (Fujiwara et al., 2018)) and the neuropeptide-like precursor 1-derived neuropeptide (IPNamide, (Shafer et al., 2006)). DN1as express the PDFR and respond to PDF with cAMP signaling. Until only recently, the existing studies of adult DN1as had been regarding their anatomy and the identity of their signaling molecules. In 2018, Fujiwara et al. published the first

characterization of adult DN1a function (Fujiwara et al., 2018). They found that DN1as also signal onto LNvs in the adult. They proposed that DN1as excite LNvs, and are important for promoting activity in the morning. A limitation of their study was that they only had specific access to DN1as via an intersectional approach: they manipulated levels of CCHa1 in all clock neurons. And since CCHa1 is not expressed in any other clock subpopulations, they could attribute behavioral phenotypes to DN1a. Because they did not have driver lines specific to DN1a, they could not look at the contributions of glutamate or IPNamide, in DN1a function. In this work, we follow up on several of their findings; discrepancies between our findings and theirs are discussed in **Chapter 3**.

The mammalian suprachiasmatic nucleus

The mouse circadian network consists of ~ 20,000 neurons that form the suprachiasmatic nucleus (SCN) of the hypothalamus (Hastings et al., 2018). Though their cell types are less defined than in the fly clock network, SCN neurons with distinct functions, connectivities, and molecular identities are topologically segregated between ventral 'core' and dorsal 'shell' regions (Welsh et al., 2010). SCN clock neurons are required for behavioral rhythms, suggesting that they generate an internal sense of time (Stephan and Zucker, 1972).

Circadian network waves

Ex vivo imaging has shown that 'waves' of calcium activity propagate across the dorsal-ventral axis of the SCN with ~24 hour periodicity: different anatomical regions of the SCN are active at different times of day (Brancaccio et al., 2013; Enoki et al., 2012; Hong et al., 2012). Analogous activity waves have been observed in the fly circadian network: recently, calcium

levels in different subpopulations were simultaneously imaged *in vivo*, over long timescales (Liang et al., 2016, 2017). Studies in flies and mice showed that peak activities for different subpopulations are biased towards specific times (Liang et al., 2016; Schaap et al., 2003), substantiating a long-standing model that a circadian representation of time is distributed across clock neural networks.

Functional evidence for a distributed representation of time

The best functional evidence for a distributed time representation is in a fly microcircuit consisting of morning and evening oscillators (Grima et al., 2004; Stoleru et al., 2004). There are two major peaks of daily locomotor activity in flies, one in the morning and the other in the evening, which are controlled by two different clock neuronal subpopulations, s-LNvs and LNds, respectively (Grima et al., 2004; Stoleru et al., 2004). These subpopulations exert semi-independent effects on locomotor activity: for example, interfering with s-LNv peptidergic output accelerates the onset of the evening locomotor activity peak (controlled by LNds), but does not prevent it (Renn et al., 1999; Schlichting et al., 2019a). Though each clock neuron has its own intracellular timer, there appear to be advantages to distributing timekeeping responsibilities across many neurons. In mammals, intercommunication between SCN neurons makes the whole network more accurate (Herzog et al., 2004; Noguchi et al., 2017; Schmal et al., 2018; Yamaguchi et al., 2003).

Measuring circadian rhythms

Masking

In light-dark cycles, flies display bimodal peaks of locomotor activity, with highest activity in the morning and in the evening. Flies appear to anticipate changing environmental conditions, by increasing locomotor activity before the lights turn on and before they turn off. Circadian rhythms are often measured in constant conditions, such as continuous darkness, because environmental reactivity can obfuscate traditional measures of circadian timekeeping (Redlin and Mrosovsky, 1999; Wheeler et al., 1993). Even arrhythmic animals react reflexively to changes in environmental luminance, which creates the appearance of rhythmicity in cycling environmental conditions. This phenomenon is called 'masking' because it can hide circadian phenotypes (Mrosovsky, 1999). In flies, these acute increases in locomotor response are sometimes called 'startle' responses (Rieger et al., 2003).

Free-running rhythms in constant conditions

In constant darkness, molecular oscillations and behavioral rhythms persist. Even without instructive environmental cues, flies, mice and humans that have been entrained to cycling environmental conditions display daytime and nighttime differences in behavioral activity. Corresponding to this, molecular clocks continue to cycle. Circadian processes are self-sustaining once set into motion (Hardin, 2011). That is, animals retain ~24 hour rhythms in physiology and behavior even if the environmental cues are removed (e.g. in constant darkness, (Konopka and Benzer, 1971).

By definition, an arrhythmic process would be consistent at all times; plotted across time, it would appear static. Rhythmic processes by contrast, are dynamic and have stereotyped, repetitive cycles. Rhythms can be quantified using different, but related metrics (Klarsfeld et al., 2003). These metrics can be applied to quantify any rhythmic process, such as behavior, transcription, or neuronal activity. One metric is periodicity, which roughly refers to the timing differences between activity peaks. For flies, a typical periodicity measurement is ~24.4 hours (Konopka and Benzer, 1971). Another typical circadian measurement is power, which roughly refers to the amplitude or robustness of the measured process. Another metric is phase, which roughly refers to 'when' the peak appears. A simple, approximate interpretation of what these terms mean is as follows: periodicity refers to the accuracy of the clock, power reflects the strength of the clock, phase refers to *when* physiological outputs are expressed.

Sensorimotor regulation by the clock

Entrainment is sometimes assessed with probing stimuli, such as with dynamic environmental conditions. The same mechanisms that entrain animals to environmental conditions, such as degradation of CRY by light, can be used to adjust to new conditions. This protocol is analogous to traveling across timezones: the speed and ease by which we adjust to new timezones is regulated by the clock.

Brief exposure to environmental inputs can reveal the state of the clock. A short exposure to nighttime light can modify the phase of the clock in subsequent days. The phase of locomotor activity in subsequent days reveals the state of the clock at the time of light pulse - if light exposure occurs early in the night, the phase of the molecular clock and behavioral rhythmicity is delayed; they are advanced if brief light exposure occurs late into the night (Suri et al., 1998).

Light exposure has little effect on phase during circadian daytime (if presented to flies in darkness).

Other protocols, that are not as commonly employed, use external stimuli to probe the state of the clock. Preference for certain environmental conditions can be tested by allowing animals choose between different lights and temperatures within their habitats. Flies display complex temperature preference rhythms, which can be roughly summarized as a preference for warmer temperatures during the day, and cooler temperatures at night (Kaneko et al., 2012). Spectral preference also changes as the day progresses – flies are attracted toward green light sources during the morning and evening, they are attracted to red light sources in the mid-day, and are repelled by blue light throughout the daytime; and they lose spectral preference during the night (Lazopulo et al., 2019). Similarly, ultraviolet light repels flies more strongly during the daytime than in the nighttime (Baik et al., 2018).

In 2008, Lu et al. established a protocol that I rely upon for the work presented here. They were first to show that *Drosophila* acute locomotor responses to light (i.e. masking) vary across a 24-hour period (Lu et al., 2008). Before this work, it was proposed that masking occurred independently of the circadian clock (Helfrich-Forster et al., 2001; Rieger et al., 2003). Lu et al. showed that dim white light evokes locomotor activity at night, but has little effect during the day. The daytime response to light is intensity-dependent; at 5 lux, locomotor activity hardly changes, but at 200+ lux, locomotor activity is suppressed by light. Using different circadian clock mutants, the authors showed that time-of-day regulation is mediated by the circadian clock. Mutants of core circadian clock factors, such as per^{01}, Clk^{ar}, and tim^{01} had stereotyped responses to light. Though these mutants all lost temporal regulation of light reactivity, there were notable differences between mutant strains: one mutant strains always had

increased locomotion in response to light, another always decreased locomotion, the other was unresponsive to light. No work, to our knowledge, has followed up on the results of this 2008 study. In **Chapter 2**, I will discuss my experiments that follow up on their work and a reinterpretation of their findings. Many results are congruent with theirs, but specific differences that arise from methodological differences are discussed in **Chapter 4**.

Summary of dissertation

Since the basic language of neurons is near-instantaneous electrical activity, how do clock neuron circuits represent time on a scale of ~24 hours? What are the principles by which timing responsibilities are passed from one circadian population to another? The answers are unclear even in the case of the extensively studied s-LNv-LNd microcircuit. The propagation of activity waves across circadian networks is suggestive of yet undiscovered circuit motifs that ensure precise alternation of active subpopulations. Finding those motifs could have broader significance since state switching is poorly understood for neural circuits in general.

In **Chapter 1**, I discussed a long-standing theory that a functional representation of time is spread across this circuit. My work substantiates and expands upon on this model. In **Chapter 2**, I discuss a noncanonical behavioral assay to study circadian timekeeping. In contrast to traditional methods that passively measure locomotor activity over the course of days, I used acute light reactivity to reveal animals' moment-to-moment internal time estimates. This protocol revealed a circadian microcircuit that contributes toward a distributed representation of time. In **Chapter 3**, I describe anatomical and functional properties of the LNv-DN1a circadian microcircuit. I show that structural plasticity that occurs within the microcircuit, and present evidence that it underlies circadian changes in time estimation. Finally in **Chapter 4**, I discuss

how mutually inhibitory microcircuits, and structural plasticity, might be general motifs network-level timekeeping. This work shows how a molecular representation of time might be transformed into a cellular and circuit-level representation.

Chapter 2: A network-level representation of time is distributed across clock neuron subpopulations

Introduction

Internal models of the external world enable evaluation of present conditions and predictions about the future. We expand upon one of the few understandings of an internal model - the molecular representation of daily time – to further ask how time is represented in circadian circuits. Here we use a noncanonical framework to assess animals' internal sense of time. Typically, locomotor activity is measured over several days in order to evaluate rhythmicity. Instead, we measured moment-to-moment time estimates by monitoring acute responsiveness to sudden light. Flies react in opposite ways to light in the middle of daytime vs. nighttime – they increase locomotion at night, and decrease it during the day. Behavioral reactivity to light therefore reports flies' internal time estimates. This protocol revealed that clocks evaluate external conditions relative to internal expectations, and enabled us to find separate clock neuron subpopulations that are functional during daytime vs nighttime. This work provides further evidence that representations of time are distributed across circadian networks.

Results

A behavioral assay to interrogate flies' sense of time

To study how circadian circuits switch between states, we searched for a behavioral assay that could reveal internal time estimates with moment-to-moment resolution. Since light is predominantly associated with daytime, we reasoned that animals differentially contextualize light depending on time of day. We modified a protocol used by Lu *et al.* to measure acute locomotor reactivity to light (Lu et al., 2008). Flies were entrained to cycles of alternating light and darkness (12 hours each) before being transferred to complete darkness for at least 24 hours. An hour-long light stimulus was then delivered to flies in darkness, at different times, and

locomotor activity was recorded (**Figure 2.1A**). As seen by Lu *et. al* (Lu et al., 2008), isogenic wild-type (Ryder et al., 2004) flies became more active in response to light during the nighttime; the opposite was true during subjective daytime (daytime, but in darkness) – locomotor activity decreased when the lights turned on (**Figures 2.1A** and **2.1B**; **Supplementary Video 1**). When locomotor responsiveness to light was examined every hour, two states lasting ~12 hours each became apparent (**Figure 2.1C**). During a period centered around mid-day (2pm) activity was suppressed by light. Conversely, during a period centered around mid-night (2am), activity was evoked by light. Locomotion seemed to be triggered by subjective mismatch (i.e. animals experiencing environmental conditions that are different than expected at that time of day). Flies not only startled to light during nighttime (**Figures 2.1A-1C**), but they also startled if darkness was imposed during daytime, in light-dark cycles (**Figure 2.2G**). Locomotor reactivity to light pulses therefore reports internal estimates of daytime vs. nighttime (**Figure 2.1D**).

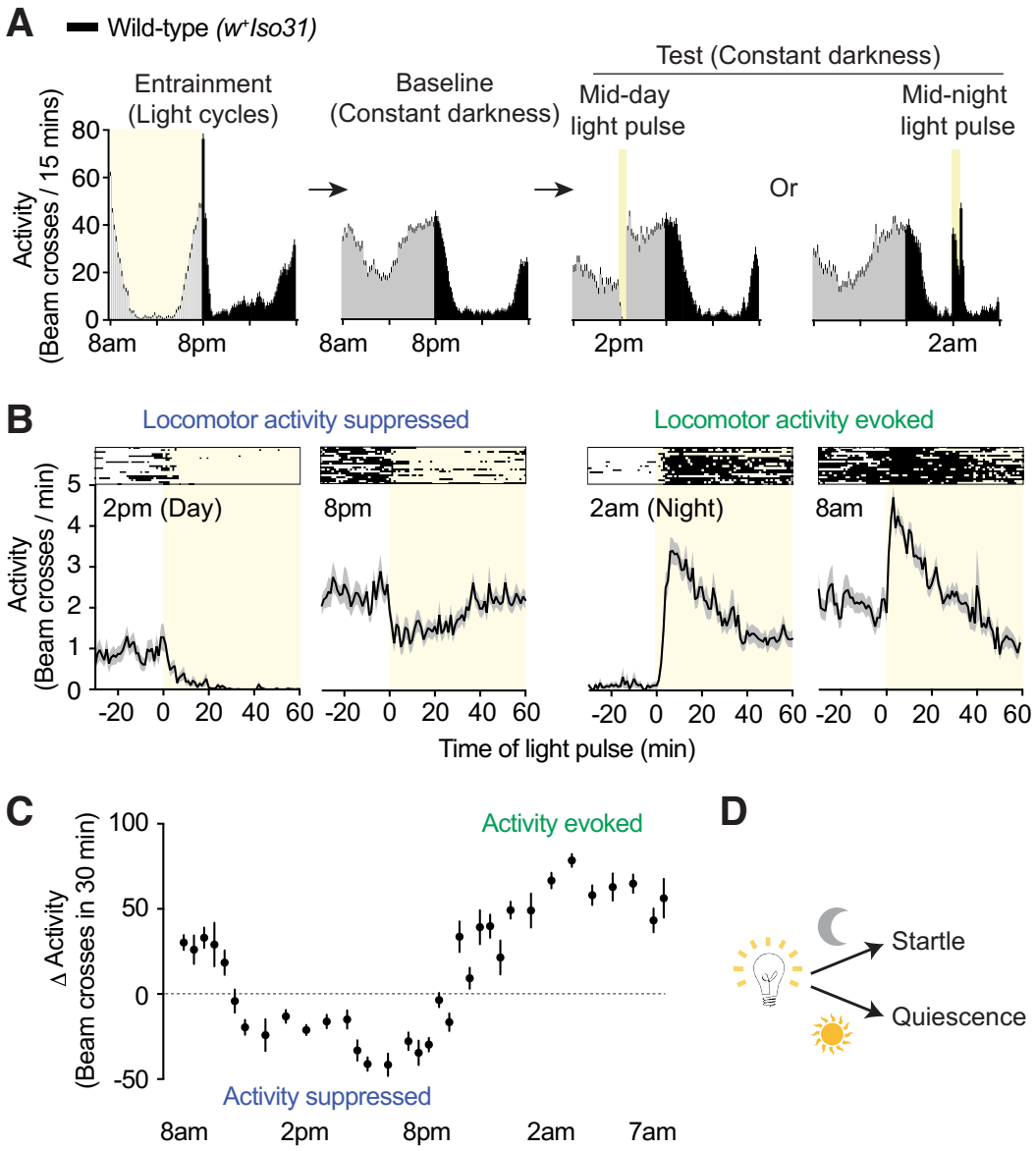

Figure 2.1. Time-of-day determines light responsiveness in wild-type flies. (A, left**)** Experimental protocol and daily locomotor activity of an isogenic wild-type strain, *w*$^{+}$*iso31*, during entrainment, baseline, and experimental periods. Vertical bars: 15 minute locomotor activity bins. Height indicates mean. Error bars, S.E.M. **(A**, right**)** Light elicits different locomotor reactivities depending on when it is presented. Yellow indicates light. At all

Figure 2.1 (continued). timepoints, lights-off transitions (at the end of the pulse) evoked large locomotor activity bouts, appearing as peaks adjacent to (but not within) yellow bars. **(B)** A closer view of acute locomotor responses to light at different times. Boxed insets show representative activities of individual flies; below, averaged activity of all tested flies. These data are collected at 1-minute intervals. Shading: error bars (S.E.M in all figures). **(C)** Change in activity evoked by light across a 24 hour period shows long-lasting behavioral states. See also Figure 2.2D. Independent cohorts were tested at each time point (so that no flies were exposed to light multiple times). **(D)** Schematic of daily light responses in wild-type flies. For all figures, behaviors were analyzed with Two-way ANOVA, Tukey's post-test, unless otherwise indicated. Supplementary Table 1 shows sample sizes for all figures.

Locomotor fluctuations do not predetermine light responses

Baseline locomotion fluctuates from day to night even in total darkness (Figure 2.1A and Figure 2.2A), so we examined whether these differences account for temporal modulation of light responses. There are three arguments against the conclusion that responsiveness is predetermined by activity levels before the light pulse: levels of locomotion were similar at 8 pm and 8 am, but diverged in opposite directions after the lights turned on (Figure 2.1B). Second, examination of individual flies showed that responsiveness to light did not correlate with baseline locomotion, and weakly correlated with sleep status prior to light. (Figure 2.2B and 2.2C). To further test this conclusion, we tried normalizing light-evoked locomotor activity to baseline activity, which recapitulated the results using our standard metric (Figure 2.1C and Figure 2.2D). Third, though male flies tend to sleep during the day while females do not (Huber et al., 2004), both sexes

responded to daytime light by decreasing activity (Figures 2.1A and 2.1B; Figures 2.2E and 2.2F).

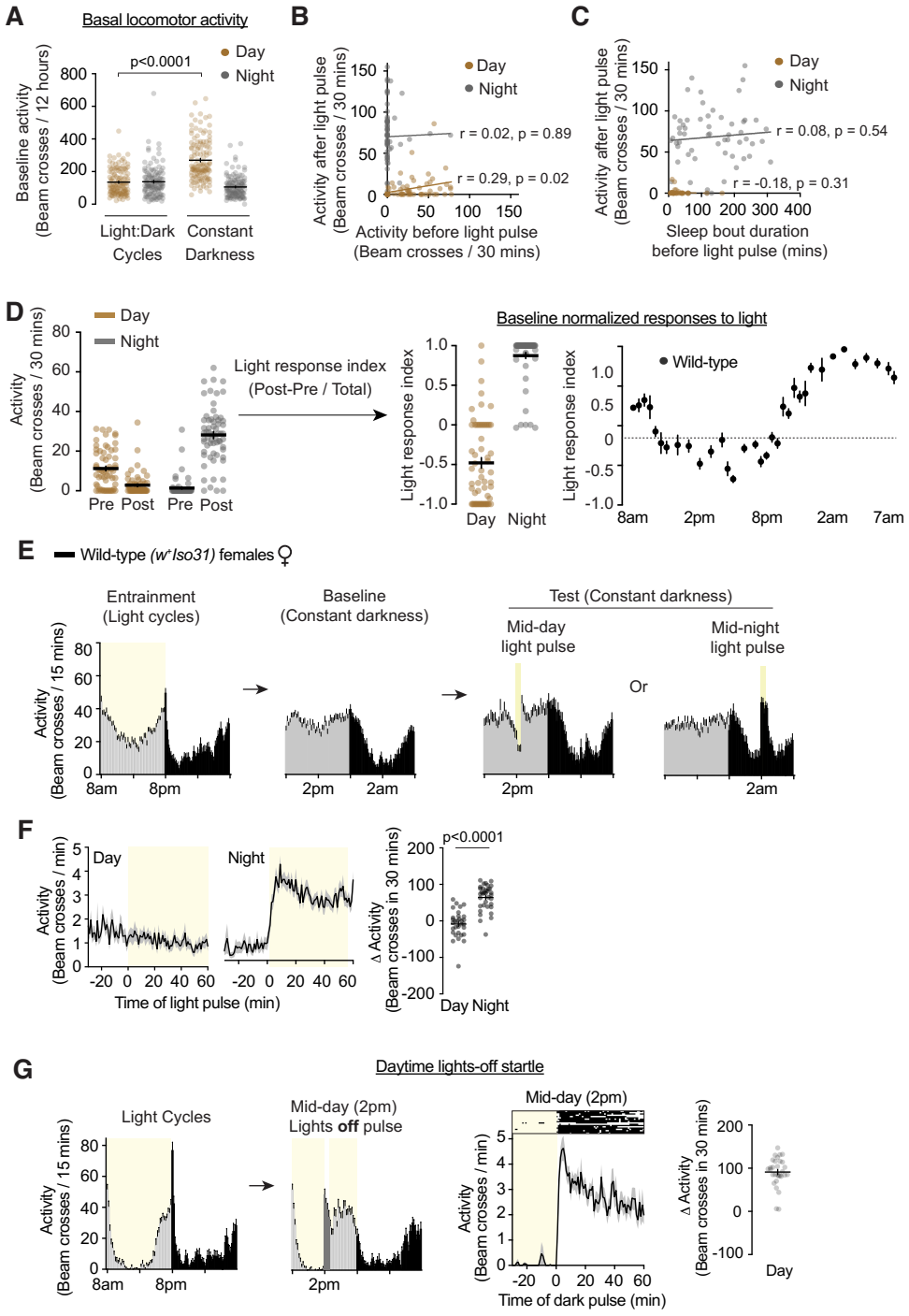

Figure 2.2. Light responsiveness is independent of circadian fluctuations in baseline locomotion. (A) Basal locomotor activity is higher in constant darkness than in light-dark cycles,

Figure 2.2 (continued). but only during daytime. **(B)** Pre-pulse locomotor activity weakly correlates with activity during the pulse given mid-day. Pre-pulse locomotor activity does not correlate with activity during the pulse given mid-night. **(C)** Sleep bout duration prior to the light pulse does not correlate with behavioral response during the mid-day or mid-night. (A-C) show the same flies as Figure 2.1, A-C. **(D)** Activity normalized to baseline still shows two distinct states. Same flies as Figure 2.1C. **(E, F)** Female flies respond to light differently during the daytime vs nighttime. Virgin female w^{+}*Iso31* flies underwent the same treatment shown in Figure 2.1A. **(G)** Lights-off during the daytime elicits startle. Unlike for experiments shown in other figures, flies were not in constant darkness but in light-dark cycles. On the experimental day, lights were turned off for 1 hour between 2pm and 3pm.

Circadian clocks bi-directionally modify responsiveness to light

When we disabled circadian clocks by knocking down the core clock protein Clock (Dubowy and Sehgal, 2017) within all clock neurons (**Figure 2.3A**; **Figures 2.4A** and **2.4B**; **Supplementary Table 2**), flies showed a similar response at both 2pm and 2am, increasing their locomotion in response to a light pulse (**Figure 2.3B**). They startled when the lights turned on, though the increase in locomotion during nighttime was lower than in controls (**Figures 2.3B**). These flies had invariant responses to light when tested across 24 hours (**Figure 2.3C**), which was also true with an analogous manipulation of a different core circadian protein Period (Per, **Figure 2.4C,** (Bargiello et al., 1984; Konopka and Benzer, 1971; Zehring et al., 1984)).

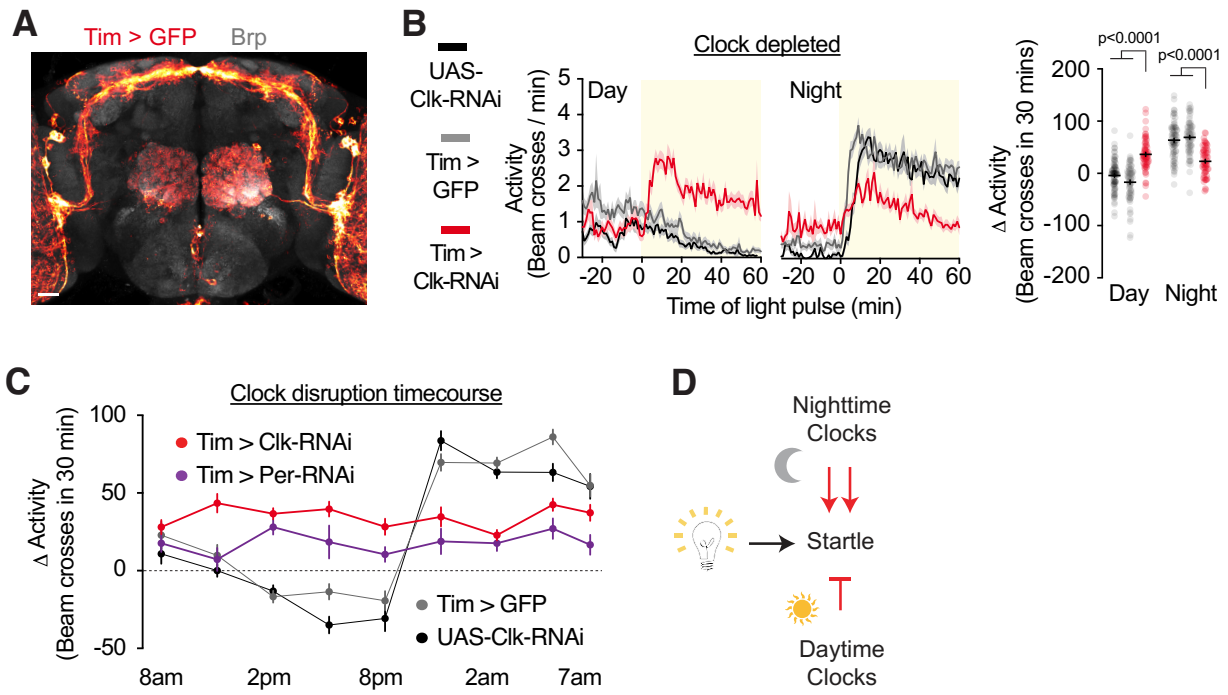

Figure 2.3. Circadian clocks bi-directionally modulate light responsiveness. (A) Left, Tim-Gal4 is expressed throughout the circadian network, visualized with GFP. The whole brain is visualized with an antibody against Bruchpilot (Brp), a presynaptic protein. For all figures, scale bars: 20 µm. Tim-Gal4 is also expressed in noncircadian neurons in the antennal lobe and glia (Gorska-Andrzejak et al., 2018), which was partially ameliorated by the inclusion of repo-Gal80 (data not shown) in all experiments using this driver. Supplementary Table 1 shows detailed genotypes for all figures. **(B)** Clock disruption (red) perturbs acute light responsiveness during daytime and nighttime. Supplementary Table 1 shows all statistical comparisons for all figures. **(C)** Light-evoked changes in activity across 24 hours in controls (black and gray), and in flies in which core circadian proteins Clock (Clk, red) or Period (Per, purple) were depleted with RNAi. Independent cohorts were tested at different time points. See also Supplemental Figure 2.2A for RNAi validation. **(D)** Proposed model for daily switches in light contextualization, regulated by the clock.

Molecular clocks direct the timing of behavioral state transitions

Circadian mutants with faster clocks (**Figure 2.4D** and **Supplementary Table 2**, (Konopka and Benzer, 1971)) had earlier transitions between light-responsive states (**Supplemental Figure 2.4E**), demonstrating that state transitions are directed by clock cycles. Together, these results suggest that the circadian system bidirectionally modifies a stereotyped startle that occurs in response to abrupt changes in environmental light. During daytime, clocks suppress the startle response, while they enhance it during nighttime (**Figure 2.3D**). We propose that clocks allow environmental conditions to be evaluated as appropriate or not relative to temporal context.

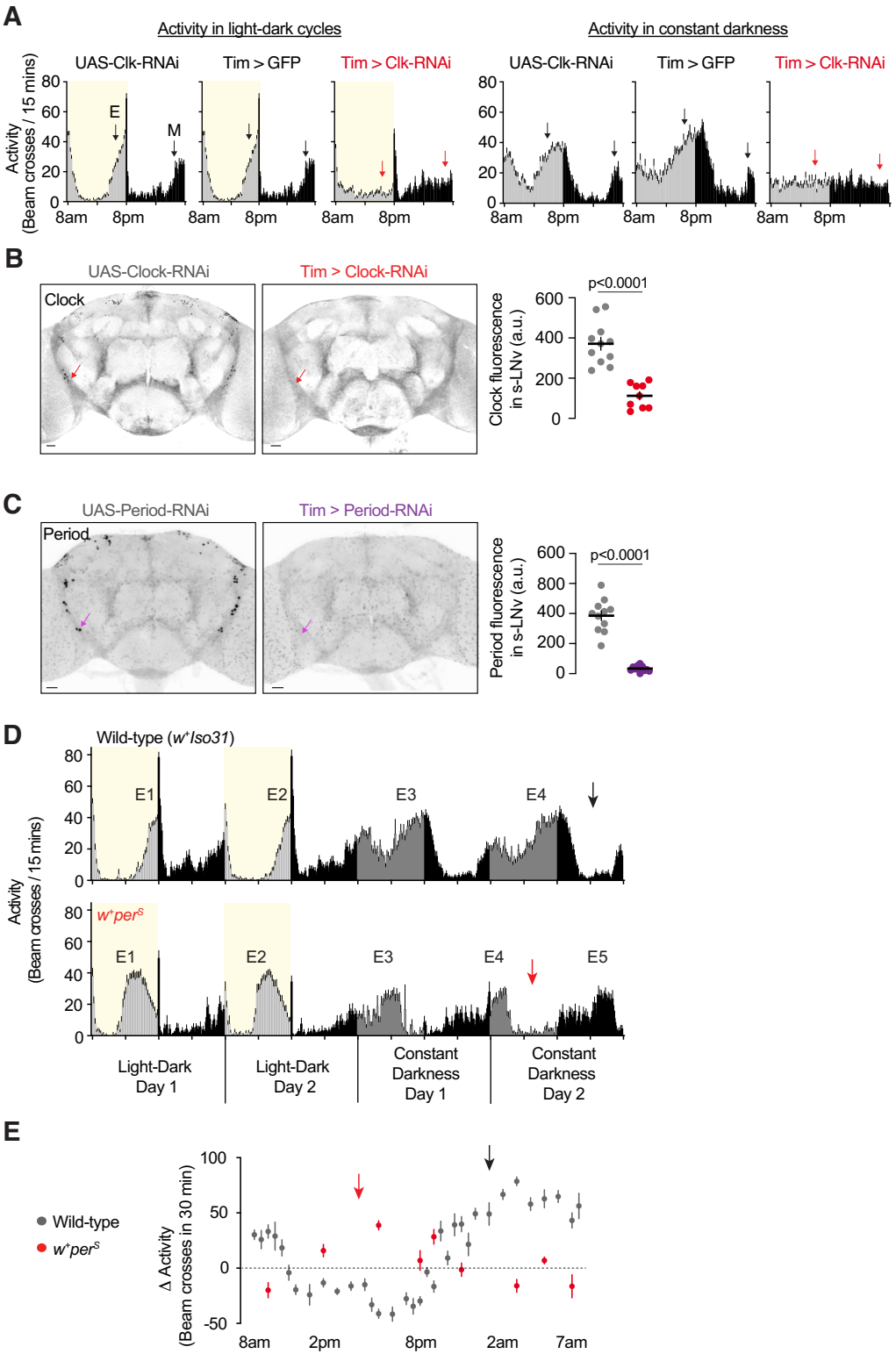

Figure 2.4. The timing of light responsiveness is directed by clocks. (A) 24-hour activity profiles in light-dark cycles and constant darkness show that targeting the core circadian protein

Figure 2.4 (continued). Clock (Clk) by Tim-Gal4-driven RNAi prevents anticipatory locomotor activity and locomotor rhythms in darkness. Arrows indicate the presence (black) or absence (red) of morning (M) and evening (E) anticipation. **(B)** Confirmation that Clk-RNAi effectively depletes Clock protein. Clock staining was arbitrarily performed at ZT6 since Clock protein levels are detectable throughout the day (Houl et al., 2008). (**C**) Confirmation that Per-RNAi effectively depletes Per protein. Period staining was perfomed at 9am (Zeitgeber Time 1, ZT1), since Period expression oscillates in controls and is near peak levels during this time (Shafer et al., 2002). Period staining is broad because of glial expression (Siwicki 1988, Zerr 1990). **(D)** A mutation in *period* (*period*^{Short} or *per*^{S}) accelerates circadian rhythms. E# indicates corresponding peaks of evening activity between control and mutant flies. Arrows indicate comparable timepoints - subjective nighttime after the fourth peak of evening activity. See also Supplementary Table 2. **(E)** This mutation also accelerates the timecourse of light responsiveness. Same control flies as in Figure 2.1C.

LNvs contextualize daytime light

We asked how molecular clocks represent time within the clock neuron network. We looked first at the best characterized clock neurons in the fly, the LNvs (**Figures 2.5A** and **2.5B,** (Dubowy and Sehgal, 2017)). LNvs regulate locomotor activity, communicate widely with other circadian neurons, and are activated by light (Dubowy and Sehgal, 2017; Renn et al., 1999; Sheeba et al., 2008b), so we suspected their potential involvement. When we optogenetically silenced LNvs via the green-light-gated chloride channel GtACR1 (Mohammad et al., 2017), flies startled in response to light during subjective daytime (**Figure 2.5C**), similar to clock-disrupted flies (**Figure 2.3B**). However, LNv-silenced flies differed from clock-disrupted flies

during the nighttime – their response to light was normal (**Figures 2.3B** and **2.5C**). RNAi-mediated depletion of the LNv-specific neuropeptide PDF (pigment dispersing factor (Helfrich-Forster, 1995)) (**Figure 2.5D**), and hypomorphic mutations in the PDF receptor (PDFR (Hyun et al., 2005)), mimicked the daytime phenotype of LNv silencing (**Figures 2.5E** and **2.5F**). PDFR mutants startled normally to the onset of nighttime light, but that response was not sustained, differing from both the controls and clock-disrupted flies. This difference was likely due to genetic background, as other PDF-silencing manipulations (**Figures 2.5C** and **2.5E**) and subsequent PDFR mutant experiments in mixed backgrounds (**Figures 2.7A** and **2.7B**; **Figure 2.8A**) revealed normal responsiveness to nighttime light.

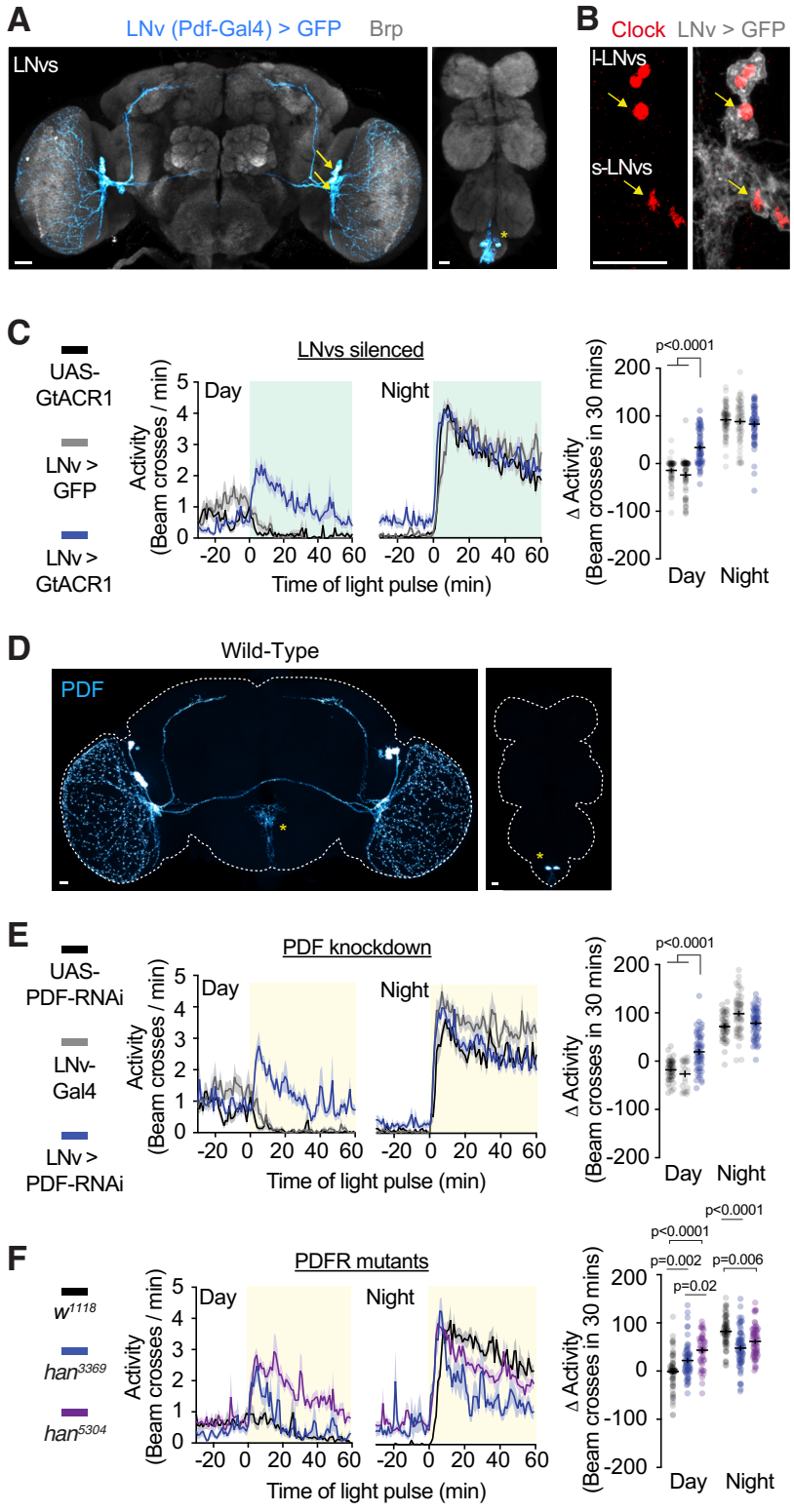

Figure 2.5. LNv clock neurons are required for normal daytime, but not nighttime, light reactivity. (A) Left, LNv neurons in the brain labeled with GFP. Arrows point to LNv cell bodies.

Figure 2.5 (continued) Right, non-LNv expression in the ventral nerve cord (VNC) indicated by asterisk. LNv-Gal4 is downstream of *pdf* regulatory elements (Park et al., 2000; Renn et al., 1999). **(B)** Clock staining in the LNvs. **(C)** Silencing LNvs using the light-gated chloride channel GtACR1 perturbs mid-day but not mid-night light responsiveness. For all optogenetic experiments, the light used for neuronal silencing simultaneously served to probe behavior. **(D)** Expression pattern of PDF in the brain and VNC. Asterisks indicate variable expression in the midline of the brain and non-circadian neurons (Shafer and Taghert, 2009) in the VNC. **(E)** Knockdown of PDF in LNvs perturbs only daytime light responsiveness. **(F)** Two hypomorphic mutations of PDF receptor (PDFR) show perturbed responsiveness to daytime light. Though nighttime light responses differ from controls, peak responses to nighttime light are similar to wild-type.

small LNvs are necessary to contextualize daytime light

Knocking down PDF in the dorsally-projecting small (s-LNv), but not large (l-LNv) subpopulation ((Helfrich-Forster, 1995), **Figure 2.6A-E**)) was sufficient to disrupt daytime light responsiveness (**Figure 2.6B**). However, PDF knockdown was incomplete in l-LNvs (**Figures 2.6C** and **2.6E**), and the phenotype was stronger when both subpopulations were manipulated simultaneously (**Figure 2.5E** and **Figure 2.6B**), so we treated the LNvs as a unit going forward.

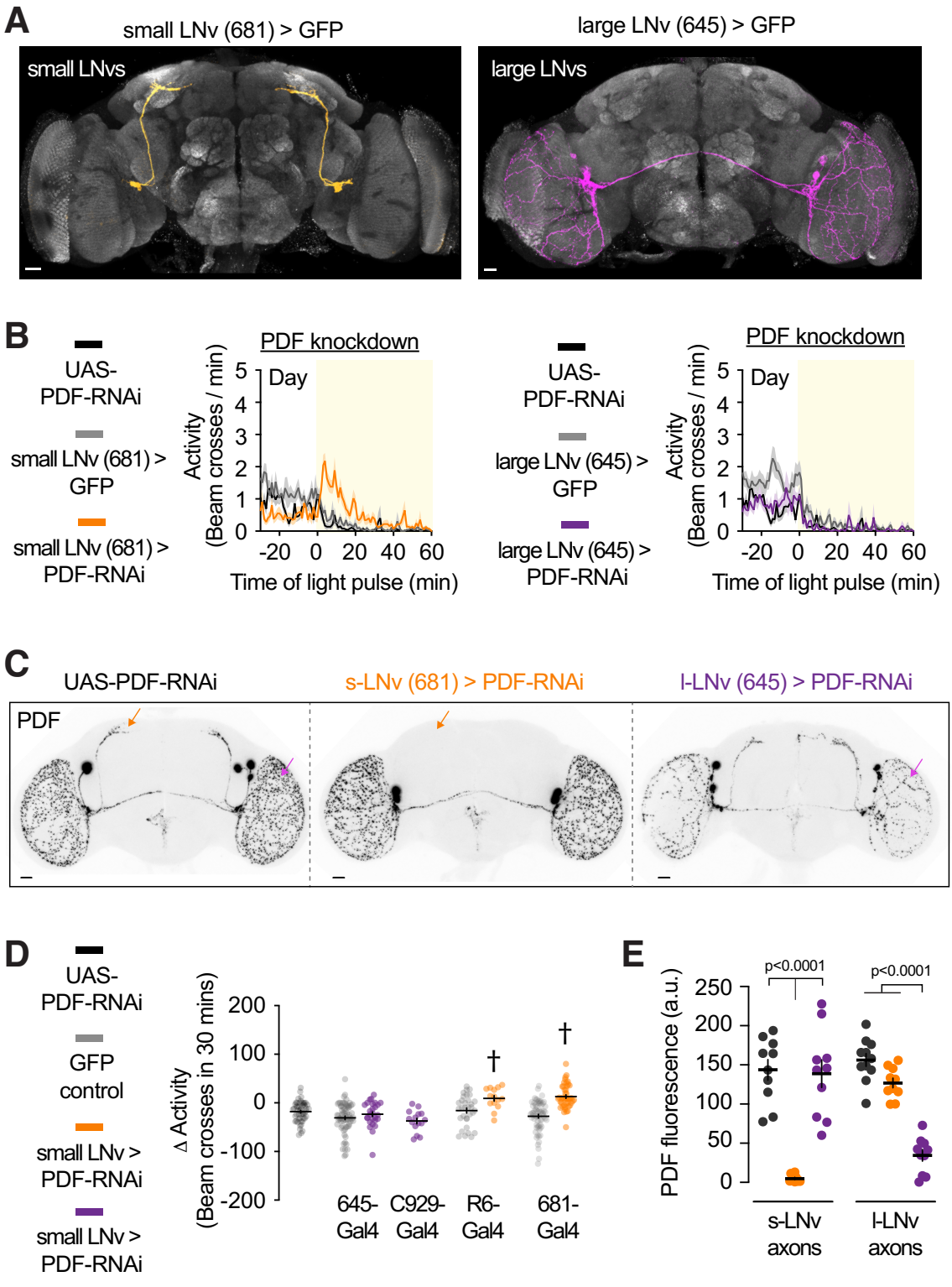

Figure 2.6. PDF from small LNvs is required for normal daytime light reactivity. (A)

Expression patterns of Gal4 drivers in small (JRC_SS00681-Gal4) or large (JRC_SS00645-Gal4)

Figure 2.6 (continued). LNv subpopulations. **(B)** PDF knockdown shows that small LNvs (681-Gal4) are a necessary source of daytime PDF. UAS-PDF-RNAi controls (grey) are duplicated between left and right panels. **(C)** Representative PDF expression patterns when PDF-RNAi was driven in either small or large LNv subpopulations. Arrows indicate quantified regions in Supplemental Figure 2.3E. Note that PDF was not completely depleted by l-LNv-Gal4-driven RNAi. **(D)** Light-evoked change in activity using two s-LNv and two l-LNv drivers to express PDF-RNAi. One-way ANOVA of daytime light responses, with Tukey's post hoc test. †significance ($p<.05$) versus all other conditions, aside from each other. **(E)** Quantification of PDF immunostaining intensity in s-LNv dorsal axons or l-LNv axons in the optic lobe.

LNv modulation of light responses is independent form general timekeeping

Because LNvs are known to be important for organizing rhythmic locomotor activity in darkness (Renn et al., 1999), a concern is that manipulating these neurons abolishes all sense of time. Three lines of evidence argue for specific rather than general loss of clock function. First, LNv-silencing manipulations did not affect nighttime responsiveness to light (**Figure 2.5C** and **2.3E**), unlike disabling the clock (**Figure 2.3B**). Second, disrupting LNv function does not prevent the increase in locomotor activity that normally occurs in anticipation of nighttime, which is clock-dependent (Renn et al., 1999; Stoleru et al., 2004). Third, rhythmicity in the first two days of constant darkness is weakened, but not abolished, by LNv manipulations (**Supplementary Table 2**, (Grima et al., 2004; Renn et al., 1999; Stoleru et al., 2004)). We conclude that LNvs signal that light is appropriate during daytime and are dispensable for contextualizing light during nighttime. This interpretation agrees with the observation that LNvs

are normally more electrically active during daytime (Buhl et al., 2016; Liu et al., 2014; Sheeba et al., 2008a; Sheeba et al., 2008b).

The DN1a subpopulation of clock neurons contextualizes light only during nighttime

The fact that LNv silencing recapitulates only the daytime phenotype of clock disruption means that the nighttime role must belong to other populations. Since LNvs signal through the peptide PDF (**Figure 2.5E**), we looked for their targets by restoring expression of the PDF receptor to various neuronal populations in the receptor mutants (**Figure 2.7A**). For this *pdfr* rescue screen, we used Gal4 lines expressed in sleep- and locomotion-regulating centers, circadian subpopulations, canonical LNv targets, and neurons expressing specific neurotransmitters or peptides. Restoring PDFR to most neuronal populations, including known LNv targets (Lear et al., 2009; Pirez et al., 2013; Zhang et al., 2010a), could not fully suppress *pdfr* mutant phenotype (**Supplementary Table 3**). Only a few of the 274 tested Gal4 lines allowed complete rescue (**Figure 2.7A** and **Supplementary Table 3**); of these, we focused on the lines with the most restricted expression. When PDF transmission was enabled onto neurons labeled by R23E05-Gal4 (Jenett et al., 2012), normal responsiveness to daytime light (decrease in locomotor activity) was restored (**Figure 2.7A** and **2.7B; Figure 2.8A**).

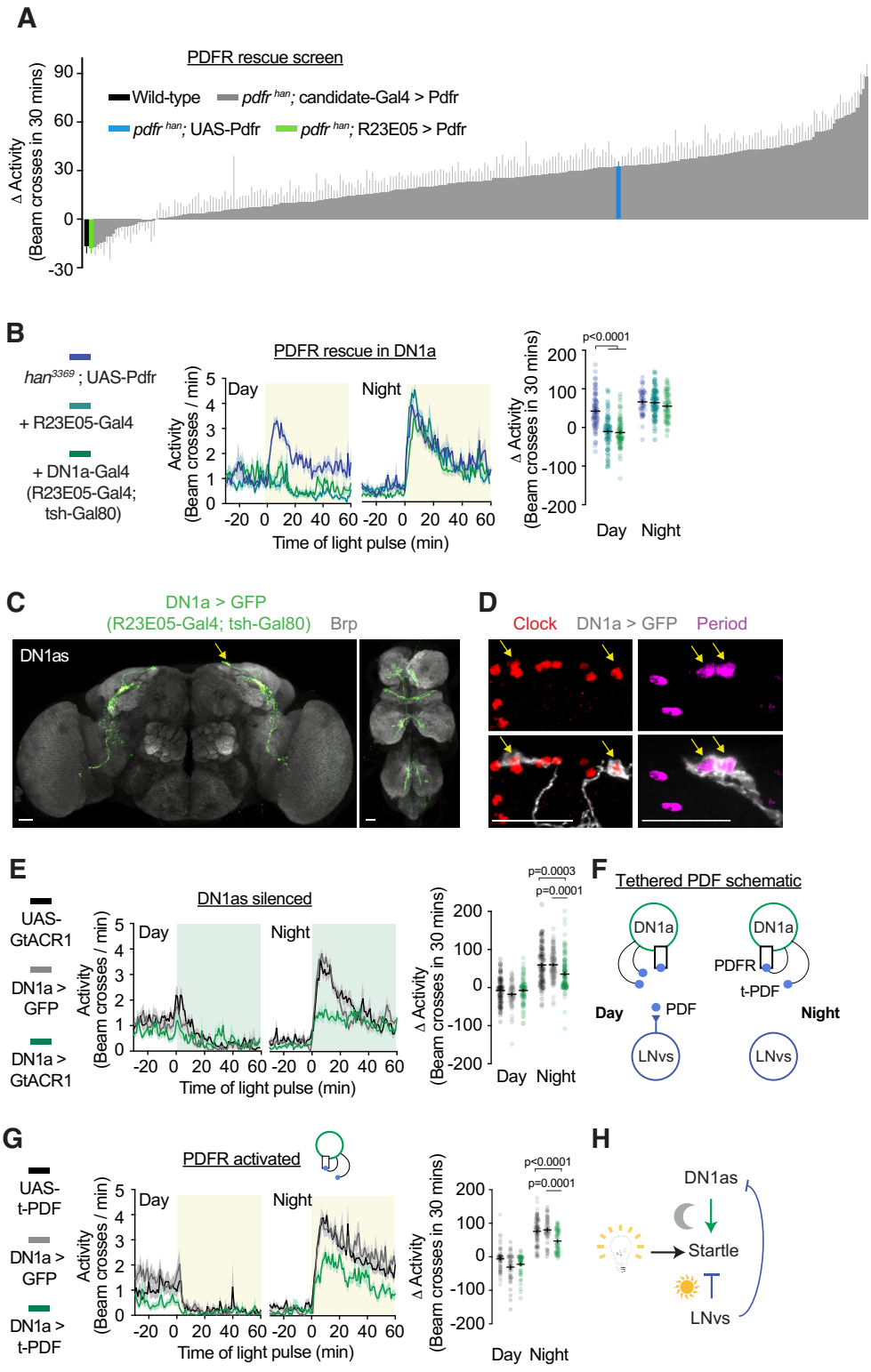

Figure 2.7. DN1as are downstream of LNvs, and are required for normal nighttime, but not daytime, light reactivity. (A) A *pdfr* genetic rescue screen reveals a role for LNv-to-DN1a

Figure 2.7 (continued). transmission in contextualizing daytime light. In *han*^{3369} or *han*^{5304} *pdfr* mutant backgrounds, PDFR was expressed in candidate neuronal populations. **(B)** Activity traces for flies in which PDFR was expressed using R23E05-Gal4 (dark green) or using R23E05-Gal4 with teashirt-Gal80 (DN1a-Gal4, light green) in the *han*^{3369} *pdfr* mutant background. This experiment was also done in the *han*^{5304} *pdfr* mutant background (Supplemental Figure 2.4A). **(C)** DN1as visualized by GFP (DN1a > GFP). See also Supplementary Figures 2.4B-2.4E. **(D)** Clock and Period staining in DN1as. **(E)** DN1a silencing perturbs mid-night but not mid-day light responsiveness. **(F)** A schematic of the tethered-PDF (t-PDF) approach. **(G)** Constitutive activation of PDFR with t-PDF in DN1as attenuates nighttime response to light. **(H)** Model of LNv and DN1a roles in contextualizing light.

Characterization of the R23E05 driver

R23E05-Gal4 labels ~20 neurons in the ventral nerve cord, and ~10 neurons in the brain (**Figure 2.8B**). The brain neurons include the four dorsal-anterior clock neurons (DN1as; **Figures 2.7C** and **2.7D; Figure 2.8C**), about which little is known (Fujiwara et al., 2018). DN1a dendrites and cell bodies are in the dorsomedial protocerebrum, and their axons descend towards the accessory medulla (**Figure 2.8D,** (Hamasaka et al., 2007; Shafer et al., 2006)). Addition of a Gal4 inhibitor Gal80 that is expressed in the ventral nerve cord (teashirt-Gal80, tsh-Gal80) diminished the expression of R23E05-Gal4 outside of the DN1a clock neurons (**Figure 2.8E**). We henceforth refer to this intersectionally-derived driver as DN1a-Gal4. Restoration of PDFR with either R23E05-Gal4 or DN1a-Gal4 restored normal daytime light responsiveness (**Figure 2.7B** and **Supplemental Figure 2.8A**). Subsequently we found that several other rescuing Gal4s are also expressed in DN1as (**Supplementary Table 3**).

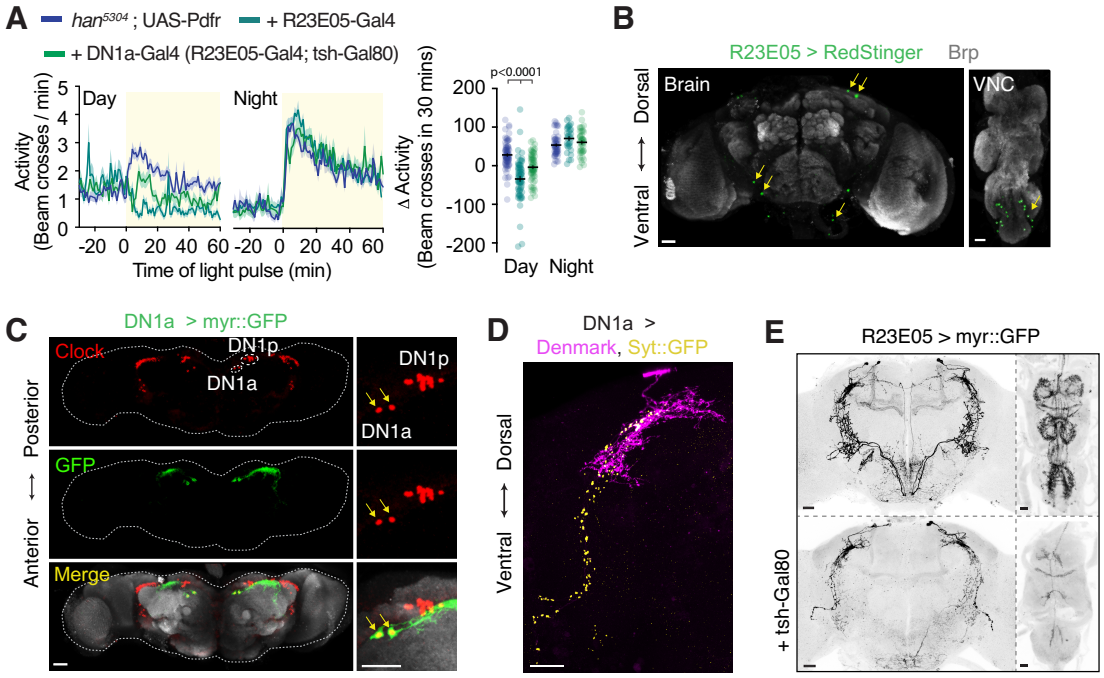

Figure 2.8. Additional anatomical and behavioral characterization of R23E05-Gal4. (A) Activity traces for flies in which PDFR was expressed using R23E05-Gal4 (dark green) or DN1a-Gal4 (light green) in the *han*^{5304} *pdfr* mutant background. **(B)** R23E05-Gal4 driving the nuclear reporter RedStinger. The nervous system expression includes 2 DN1as, 2 neurons in the saddle, 1 cell in the inferior posterior slope, and ~10 neurons in the ventral nerve cord, per hemisphere. With some reporters, we saw weak expression in the mushroom body. **(C)** Dorsal view of DN1a-Gal4 expression pattern confirms expression in anterior, and not posterior, DN1 subpopulations. **(D)** DN1a-Gal4 driving markers of postsynaptic sites (Denmark) and presynaptic sites (Synaptotagmin:::GFP, Syt::GFP). **(E)** Restriction of R23E05 primarily to DN1as using teashirt-Gal80 (tsh-Gal80). Expression was diminished in most VNC neurons and in some central brain neurons.

The DN1a subpopulation of clock neurons contextualizes light only during nighttime

DN1a silencing perturbed only the *nighttime* response (**Figure 2.7E**), which was the opposite pattern than seen with LNv silencing (**Figure 2.5C**). The attenuated startle to nighttime light was similar to the response of clock-disrupted flies (**Figure 2.2B**), suggesting that DN1as might provide context that light during the nighttime is inappropriate. If DN1as contextualize light during the nighttime, why is LNv-to-DN1a signaling required for normal responsiveness to light during the daytime (**Figures 2.7A** and **2.7B; Figure 2.8A**)? One possibility is that daytime LNv-to-DN1a signaling is inhibitory. We tested the consequence of expressing a membrane-tethered variant of the peptide PDF (Choi et al., 2009) in DN1as. Since tethered PDF is anchored by a short glycosylphosphatidylinositol glycolipid anchor, it can only have short-range, cell-autonomous effects on cells that natively express PDF receptor (**Figure 2.7F,** (Choi and Nitabach, 2013)). The nighttime startle to light was weakened by this manipulation (**Figure 2.7G**), which was similar to the DN1a silencing phenotype (**Figure 2.7E**). This result confirms that DN1as express PDFR (Im et al., 2011; Shafer et al., 2008) and suggests that PDF has inhibitory effects on DN1as. While PDF is classically thought to have neuromodulatory effects via cAMP signaling (Shafer et al., 2008), it can also be excitatory (Chatterjee et al., 2018; Seluzicki et al., 2014; Vecsey et al., 2014; Yao et al., 2012) or inhibitory (Cavey et al., 2016; Chatterjee et al., 2018; Liang et al., 2017; Potdar and Sheeba, 2018). Taken together, results presented thus far suggest that LNvs and DN1as have opposite roles in contextualizing light during daytime vs. nighttime, and that the peptide PDF is a crucial organizational signal between these subpopulations (**Figure 2.7H**).

DN1a silencing does not impair locomotor ability

Since weak responsiveness could indicate a general problem, it was important to test for locomotor and visual deficits. To determine whether flies were capable of reaching high levels of locomotion, we reanalyzed nighttime activity from key experiments (**Figures 2.2B, 2.5C** and **2.7E**). Comparing the maximal locomotor activities that individuals reached during testing (activity/minute) revealed little difference between the experimental animals and the controls (**Figure 2.9A**). The lower population-averaged responsiveness in DN1a-silenced, or clock-disrupted flies, is instead accounted for by infrequency of high activity bouts (**Figure 2.9A**). In addition, flies with nighttime phenotypes reacted vigorously to mechanical stimulation, easily exceeding the highest levels of locomotor activity that is elicited by light (**Figure 2.9B**). A visually guided behavior, courtship (Markow and Manning, 1980; Ribeiro et al., 2018), was also normal (**Figure 2.9C**, see methods for details). Taken together, these data suggest that clock neuron manipulations do not simply impair sensory input or motor output, but instead disrupt the ability to contextualize light.

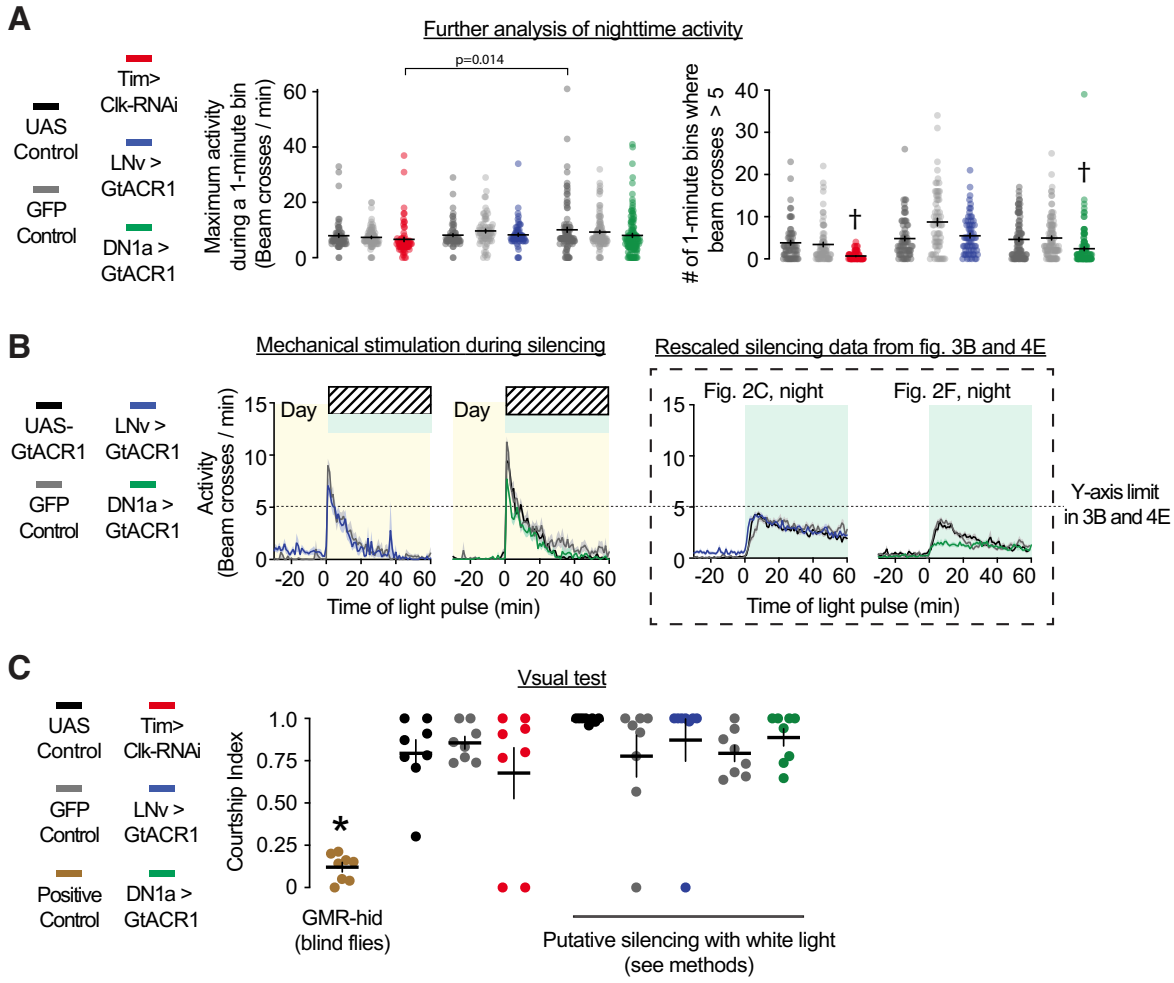

Figure 2.9. Manipulating LNv or DN1a activity does not cause general visual or locomotor defects (A) Left, peak locomotor activity per 1-minute bin, during nighttime light pulses (same flies as Figure 2.4B) or during nighttime optogenetic silencing (same flies as Figure 2.3C and Figure 2.4E). Right, number of high activity bouts (animals cross the middle of the tube more than 5 times per 1 minute bin). Cross symbols within panel indicate significance against all other conditions (except against each other). The LNv > GFP control genotype was significantly higher than all conditions, which is not indicated in the figure. One-way ANOVA with Tukey's post hoc test. **(B)** Mechanical stimulation of LNv-silenced and DN1a-silenced flies shows that all genotypes are capable of reaching high levels of locomotion. **(C)** Courtship of clock-disrupted

Figure 2.9 (continued). flies and subpopulation-silenced flies, which is compared to GMR-hid flies, a positive control with visual defects. See methods for details about optogenetics.

Discussion

Locomotor reactivity to light: masking or startle?

Our noncanonical framework insinuates that flies assign valence to experienced environmental conditions. Of course, we cannot know whether flies 'startle' because luminance conditions are unexpected, or if there is an alternative motive to increase locomotion. Previous studies of circadian modulation of light reactivity have observed similar phenomena (Lu et al., 2008) but our interpretation is new. What we call 'startle' and 'quiescence' are traditionally referred to as positive and negative 'masking' (Mrosovsky, 1999) because environmental reactivity can obfuscate traditional measures of circadian timekeeping (Redlin and Mrosovsky, 1999; Wheeler et al., 1993). Even arrhythmic animals react reflexively to changes in environmental luminance, which creates the appearance of rhythmicity in cycling environmental conditions (**Figure 2.4A**). We show that acute reactivity to light can also be an informative indicator of internal timekeeping. One advantage of this paradigm is that we can immediately measure moment-by-moment representations of time, rather than relying on passive measurements over the course of days. We demonstrate this utility with the use of optogenetics, which is not compatible with many circadian measurements; light will reset the clock and affect periodicity of subsequent days (Emery et al., 1998; Stanewsky et al., 1998).

Generalization to other models

Though we use light as a stimulus, our goal was to uncover general principles by which internal predictions are compared to external conditions. Light itself may be an idiosyncratic stimulus depending on the species. Unlike for flies, bright nighttime light presented to mice induces quiescence (Mrosovsky, 1999) , which does not fit the model where unexpected conditions induce startle characterized by high locomotion. This may be because inactivity can be a freezing response in mice, a behavioral correlate of fear (Pellman and Kim, 2016). Alternatively, nocturnal animals like mice may have evolved specific mechanisms to cope with light. Given the conservation of the core molecular clock, the use of circadian clocks to contextualize environmental conditions is likely retained.

The remaining subpopulations

The other circadian subpopulations may also contribute to changing predictions about light. The optogenetic silencing phenotypes of LNvs and DN1as together recapitulate the phenotype produced by network-wide loss of clock function (**Figures 2.3B, 2.5C** and **2.7E**). However, the native circuit signal may be built by the cooperative action of multiple subpopulations with overlapping tuning. Hints of subpopulation cooperativity are apparent in our data - there was a stronger phenotype when PDF was knocked down in both small and large LNvs, compared to s-LNvs alone (**Figure 2.5E; Figures 2.6B** and **2.6D**). We focused on two timepoints, but other populations may be more influential during other times of day (e.g. LNds in the evening).

Methods

Drosophila melanogaster

All *Drosophila* used in this study are listed in **Supplementary Table 4**. Flies were grown on cornmeal-agar medium at 25°C under 12 hour light : 12 hour dark conditions in a room with ~70 lux white light. UAS-myr::GFP, UAS-mCD8::GFP, UAS-tethered PDF, and UAS-Dicer2 lines were outcrossed six or seven times into the control *iso31* background. No differences in light responses were observed between outcrossed and non-outcrossed lines. Few experiments (**Figures 2.3B** and **2.3C (**2pm and 2am only); and **Figure 3.3C**) had UAS-mCD8::GFP controls included in the GFP condition, where the genotype is UAS-myr::GFP elsewhere in the paper. No behavioral differences were seen between UAS-mCD8::GFP and UAS-myr::GFP. RNAis were co-expressed with Dicer2 (Dcr) to increase efficiency (Ni et al., 2008). "LNv-Gal4" used in this study has two copies of Pdf-Gal4, on the second and third chromosomes. Similar results for silencing and neuropeptide knockdown were found using a single copy of Pdf-Gal4 on the second chromosome, although effect sizes were smaller (data not shown). Wild-type w^{+}*iso31* wild-type strains were created by backcrossing *Canton S* six times into the *iso31* background. Detailed genotypes and samples sizes for each experiment are provided in **Supplementary Table 1**. Origin of fly stocks and reagents are shown in **Supplementary Table 4**. Stocks are available upon request.

Locomotor activity measurements

Male flies, 1-9 days old, were collected and individually housed in 65 mm glass tubes with approximately 20 mm of cornmeal-agar media. To avoid cumulative effects of repeated exposure to light, separate cohorts were tested for each trial. They were given at least 48 hours to

acclimate before experiments began. Female flies were collected as virgins (<1 day old) upon eclosion, and group housed for at least 3 days before testing. Activity and sleep were measured using the Trikinetics *Drosophila* activity Monitor system, which counts infrared beam crosses through the midline of the glass tube. Experiments were conducted in DigiTherm CircKinetics incubators (Tritech Research, DT2-CIRC-TK) at 25°C. Aside from optogenetics experiments, light pulses were delivered using white incubator lights (~260 lux white fluorescent bulbs, ~102 $\mu W/mm^2$ in the 470 nm range). Most experiments in **Figure 2.7A**, and all experiments in **Figure 2.9B** and **Supplementary Video 1** were conducted in larger incubators (Percival, DR-41VL) to accommodate screening, video cameras or the mechanical stimulation apparatus.

Optogenetics

For 48-96 hours before the experiment, control and experimental flies were fed 50 mM all-trans-retinal (Sigma Aldrich R2500) that was diluted in ethanol (Koptec, V1001) and coated onto rehydrated potato food (Carolina Bio Supply Formula 4-24 Instant *Drosophila* Medium, Blue). For GtACR1 experiments, six 530 nm green LEDs (Luxeon Rebel, LXML-PM01-0100) were driven by a 700 mA constant current driver (LuxDrive BuckPuck, 03021-D-E-700), and pulse-width modulated signal to an averaged intensity of ~202 $\mu W/mm^2$. LEDs were placed along the wall of the incubator and controlled with an Arduino Uno Rev3 (Arduino, A000066) microcontroller using a custom script. Between replicates, genotypes were positionally counterbalanced within the incubator to control for nonuniform illumination from the light source (LEDs or white fluorescent bulb). Silencing motor neurons with VGlut-Gal4 allowed us to confirm that all flies received enough illumination to access neurons expressing GtACR1 (Mauss et al., 2017; Mohammad et al., 2017), regardless of position within the incubator.

Light measurements

Light intensity measurements were recorded using a power meter (Thorlabs, PM100D). Lux measurements were recorded using a light meter (Extech, LT300). The spectra of ambient white light in the laboratory and in experimental incubators were measured with a spectrometer (Thorlabs, CCS200). All reported measurements were taken with devices facing the light source. Power measurements for white light were taken at the 470 nm range.

Mechanical stimulation

Flies were shaken using a multi-tube vortexer (Trikinetics TVOR-120) modified to house *Drosophila* Activity Monitors (Trikinetics). The vortexer was programmed to deliver medium intensity vibrations for an hour.

Courtship assay

Courtship assays were conducted as previously described (Zhang et al., 2016). Briefly, male flies were isolated at least five days before the assay, to allow recovery of mating drive (Boutros et al., 2017; Zhang et al., 2016). On the day of the assay, one male was aspirated into a cylindrical chamber (10mm diameter and 3mm height) with one virgin w^{+}*iso31* female. Flies were videotaped from above using a handheld camera (Canon, Vixia HRF800) and videos were manually scored for courtship behaviors. Courtship indices were calculated from the percentage time engaged in mating behaviors during a five minute window following courtship initiation (as indicated by unilateral wing extension). If flies did not engage in courtship throughout the entire 15 minute assay, they were given a courtship index value of 0. Flies were illuminated from below (~3.7 $\mu W/mm^2$ in the 475 nm range) using a light pad (Artograph,

LightPad 930), in addition to aforementioned overhead white room lighting. Because optogenetic LEDs interfered with the ability to visualize and record flies, we relied on the white light from the light pad as an optogenetic effector. While the lightpad was substantially dimmer than the LEDs used in our optogenetic silencing experiments, our control experiments with other drivers showed that this light could in principle penetrate the cuticle to effect GtACR1 in the nervous system. For positive controls, we verified the lightpad's efficacy in inducing paralysis or extending mating duration in flies where GtACR1 was expressed by VGLUT-Gal4 or Corazonin-Gal4 respectively (data not shown, (Mohammad et al., 2017; Tayler et al., 2012)).

Immunohistochemistry

Flies were anesthetized under CO2. Brains were then dissected in cold Schneider's medium (Gibco, 21720-001) and immediately fixed in 4% paraformaldehyde (PFA, Electron Microscopy Sciences, 15710). After a 20 minute fixation at room temperature, brains were washed three times with PBS containing 0.3% Triton X-100 (Amresco, M143-1L), 20 minutes per wash, and blocked overnight with 10% donkey serum (Jackson ImmunoResearch, 017-000-121) at 4°C. Primary and secondary antibodies were diluted in donkey serum and incubated with brains for 48 hours each. For Brp (nc82) stainings, the primary antibody incubation was conducted for 72 hours due to the large number of Brp epitopes in the brain. Three 20 minute washes were done after primary and secondary antibody incubations. Antibodies used:

Guinea pig anti-Clock antibody (Gift from Paul Hardin, 1:2000 dilution)

Chicken anti-GFP antibody (Aves, GFP-1020, 1:1000 dilution)

Mouse anti-Brp antibody (Developmental Studies Hybridoma Bank (DSHB), NC82, 1:7 dilution)

Mouse anti-PDF antibody (DSHB, PDF C7, 1:100 dilution)

Rabbit anti-DsRed antibody (Clontech, 632496, 1:100 dilution)

Guinea pig anti-Period antibody (Gift from Amita Sehgal, 1:50 dilution)

Rabbit anti-CCHa1 (Our lab raised antibodies against the peptide QIDADNENYSGYELT (Veenstra and Ida, 2014), Genscript, 1:50 dilution)

Donkey anti-Mouse 488 (Thermo Fisher Scientific, A-21202, 1:1000 dilution)

Donkey anti-Rabbit 568 (Thermo Fisher Scientific, A-10042, 1:1000 dilution)

Donkey anti-Mouse 647 (Thermo Fisher Scientific, A-31571, 1:1000 dilution)

Donkey anti-Guinea Pig 488 (Jackson ImmunoResearch, 703-545-148, 1:100 dilution)

Donkey anti-Chicken 488 (Jackson ImmunoResearch, 703-545-155, 1:100 dilution)

Donkey anti-Guinea pig Cy3 (Jackson ImmunoResearch, 706-165-148, 1:100 dilution)

Donkey anti-Guinea pig 647 (Jackson ImmunoResearch, 706-605-148, 1:100 dilution)

Tissues were whole-mounted in Prolong Gold antifade reagent (Invitrogen, 1942345) on glass slides and coverslips (Electron Microscopy Sciences, 64321-10, 72230-01). Confocal images were obtained using a Leica SP8 confocal microscope at 20x, 1 μm intervals for expression patterns, and 63x,. Maximum projection images and quantifications were obtained using FIJI. Levels of brightness and contrast were adjusted across the whole image using FIJI or Adobe Photoshop.

Quantifying locomotor activity

Sleep and activity data were analyzed using custom Matlab software (available on github at https://github.com/CrickmoreRoguljaLabs) and plotted in Graphpad Prism 8 for Macintosh. Activity counts were collected at 1 minute intervals. A sleep episode was defined as inactivity

lasting at least five minutes (Hendricks et al., 2000; Shaw et al., 2000).

Circadian analysis was conducted using the Cycle-P function in FaasX, using 30 minute bins (Klarsfeld et al., 2003). Our experiments occurred during the second day of darkness, but rhythmicity, tau and power of locomotor rhythms (**Supplementary Table 2**) were calculated after 4 days in darkness. Additional days of analysis allowed us to acquire more accurate measurements (Klarsfeld et al., 2003; Zielinski et al., 2014). This analysis is conservative, because circadian deficits grow stronger with more time spent in darkness (Renn et al., 1999).

Statistical analysis

All statistical tests were conducted with Prism 8 for Macintosh (GraphPad). All data are presented as mean ± S.E.M. For significance indicators (asterisks) referring to multiple post hoc tests, we conservatively report the largest (least significant) p-value from each of the tests. Only significant comparisons are indicated. For light probe experiments, group means were compared using a Two-way ANOVA with Tukey's post-hoc comparisons against all possible conditions. For all behavioral panels using two-way ANOVA, multiple comparisons between time points are not reported. Significant differences between control genotypes are not indicated in figures. We report them here: the two parental controls significantly differed in **Figure 2.7F** (day, $p < 0.05$), the two parental controls in **Figure 2.5E** significantly differed (night $p < 0.0001$). Exact p values for all comparisons are reported in **Supplementary Table 1**. Behavioral experiments in main figures each had at least three replicates of approximately sixteen flies each. In cases where genotypes were only tested at one time point, we used a One-way ANOVA followed by Tukey's post-hoc test. For imaging experiments in **Figures 3.4** and **3.5**, we noticed substantial variability

between hemispheres, so each hemisphere was treated as a single sample. Power analyses to predetermine sample size were not conducted. Experimenters were not blind to conditions. Sample sizes are shown in **Supplementary Table 1**.

Quantifying immunostaining intensity

For quantifications of fluorescence intensities used to validate the efficiency of RNAi, the experimenter was not blinded during quantification, which we deemed acceptable due to the large and consistent effect sizes. Regions of interest were selected using the freehand selection tool in FIJI, on summed intensity projections of whole brain z-stacks. For measurements of Clock and Period RNAi, intensity measurements were taken within one s-LNv cell body per brain. For measurements of GFP intensity, when comparing the strength of LexA drivers, there was substantial variability between hemispheres. Thus measurements were taken for both hemispheres and subsequently averaged.

Additional acknowledgements

Stephen Zhang helped with coding and curated FlyLight for sparse driver lines. Stephen Thornquist helped with optogenetics. For fly stocks, we thank David Anderson, Andreas Bergmann, Justin Blau, Adam Claridge-Chang, Michael Crickmore, Barry Dickson, Paul Hardin, Robert Kittel, Michael Nitabach, Matt Pecot, Jeff Price, Orie Shafer, Amita Sehgal, Paul Taghert and Rachel Wilson. We are especially grateful to Dr. Gerry Rubin and the Howard Hughes Medical Institute's Janelia Research Campus for access to JRC_SS00681-Gal4 and JRC_SS00645-Gal4 lines prior to their publication. These strains will be described further in Dionne, Rubin, and Nern (manuscript in preparation). For antibodies, we thank Paul Hardin and Amita Sehgal. This work was supported by the National Science Foundation Graduate Research

Fellowship Program under Grant No. (BS, NSF Grant No. DGE1144152). Any opinions, findings, and conclusions or recommendations expressed in this material are those of the author(s) and do not necessarily reflect the views of the National Science Foundation. BS was also supported by the National Institutes of Health (F31 EY027252). DR is a New York Stem Cell – Robertson investigator. This work was supported by a New York Stem Cell Foundation grant, and a Klingenstein-Simons Fellowship Award in the Neurosciences.

Chapter 3: Structural plasticity in a circadian microcircuit regulates behavioral state transitions

Introduction

Many behavioral states are stable across long timescales, but flexible to changing circumstance. States like sleep and hunger are uninterrupted for hours, and somehow undergo dramatic transitions to antithetical states at predictable intervals. The mechanisms of neural circuit state transitions are poorly understood, and this shortcoming is especially poignant considering the prevalence of psychiatric disorders, such as bipolar disorder or depression, where dysregulated transitions are implicated. Given the enormous complexity of the human brain, there is utility in searching for circuit motifs and transition mechanisms in a tractable model organism, such as *Drosophila melanogaster*.

Here we describe cellular mechanisms that enable circuit state switching in a clock microcircuit. The behavioral experiments in **Chapter 2** imply that the LNvs and DN1as have distinct activity patterns during the daytime vs. nighttime. In this chapter we show that LNvs and DN1as form a microcircuit. Analysis of putative connectivity regions show that this microcircuit is in distinct physical configurations during daytime vs. nighttime. This is due to clock-driven axonal remodeling occurring with antiphase timing in the two populations, which requires the GTPase Rho1, a cytoskeleton-reorganizing signal. In summary, we describe the molecular, cellular and circuit mechanisms that allow for predictable and reversible switching between circuit, and consequently behavioral, states.

Results

LNvs and DN1as are reciprocally connected

To study the populations simultaneously, we created an R23E05-LexA line (**Figure 3.2A**). The LexA/LexAop system (Lai and Lee, 2006) functions similarly to the Gal4/UAS system, but

does not interact with it, allowing us to study the subpopulations in parallel. The interdigitated arrangement of LNv and DN1a projections (**Figure 3.1A**, **Figure 3.2B** and **Supplementary Video 2**) is suggestive of reciprocal communication. Genetically encoded markers of pre-and post-synaptic sites (Nicolai et al., 2010; Zhang et al., 2002) showed that LNv axons terminate onto DN1a dendrites within the superior lateral protocerebrum, while DN1a axons terminate onto LNv dendrites within the accessory medulla (**Figures 3.1B**, **Figure 3.2B**, **Supplemental Videos 3** and **Supplemental Video 4**). The trans-synaptic tracing tool *trans*-Tango (Talay et al., 2017) indeed reported LNvs and DN1as as mutual synaptic targets (**Figures 3.1C** and **Figure 3.2B**). To test whether these putative connections are functional, we activated each population at times when their activity is predicted to be low, and looked at the response of the other population *ex vivo.* When LNvs were stimulated via the ATP-gated cation channel $P2X_2$ (Lima and Miesenbock, 2005; Yao et al., 2012), the calcium sensor GCaMP6s (Chen et al., 2013) reported transient inhibition in DN1as (**Figures 3.1D**; **Figures 3.2C** and **3.2D**). Conversely, stimulating DN1as led to transient LNv inhibition (**Figures 3.1E**; **Figures 3.2E** and **3.2F**). The effects of DN1a stimulation were substantially weaker, potentially due to the R23E05-LexA line having lower levels of expression than PDF-LexA (**Figure 3.2G**).

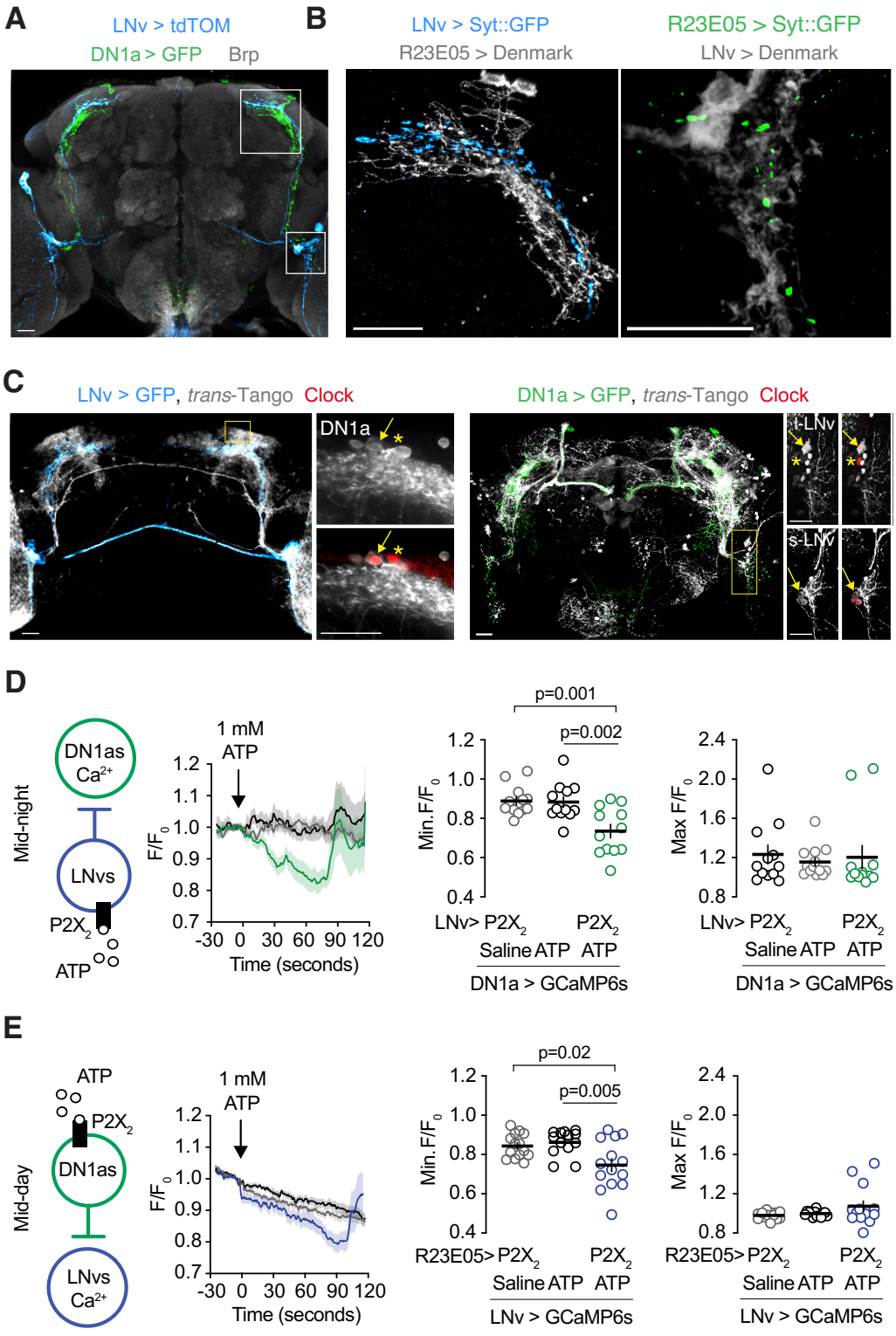

Figure 3.1. Reciprocal targeting between LNvs and DN1as. (A) Expression of GFP in DN1as, and tdTomato in LNvs, reveals overlapping projections. See also Supplemental Figure 3.1, A and

Figure 3.1 (continued). B and Supplementary Video 2. **(B)** LNv axons overlap with DN1a dendrites (left), and *vice versa* (right). Synaptotagmin (Syt): presynaptic marker; Denmark: postsynaptic marker. Left, area outlined on the top in (A). Right, area outlined on the bottom in (A). See also Supplementary Videos 3 and 4. **(C)** Postsynaptic targets labeled by *trans*-Tango indicate that LNvs and DN1as target each other. Arrows point to target cells expressing Clock. Asterisks: DN1as and LNvs not labeled by *trans*-Tango. See also Supplemental Figure 3.1B. **(D)** Chemogenetic activation of LNvs during the nighttime silences DN1as *in vitro*. See also Suplementary Figures 3.1C and 3.1D. **(E)** Chemogenetic activation of DN1as during the daytime silences LNvs *in vitro*. See also Figures 3.2E and 3.2F. For D and E, measurements were taken from flies that were in light-dark cycles (at ~2pm (ZT6) for daytime, at ~2am (ZT18) for nighttime). Minimal and maximal changes in calcium are reported for each trial. One-way ANOVA with Tukey's post-hoc test.

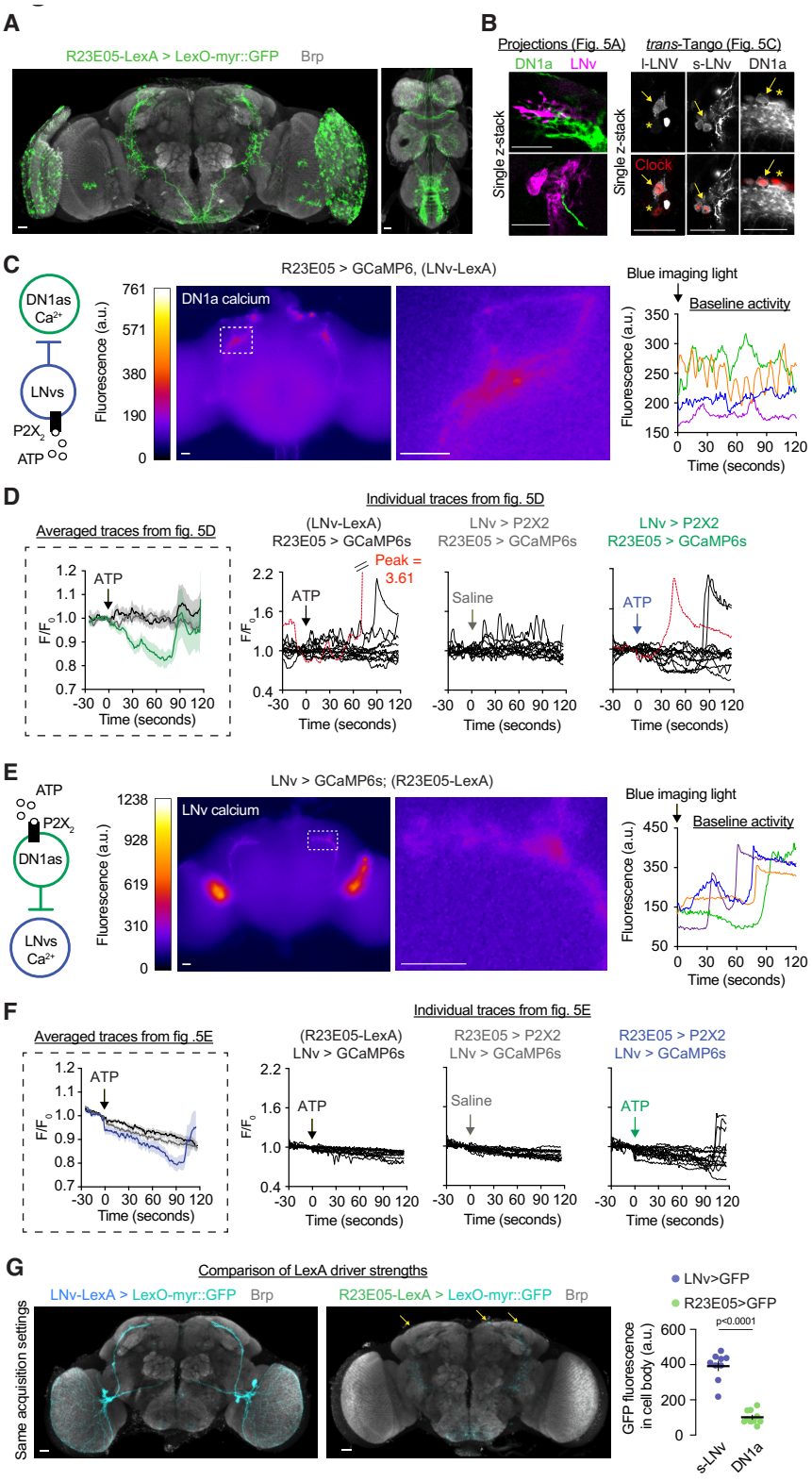

Figure 3.2. Additional data for functional imaging and mutual connectivity experiments. (A)

Single confocal z-stacks with imaging depths of 0.3 µm show proximity of LNv and DN1a

Figure 3.2 (continued). terminals (left) and specificity of trans-Tango experiments. **(B)** Expression pattern of R23E05-LexA. We saw strong expression in the lamina, which was not seen with R23E05-Gal4. **(C)** Left, representative fields of view during LNv-to-DN1a circuit tracing experiment. Dashed box shows magnified DN1a dendritic region selected for analysis. Left, representative baseline calcium fluctuations in DN1as before ATP stimulation. Right, representative calcium fluctuations in DN1a dendrites during two minutes of baseline imaging before ATP stimulation. Each color shows an independent trial. **(D)** All trials for experiments shown in Figure 3.1D. Red traces are one experimental and one control trial that were excluded from analysis because of non-representative depolarizations (see methods for more details). **(E)** Left, representative fields of view during DN1a-to-LNv circuit tracing experiments. Inset represents LNv axonal area selected for analysis. Dashed box shows magnified region of analysis in LNv axons. Right, representative calcium fluctuations in LNv axons during two minutes of baseline imaging before ATP stimulation. Each color shows an independent trial. **(F)** All trials for experiments shown in Figure 3.1E. **(G)** Representative GFP staining of LNv-LexA and DN1a-LexA when imaged under identical acquisition settings. Quantification of staining intensity within cell bodies is shown in the right panel.

DN1a output signals

The function of DN1as in adults has been unexplored, save for one study (Fujiwara et al., 2018). Fujiwara *et al* examined solely the role of the DN1a-produced neuropeptide CCHamide1 (CCHa1, **Figure 3.3A**, (Fujiwara et al., 2018)) in circadian rhythmicity. Consistent with our findings, they presented evidence that DN1as signal onto LNvs, that CCHa1 levels in DN1as are highest during mid-night and lowest during mid-day, and that the absence of CCHa1 results in

increased levels of PDF in LNvs. The authors proposed that DN1as release CCHa1 onto LNvs as an excitatory signal that promotes locomotor activity during the daytime. In contrast to their model, we found that DN1a silencing only had an effect during the *nighttime* in our assay (**Figure 2.7E**). The inhibition of LNvs that we saw when we stimulated DN1as (**Figures 3.1E** and **Figure 3.2E**) appears not to require CCHa1, as RNAi-mediated knockdown of CCHa1 or its receptor (CCHa1R) had no effect on light response behaviors (**Figure 3.3B**). We considered glutamate as an alternative candidate output signal, as in larvae this neurotransmitter is released from DN1as to inhibit LNvs. (Collins et al., 2012)). Consistent with this hypothesis, glutamate continues to be expressed in adult DN1as (Hamasaka et al., 2007). In adult brains, glutamate inhibits s-LNvs via the inhibitory metabotropic glutamate receptor A (mGluRA) (Guo et al., 2016; Hamasaka et al., 2007). Knockdown of mGluRA in LNvs partially phenocopied the effects of DN1a silencing (**Figure 3.3C**), though we cannot rule out the possibility that glutamate comes from another cell population such as DN1ps (Guo et al., 2016). Our data, when considered alongside existing knowledge, support a model where reciprocal connections between LNvs and DN1as can be refined by distinct output pathways, including ones that are inhibitory.

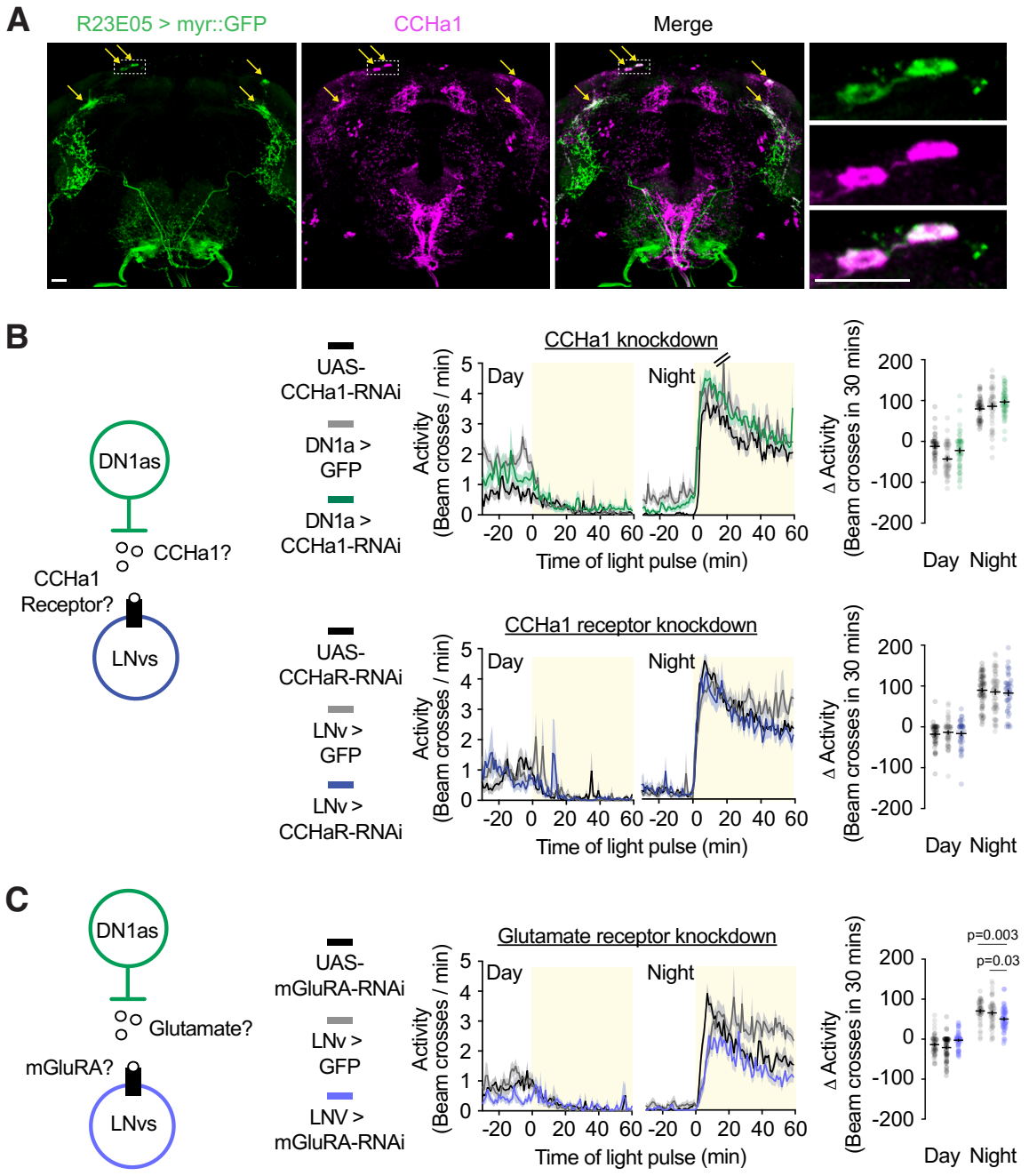

Figure 3.3, The peptide CCHa1 is not the relevant nighttime DN1a-to-LNv signal. (A) Co-staining of CCHa1with GFP in DN1as. **(B)** RNAi against CCHa1or its receptor does not mimic the effects of DN1a silencing. **(C)** RNAi against mGluRA partially recapitulate the nighttime effect of DN1a silencing.

LNv and DN1a axons are physically remodeled with anti-phase timing

LNv and DN1a neurons are required to contextualize light at different times of day and are mutually connected. How does the LNv-DN1a circuit alternate between the states during which one population or the other is required? Previous studies showed that s-LNv axons undergo daily structural remodeling, spreading out in the morning and bundling up at night (Fernandez et al., 2008; Gorostiza et al., 2014; Petsakou et al., 2015; Sivachenko et al., 2013). The function of this change has been unclear (Agrawal and Hardin, 2016; Kula et al., 2006; Muraro et al., 2013; Prakash et al., 2017) but has been proposed to regulate communication to downstream targets (Gorostiza et al., 2014; Petsakou et al., 2015). We confirmed the LNv axonal plasticity rhythms (**Figure 3.4A**, top) and discovered that DN1a axons are also remodeled daily (**Figure 3.4A**, bottom), in the ventromedial region where they overlap with LNv dendrites (**Figure 3.1A**). The daily DN1a plasticity rhythms follow a schedule antiphase to LNvs - their axons are extended at night and retracted during the day (**Figure 3.4A**, bottom). The fluorescently tagged presynaptic protein Bruchpilot (Brp) showed that changes in presynaptic area correspond with changes in synapse number, for both LNvs and DN1as (**Figures 3.4B**; **3.4C** and **3.4D**). The rhythmicity of axonal remodeling is set by the circadian clock, as it was absent in *period* mutants (**Figure 3.4E**).

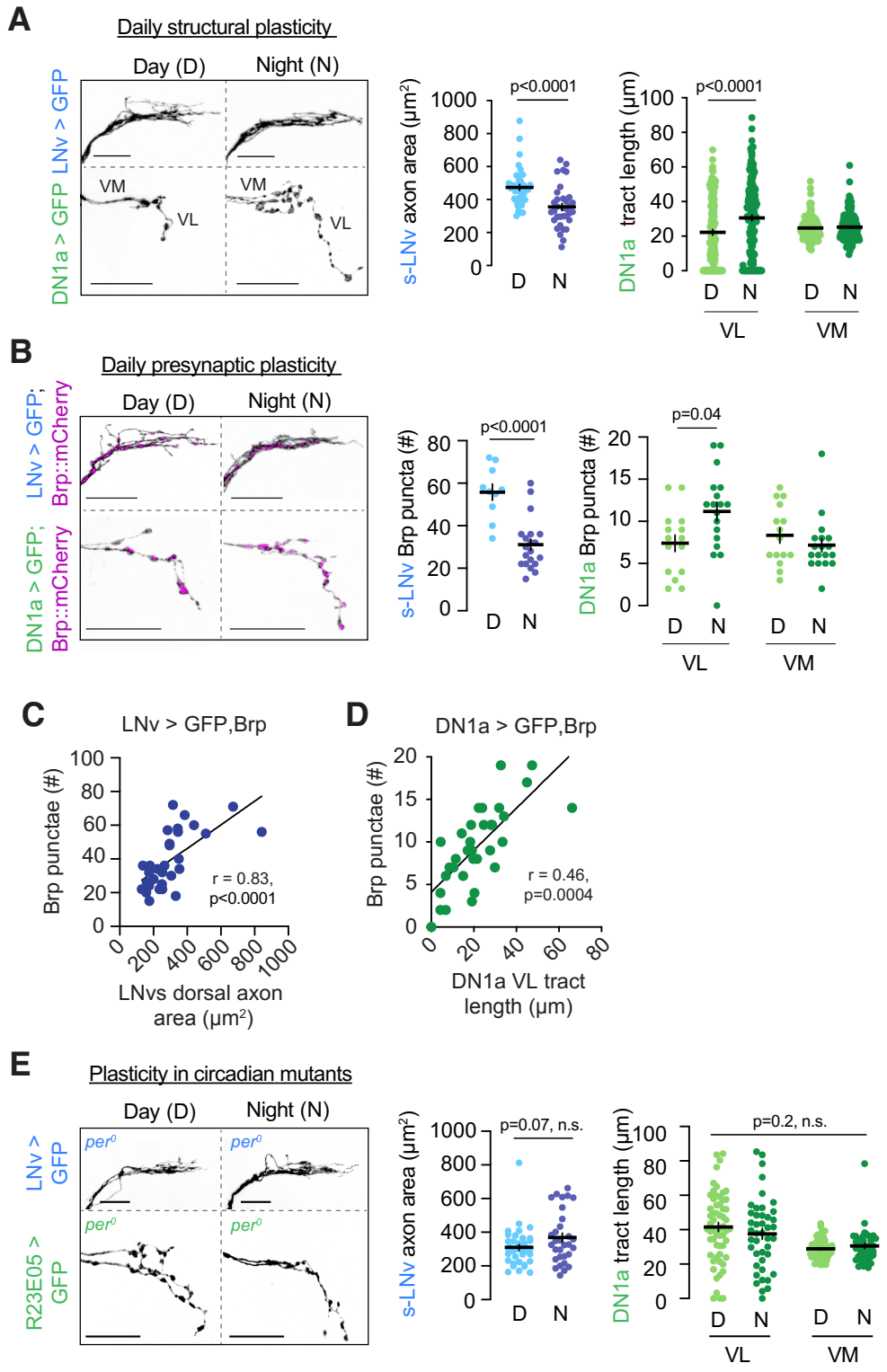

Figure 3.4. Daily axonal remodeling in LNvs and DN1as. (A) LNvs and DN1as show antiphase oscillations in neurite morphology. Measurements were taken from flies that were in light-dark

Figure 3.4 (continued). cycles (at 2pm (ZT6) for daytime, at 2am (ZT18) for nighttime). Quantifications show data for individual brain hemispheres. For this figure, t-Test in LNvs, Two-way ANOVA with Tukey's post-hoc test in DN1as. Ventromedial (VM) tracts are internal controls for ventrolateral (VL) tracts in DN1as. **(B)** Daily changes in presynaptic site number in LNvs and DN1as, as reported by a synaptic marker Brp:mCherry (magenta) within GFP-labeled neurites (black). **(C)** s-LNv synapse number as a function of s-LNv axon area. **(D)** DN1a synapse number as a function of DN1a axon length. C and D are reanalyses of the same animals shown in Figure 3.4B. (E) *Period* mutants lack LNv and DN1a plasticity rhythms.

Rho1 bidirectionally affects structural plasticity

The LNv-DN1a circuit appears in distinct physical configurations during the day (more LNv output sites) vs night (more DN1a output sites). Our behavioral experiments suggest that the activity configuration of this circuit also changes from day to night. These data fit a model in which structural plasticity biases the outcome of LNv-DN1a reciprocal inhibition. To test this model, we looked for manipulations that can affect remodeling in the two populations. LNv axons are remodeled through a cellular program that depends on the GTPase Rho1 for fasciculation (bundling, (Petsakou et al., 2015)). We confirmed that manipulating Rho1 levels can bidirectionally affect plasticity - Rho1 overexpression (OE) kept LNv axons fasciculated (nighttime configuration) while RNAi-mediated Rho1 depletion kept them defasciculated (daytime configuration, **Figure 3.5A**). Similar mechanisms might be used to remodel DN1as, as Rho1 overexpression kept their axons shorter (daytime configuration), while Rho1-RNAi kept them extended (nighttime configuration, **Figure 3.5B**).

LNv and DN1a axonal remodeling is required for behavioral state transitions

If the physical remodeling of LNv or DN1a axons contributes to transitions between light-responsive states, blocking plasticity should perturb behavioral flexibility. In agreement with this prediction, Rho1 overexpression in LNvs caused increased locomotion in response to daytime light, while overexpression in DN1as attenuated the startling effect of nighttime light (**Figure 3.5C**). That is, preventing presynaptic area from increasing resembles optogenetic silencing phenotypically (**Figure 2.5C** and **2.7E**). Rho1 overexpression did not appear to overtly damage the LNv neurons, as animals had relatively intact locomotor activity rhythms (**Figure 3.6A** and **Supplementary Table 2**) and did not have accelerated evening locomotor activity onset, which occurs when LNvs are ablated or constitutively silenced (**Figure 3.6A,** (Renn et al., 1999; Wu et al., 2008)). The daytime phenotype of Rho1 overexpression in LNvs, and nighttime phenotype of Rho1 overexpression in DN1as, together match the light response phenotypes seen when circadian clocks are disabled (**Figure 2.3B**). These experiments support a model where shifting synaptic weights can tip the equilibrium between the mutually repressive LNvs and DN1as, leading to daily behavioral state transitions (**Figure 3.5D**).

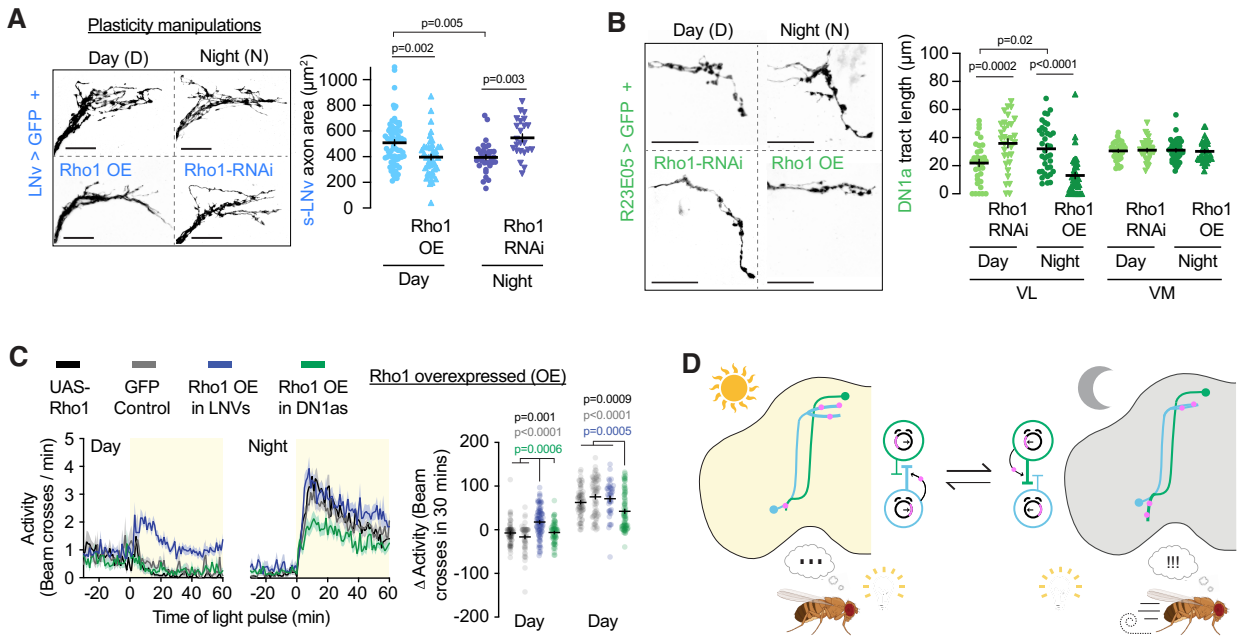

Figure 3.5 Axonal remodeling in LNvs and DN1as is required for behavioral state transitions

(A) Manipulating Rho1 in LNvs (Rho1-RNAi vs Rho1 overexpression (OE)) bi-directionally changes axonal fasciculation. One-way ANOVA with Tukey's post-hoc test. **(B)** Manipulating Rho1 in DN1as bi-directionally changes axonal fasciculation. One-way ANOVA with Tukey's post-hoc test. **(C)** Flies with fasciculated (closed) dorsal LNv axons (Rho1 OE in LNvs, blue) have perturbed daytime, but not nighttime, light responsiveness. The opposite is true in flies in which DN1a axons are kept short (Rho1 OE in DN1as, green). 'GFP control' is LNv > GFP during the daytime, and DN1a > GFP during the nighttime. **(D)** Schematic summary of LNv-DN1a circuit state transitions that regulate behavioral responsiveness to light.

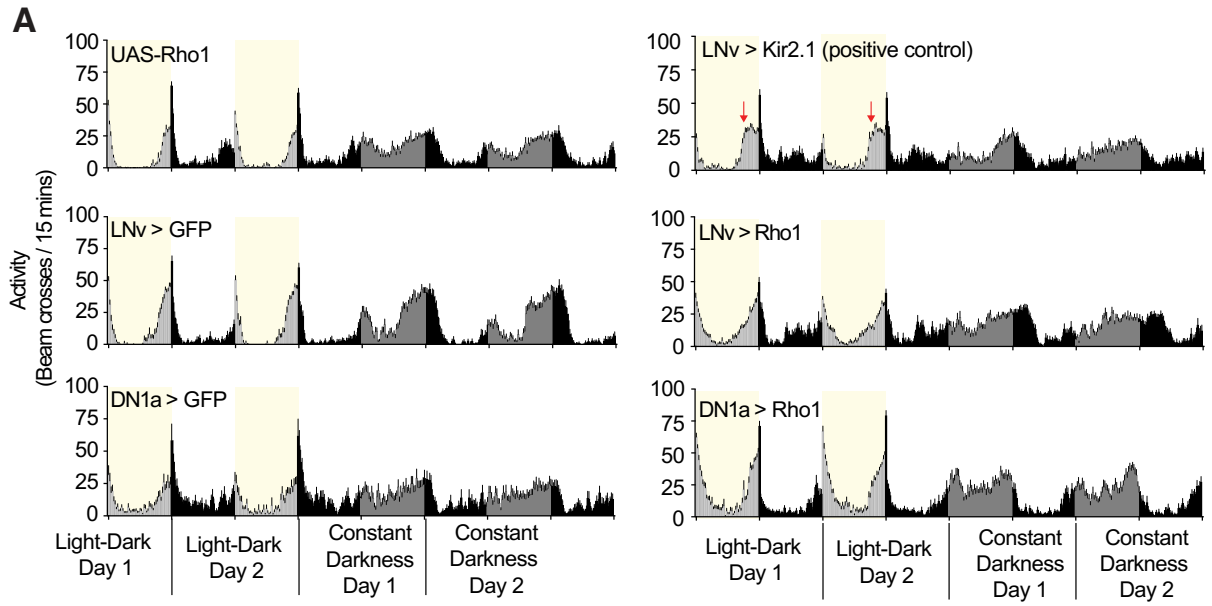

Figure 3.6. 24-hour activity rhythms with plasticity manipulations. (A) Rho1 overexpression does not overtly perturb rhythmic locomotor activity. Locomotor activity of flies expressing Rho1 in LNvs or DN1as, across two days in light-dark cycles and two days in continual darkness. Red asterisks indicate advanced evening activity that occurs when LNvs are constitutively silenced using overexpression of inwardly rectifying potassium channel Kir2.1 (Baines et al., 2001).

Discussion

Decades of work have uncovered representations of daily timescales in cell-autonomous molecular cycles and circuit activities (e.g. activity waves prorogating across circadian neuron subpopulations (Enoki et al., 2012; Liang et al., 2016)). Our work bridges molecular and circuit understanding by showing how circuit activity can be patterned by a clock-controlled cellular program. Rhythmic remodeling was described in s-LNvs a decade ago (Fernandez et al., 2008) and we have now shown that DN1as are also remodeled, but on their own schedule. Structural

plasticity is a potential mechanistic answer to how the circadian clock network transitions between the distinct network states observed by Liang et al. (Liang et al., 2016).

We and others have shown that recurrent inhibition is prevalent in the circadian networks of flies (Chatterjee et al., 2018; Frenkel et al., 2017; Guo et al., 2016; Liang et al., 2017) and mice (Albus et al., 2005; Gribkoff et al., 2003; Moore and Speh, 1993; Ono et al., 2019; Wagner et al., 1997). In the absence of external influence, reciprocal inhibition can stabilize a winner-take-all steady state (Kim et al., 2017). Structural plasticity offers a potential solution to this problem, by providing a molecular mechanism to overcome electrical inhibition. We have demonstrated how changes in activity and plasticity line up with a changing clock, and proposed a model where the clock directs plasticity rhythms through molecular effectors, such as Rho1. However, we cannot yet disentangle the complex interplay between activity, structural plasticity, and the molecular clock. This is because in *period* mutants, clock neurons lack both transcriptional (Kula-Eversole et al., 2010) and electrical activity rhythms (Flourakis et al., 2015), and it has been shown that electrical activity can induce structural remodeling (Depetris-Chauvin et al., 2011; Fernandez et al., 2007). Which events are causal within this complex web of cellular and circuit dynamics remains an open and intriguing question.

Plasticity is an apparently straightforward answer to the profoundly complex question of how circuits transition between network states. Synaptic plasticity, the experience-dependent regulation of receptor trafficking, active zone assembly, and spine dynamics, is a ubiquitous and well-understood mechanism for modifying circuits (Citri and Malenka, 2008). Neuritic remodeling, in contrast, is an enigmatic phenomenon whose frequency and breadth of occurrence remain unknown (Mehnert and Cantera, 2011; Muraro et al., 2013). Relative to synaptic plasticity, neurite remodeling is a decisive process with a high energetic barrier. This may be advantageous

for encoding relatively stable states that change over slower timescales. Studies have shown changes in neuronal morphology that correlate with other slowly changing states, such as hunger (Liu et al., 2017), sexual experience (Hart and Hobert, 2018) and foraging experience (Farris et al., 2001). Notably, these studies have all been conducted using invertebrates, perhaps due to the difficulty in complex systems to reproducibly and specifically assess individual arbors. Some studies using mammalian models have uncovered hints of structural plasticity in more complex systems. In the SCN and in mammalian circuits underlying stress, hunger, sexual experience, changes in the bulk density of presynaptic arbors have been observed (Appelbaum et al., 2010; Girardet et al., 2010; Inoue et al., 2019; Kasugai et al., 2019; von der Ohe et al., 2007), which could be due to axonal remodeling. Considering that the circadian clock is remarkably conserved, similar mechanisms may operate in the SCN (Freeman et al., 2013), but may have remained hidden due to lack of sparse, well-defined subpopulation neurites that can be reproducibly traced.

Methods

Generation of R23E05-LexA and R23E05-Gal80

Standard Gateway cloning protocols (Thermo Fisher Scientific, 11791020 and 11789020) were followed to derive constructs in which either LexA or Gal80 are driven by the R23E05 enhancer. gtcccgatttcgtcgaaggattcaa forward and gctaaccggatgacggtaccaggag reverse primers were used to PCR-amplify a 644kb enhancer fragment from R23E05-Gal4 flies. This product was subcloned into pBPLexa:P65UW (Addgene plasmid # 26231, (Pfeiffer et al., 2010) or pBPGal80uw-6 (Addgene plasmid # 26236, (Pfeiffer et al., 2010)), which were gifts from Gerry Rubin. Resulting constructs were inserted into the attP2 landing site by embryo injection (Rainbow Transgenics).

Calcium imaging

Experiments were conducted in a 6-hour window centered around periods of putative peak activity (mid-day for DN1a->LNv and mid-night for LNv->DN1a), alternating between control and experimental samples. *Ex-vivo* whole mount brains were explanted in Nunclon cell culture dishes (Thermo Scientific, 150318) which contained 3 mLs of chilled *Drosophila* saline (Gift from Rachel Wilson, 103 mM NaCl, 3 mM KCl, 5 mM N-tris (hydroxymethyl) methyl-2-aminoethane-sulfonic acid, 8 mM trehalose, 10 mM glucose, 26 mM NaHCO3, 1 mM NaH2PO4, 1.5 mM CaCl2, and 4 mM MgCl2 (osmolarity adjusted to 270–275 mOsm). Saline was bubbled with 95/5% carboxygen prior to the experiment. Brains were dissected in the same media used to conduct the experiment. Brains in which GCaMP was expressed in LNvs were allowed to rest for 2.5 minutes prior to the experiments under the blue imaging light. Brains in which GCaMP was expressed in DN1as were allowed to rest for 5 minutes prior to the experiments under the blue imaging light. During this baseline period, we noticed increased large calcium transients (**Figures 3.2C** and **3.2E**), likely due to control of clock neuron activity by the light-sensitive protein Cryptochrome (Fogle et al., 2015; Fogle et al., 2011). During pilot experiments we chose baseline intervals that were usually sufficient to allow activity to stabilize. Two trials were excluded (one experimental and one control) because baseline activities were not stable. These trials are shown as red traces in **Figure 3.2D**. For $P2X_2$ experiments, 20 μL of 150 mM ATP (Sigma, A2383), diluted in *Drosophila* saline, was pipetted gently down the side of the dish, to a final concentration of 1 mM. Positive control experiments in which both $P2X_2$ and GCaMP were expressed in LNvs showed that ATP delivered this way could start inducing small changes within a few frames of delivery. Acquisition occurred at 1 frame/second.

Immunostaining

Tissues were whole-mounted in Prolong Gold antifade reagent (Invitrogen, 1942345) on glass slides and coverslips (Electron Microscopy Sciences, 64321-10, 72230-01). Confocal images were obtained using a Leica SP8 confocal microscope at 10x, 2.4 μm intervals, for morphology quantifications; 20x, 1 μm intervals for expression patterns, and 63x, 0.3 μm intervals for imaging of pre- and postsynaptic sites. Maximum projection images and quantifications were obtained using FIJI. Levels of brightness and contrast were adjusted across the whole image using FIJI or Adobe Photoshop.

For quantifications comparing neurite morphologies between mid-day and mid-night, whole heads were fixed because prolonged exposure to light (required for dissections) can modify the operation of the clock. Heads were fixed for 50 minutes at room temperature with fixative containing 4% PFA and 03.% Triton X-100. For mid-night samples, heads were fixed with minimal light exposure, using red light that is less disruptive to the light-sensitive clock protein Cryptochrome (Berndt et al., 2007; Busza et al., 2004; Hanai et al., 2008; VanVickle-Chavez and Van Gelder, 2007). Acquisitions were conducted at 10x due to the large number of samples; as the drivers we used are expressed sparsely, this resolution was sufficient. Because the z-axis of the slide/coverslip chamber is slightly shorter than the height of the brain, all of the brains were pressed slightly, and in similar orientation.

For *trans*-Tango experiments, flies were raised for 5 weeks at 18°C, which permits stronger expression than 25° (Talay et al., 2017). We often noticed aberrant morphology in cells expressing the *trans*-Tango construct, likely due to overexpression of neurexin and the cell adhesion molecule ICAM1 at presynaptic sites (Talay et al., 2017).

Quantifying morphological imaging data

Measurements were conducted blind using the segmented line tool in FIJI on the maximum intensity projection of whole brain z-stacks. No obvious daytime-nighttime differences were observed in the z-axis for the DN1a ventrolateral tract. For Brp quantifications, acquisitions were done at 63x. The sparsity of synaptic sites along the ventrolateral DN1a tract allows for visualization and counting of individual punctum. Brp counts were conducted blind. Each hemisphere was computed as an independent sample because of variability between hemispheres.

Quantifying ex vivo calcium imaging

Data were analyzed with ImageJ, using the freehand selection tool to choose a ~100μm ROIs from s-LNv dorsal terminals. Only the brighter hemisphere was used for analysis. For figures, 2-3 frames (two seconds) of data was removed from each sample because of motion artifacts from pipetting. Unaltered trials are in reported in **Figures 3.2D** and **3.2F**. Baseline fluorescence was calculated from the average of ten frames prior to ATP delivery, excluding the first frame before ATP. Minimum and maximum fluorescence was calculated using standard Excel functions from all frames after ATP delivery except for the first five frames, to exclude potential residual motion artifacts. 1-3 samples per condition showed drift after pipetting, thus we used an ImageJ registration plugin (TurboReg) to create a new series corrected against a time-series averaged reference. Two nonrepresentative trials (one experimental trial and one control) were excluded from averaged results shown in **Figure 3.1D**. These excluded trials are shown in **Figure 3.2D** and were excluded due to unusually large and early depolarizations that were putatively due to the effects of blue light stimulation.

Statistical analysis

For imaging experiments, we noticed substantial variability between hemispheres, so each hemisphere was treated as a single sample. In **Figure 3.3** and **Figure 3.4**, comparisons between VL and VM DN1a tracts are not reported. In **Figure 3.4**, comparisons between Rho1 overexpression and Rho1-RNAi are not reported. Power analyses to predetermine sample size were not conducted. Experimenters were not blind to conditions except during quantifications of morphology. Sample sizes are shown in **Supplementary Table 1**. Significant differences between control genotypes are not indicated in figures. We report them here: DN1a>GFP was significantly different from both other conditions in **Figure 3.3B** (day, $p<0.05$), and LNv>GFP was different from the experimental condition in **Figure 3.3C** (day, $p<0.05$). Power analyses to predetermine sample size were not conducted. Experimenters were not blind to conditions except during quantifications of morphology.

Additional acknowledgements (that are not mentioned in Chapter 2)

We thank Rachel Wilson and her lab for saline and for calcium imaging advice; and Corey Harwell for microscope access.

Chapter 4: Extended discussion and future directions

Summary

An internal representation about the external world allows animals to evaluate whether experienced conditions (such as light) are appropriate or inappropriate. During entrainment (repetitive light:dark cycles), animals form associations between time-of-day and environmental conditions. In **Chapter 2**, we showed that circadian clocks may inform animals about present conditions, through the lens of past experience. In **Chapter 3**, we provide a potential mechanism by which the circadian clock operates a switch between predictive states: structural plasticity. In the LNv-DN1a microcircuit, competitive interactions between specialized neuronal subpopulations are poised to sharpen an internal representation of time. Further, structural plasticity may be an appropriate transition mechanism for slowly changing internal states. Together, these motifs converge in a microcircuit that has properties of stability (mutual inhibition) and flexibility (structural plasticity). The principles we find may be relevant for states like sleep, mood and hunger that are stable across long timescales, but flexible to changing circumstance.

A prediction error framework for explaining circadian modulation of locomotion

Our data may also explain three behavioral features normally seen under standard lab conditions used to study circadian clocks. Flies that are entrained to light-dark cycles and transferred to constant darkness have higher baseline activity during subjective daytime, compared to flies that remain in oscillating conditions (**Figure 2.1A**). Light is known to promote daytime sleep (Schlichting et al., 2019b), but to our knowledge, no explanation for why flies are more active in the dark has ever been offered. Based on our data, we propose that these animals are essentially in a continuously agitated (startled) state during subjective daytime, because their

internal prediction (lights should be on) does not match actuality (darkness). Though it is impossible to prove whether animals feel subjectively agitated by internal-external mismatch, we can test some predictions from this model. Consistent with the mismatch model, activity during subjective daytime gradually decreases over days spent in darkness (**Figure 4.1A**). This 'dampening' effect has been proposed to stem from declining robustness of the clock (Peng et al., 2003; Stanewsky et al., 1997) that occurs because the TTFL is detached from its instructive cues (light or temperature cycles). An alternative interpretation is that flies habituate to their new environment. A second puzzling phenomenon is seen in light-dark cycles – flies normally startle when lights turn on or off at predictable transition times, despite robustly anticipating these transitions. That is, when night turns into day (lights turn on after 12 hours of darkness) or day turns into night (lights turn off after 12 hours of darkness), animals startle (**Figure 4.1B**). This might be because transitions are periods of ambiguity, and not all animals have made the estimation that daytime or nighttime has arrived. The prediction that follows is that delaying the onset of light in the morning would allow more animals to transition into a new state, which means that fewer animals should startle. In support of this hypothesis, delaying morning light onset prevented startle; conversely, advancing morning light potentiated startle (**Figure 4.1C** and **4.1D**). Third, our predictive framework could also account for why *Drosophila* locomotor activity is organized around lights-on and lights-off. The 'ramping' of locomotor activity (i.e. anticipation) seen at the population level (**Figure 4.1B**) could reflect increased proportions of flies exiting the state where current conditions feel appropriate.

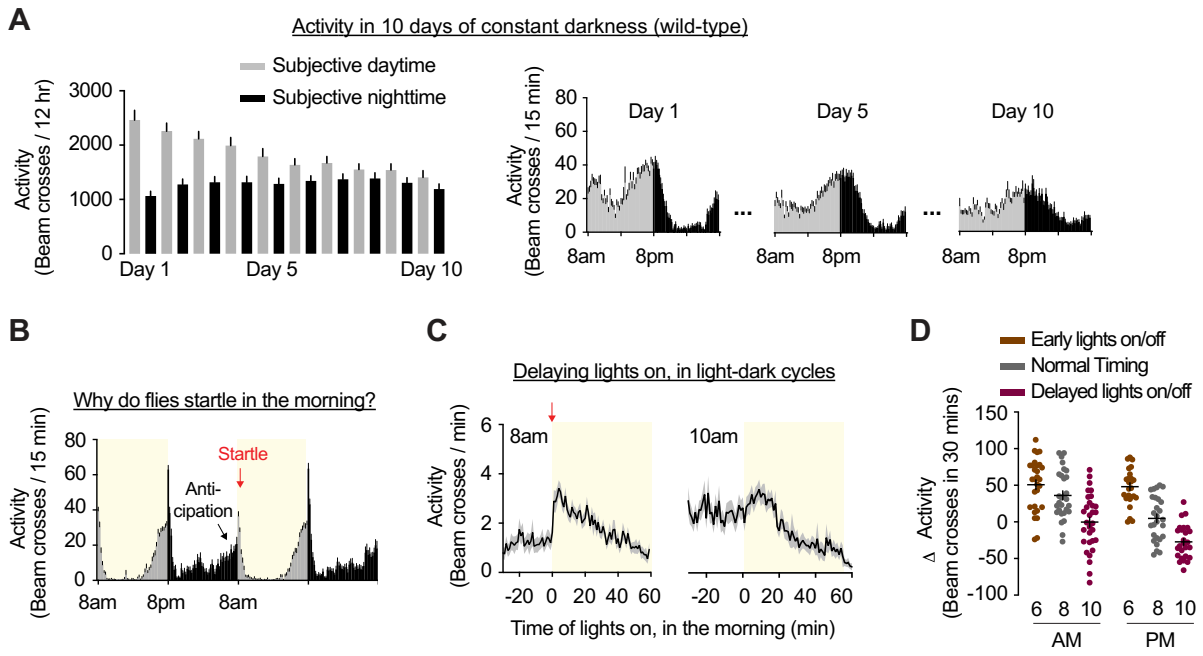

Figure 4.1. Testing predictions from the mismatch model of locomotor activity. (A) Daytime locomotor activity is dampened during 10 days in continuous darkness. **(B)** Anticipation and startle in typical cycling light-dark cycles. **(C)** Delaying when the lights turn on in the morning (in cycling light-dark conditions) prevents startle to light. **(D)** For both morning and evening, delaying when the lights turn on prevents startle; turning on the lights preemptively increases startle.

Considering that the circadian clock can be entrained by temperature (Sehadova et al., 2009), mechanical stimulation (Simoni et al., 2014), and other cues (Aschoff et al., 1971), our framework predicts that the ability to contextualize environmental conditions could generalize to other modalities. In order to test whether clock neurons contextualize light specifically, or whether they provide general temporal context about the time of day, it would be worthwhile to test whether predicted cues can still elicit quiescence responses, if the predictions are entrained through temperature or mechanical input pathways.

As noted in **Chapter 2**, we are the second group to use acute light at different times to assay timekeeping in *Drosophila*. Though many of our conclusion align with the prior report (Lu et al., 2008), three of our conclusions differ. First, in their dataset, wild-type strains do not become quiescent in response to daytime light, but rather are unreactive. This is likely due to differences in light stimulus intensity – the authors used a dim, ~5 lux light presentation throughout most of their experiments while ours was ~260 lux. Indeed, in the single panel where the authors tested the intensity-dependence of this behavior, they also found that 200+ lux light causes locomotor activity suppression during the daytime. A second difference is that the authors conclude that "LNvs and PDF are not necessary for the rhythms of light-induced locomotion responses" (Lu et al., 2008). Superficially, this appears to be a major difference between our conclusions and theirs. However, further inspection of their data shows clear differences between controls and PDF manipulations, specifically during the daytime. Their interpretation of the data is not incorrect: in our data and in theirs, PDF-signaling disrupted flies have rhythms: daytime responses to light look different from nighttime responses to light. Unlike Lu et al., we do not interpret this to mean that timekeeping is intact, as the daytime responses to light in PDF-disrupted flies are very similar to clock-disrupted flies (**Figure 2.3B** and **Figure 2.5C**). A third

difference between our results and theirs, is that they find that different mutations do not always cause startle. In their dataset, some mutants always show quiescence or are always unreactive. With the two manipulations we tried, light always evoked startle. However, it is possible that different mutations can lock the circadian clock in persistent daytime, nighttime or intermediate states, e.g. perhaps the outputs of the clock always signal daytime for clk^{jrk} mutants, for whom light always induces locomotor quiescence (Allada et al., 1998).

The unknown origin of subpopulation diversity

Our optogenetic perturbation experiments (**Figure 2.5C** and **Figure 2.7E**) imply that LNvs and DN1as are functionally active at different times of day. Further, we show that LNvs and DN1as have antiphase plasticity patterns. All of the subpopulations have indistinguishable TTFL operations (at least at the level of PER or VRI cycling). This raises again a question posed by Liang, Holy and Taghert: how do synchronous molecular pacemakers drive nonsynchronous physiological cycles (Liang et al., 2016)? Since the clock directs electrophysiological activity (Flourakis et al., 2015) and plasticity (**Figure 3.4E,** (Depetris-Chauvin et al., 2011) cycles, there must be diversity in the intracellular programs of LNvs and DN1as that interpret and execute instructions from the molecular clock. Catalogs of transcriptional diversity between clock neurons subpopulations have regrettably excluded the DN1as (Abruzzi et al., 2017; Kula-Eversole et al., 2010), likely due to lack of DN1a-specific drivers. No work, to our knowledge, has led to an understanding of how different clock neuron subpopulations come to have different temporal tuning properties (Liang et al., 2016). Future studies should investigate the transcriptional and epigenetic differences between LNvs and DN1as, during daytime and nighttime, which is now enabled by our characterization of DN1a-Gal4. Many pathways, such as

channel trafficking, neuropeptide expression, or presynaptic modifications could potentially endow subpopulations with their unique functional profiles. A worthwhile path of investigation would be to distinguish whether differences emerge from the expression of different genes; or alternatively perhaps, shared genes are expressed at different times through epigenetic regulation or by posttranscriptional modifications like alternative splicing (Wang et al., 2018).

The locus of comparison between internal predictions and external experience

It is of great interest to explore where internal representation is compared with external predictions. One possibility is that the comparisons occur within circadian cells, since *Drosophila* express cell-autonomous light detectors Cryptochrome (Busza et al., 2004), Rhodopsin 7 (Ni et al., 2017), and receive input from the visual system (Helfrich-Forster et al., 2001). Li et al. recently accomplished an impressively comprehensive documentation of clock neuron light sensitivity, using electrophysiology (Li et al., 2018). These experiments, if applied at different times of day, are poised to answer the question of whether clock neurons can intrinsically integrate external sensory information with internal temporal status.

Another possibility is that the comparison occurs somewhere downstream of circadian circuits. In this scenario, clock neurons would simply provide the temporal context that is being utilized by light-sensitive circuits somewhere downstream of clock neurons. There are several non-circadian populations that have been shown to receive output signals from clock neurons (Barber et al., 2016; Cavanaugh et al., 2014; Cavey et al., 2016; Guo et al., 2018; King et al., 2017; Lamaze et al., 2018; Liang et al., 2019; Pirez et al., 2013). In mammals, comparisons between expected and received reward have been proposed to be encoded in the activities of midbrain dopaminergic neurons (Schultz, 2016). Dopaminergic PPM3 neurons have been

recently found to relay timing signals between circadian neurons and locomotor circuitry (Liang et al., 2019; Potdar and Sheeba, 2018). These neurons are a compelling candidate for the integration of internal expectations with external sensory signals.

A proposed circuit model for circadian timekeeping

A representation is tiled across the circadian network: distinct subpopulations reach peak activity at different times of day. It remains unclear how the network ensures the reliability of this patterns. For a clock to provide meaningful utility, it must only display one time at any given moment. Specifically, how does the circadian circuit ensure that one cluster is most active at any given time? If two clusters encoding different times-of-day reached peak activity simultaneously, temporal signals would be difficult to decode. A useful reference for comparison are studies of the E-PG navigational circuit in *Drosophila*. Projections from E-PG neurons form a donut-like anatomical structure (Hanesch and Heisenberg, 1989); wedges within the ring encode the body orientation relative to visual references in the external world (Fisher et al., 2019; Green et al., 2017; Kim et al., 2019; Seelig and Jayaraman, 2015; Turner-Evans et al., 2017). The function of the E-PG circuits as an internal compass is analogous to head-direction neuron populations that are found in mammals (Taube, 2007). Observation of calcium dynamics within the E-PG, as the animal navigates a virtual environment, reveals that the E-PG circuit maintains a singular representation of heading orientation at any given time - as the animal turns, a 'bump' of calcium activity rotates around the ring (Seelig and Jayaraman, 2015).

From these studies, we can infer multiple circuit implementations that could also result in the singularity of temporal representation in the circadian circuit. Possibilities include winner-take-all networks and ring attractors (Kim et al., 2017; Taube, 2007). In **Chapter 3**, I discussed

the likelihood that each subpopulation communicates widely with many of the other subpopulations in the network. Further, we discussed the evidence that many of these interactions are competitive signals between subpopulations with different activity timings. A productive avenue for future research would be to systematically investigate the strength and sign of connectivities between each subpopulation, and to monitor how these connectivities change over time. One could begin by testing four potential models outlined by Kim et al. in their investigations of circuit organizations underlying E-PG bump singularity (**Figure 4.2A to Figure 4.2D**) (Kim et al., 2017).

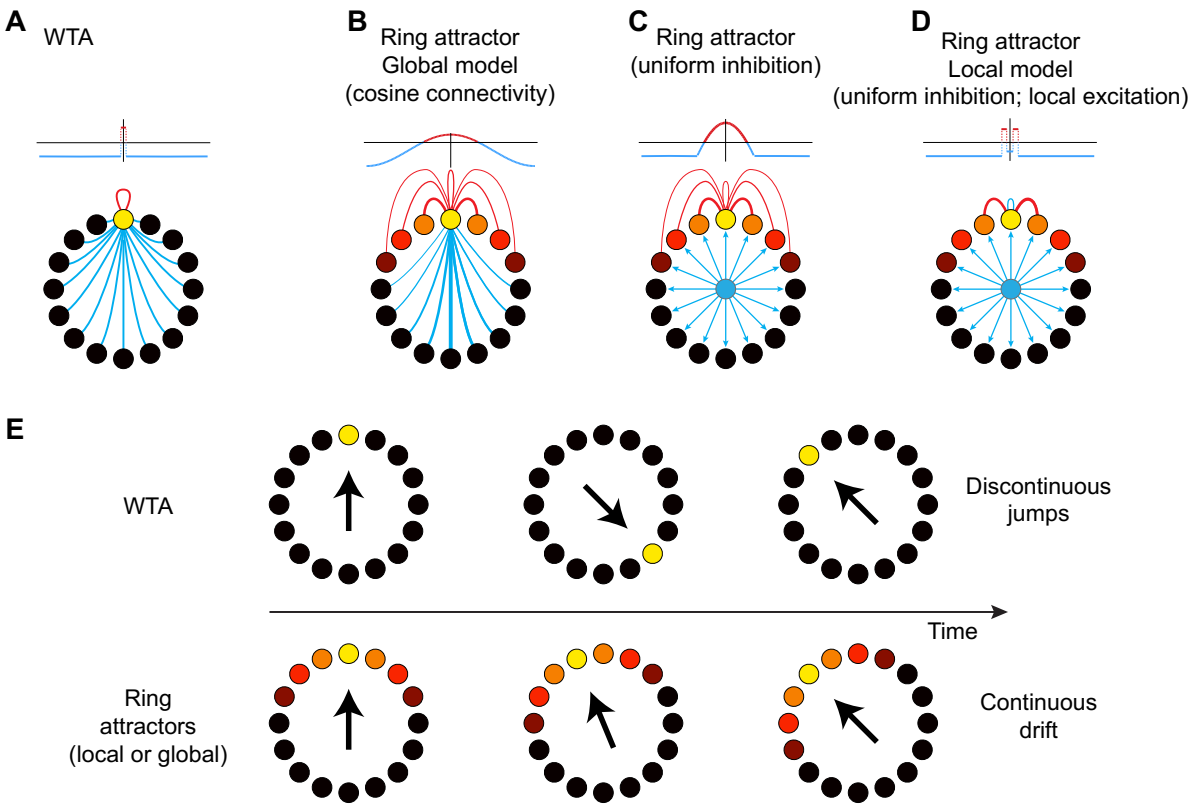

Figure 4.2. Circuit models that result in singular subpopulation activity expression. This figure is reprinted from Kim, S.S., Rouault, H., Druckmann, S., and Jayaraman, V. (2017). Ring attractor dynamics in the Drosophila central brain. Science *356*, 849-853, with permission from The American Association for the Advancement of Science. Captions are my own. **A-D)** Hypothetical models of E-PG structure. Subpopulations of ring neurons are arrayed around the ring. Neurons at opposite points of the ring represent antithetical heading orientations. Blue lines refer to inhibitory connections. Red lines indicate excitatory connections. (WTA, winner-take-all). **E)** Predicted state transition dynamics from WTA versus ring attractor models.

In winner-take-all networks, the most active subpopulation inhibits all others (**Figure 4.2A**). Ring attractor model have multiple possible implementations (**Figure 4.2B to Figure 4.2D**) (Kim et al., 2017). Ring attractor variants vary along two parameters: the breadth of inhibitory influence, and the breadth of excitatory influence. Inhibition can reach specific targets (**Figure 4.2B**, blue) or be uniform across the circuit (**Figure 4.2C** and **Figure 4.2D**, blue). Similarly, excitation can be local (**Figure 4.2D**, red) or most strongly biased towards subpopulations with similar tuning properties (**Figure 4.2B** and **Figure 4.2C,** red). Abrupt excitatory transitions, enabled with optogenetics (concurrently with calcium imaging), can be used to test whether any of these models are true in the circadian clock network. Ring attractor models predict a smooth transition to new states, while winner-take-all circuits should allow instant transition to new states (**Figure 4.2E**) (Kim et al., 2017). The E-PG circuit uses excitation biased towards similar subpopulations, and inhibition biased towards opposite ones, to ensure that only a singular orientation representation is active in the circuit at any given time (Kim et al., 2017). Systematic mapping of connectivity rules of the *Drosophila* circadian clock networks could be achieved using optogenetics in conjunction with calcium imaging. These experiments could reveal whether *Drosophila* circadian network has ring attractor properties, or by what other measures specificity of temporal representations are achieved.

Is neurite remodeling a general mechanism?

Plasticity allows for adaptive interactions with dynamic environments. The pace and decisiveness by which modifications are made in neural circuits may vary according to need and circumstance. Structural plasticity may be appropriate for changes that occur more slowly. There are few documented cases of neurites undergoing morphological restructuring (also reviewed in

Chapter 1 and **Chapter 3**). Neurite remodeling may be a mechanism specifically amenable for circuits that function on hours-long timescales. Another possibility is that neurite remodeling is a general phenomenon that many neurons have the potential to achieve. The latter case is supported by the fact that most examples of structural plasticity have come from well-defined sensory areas in invertebrate systems (Cohn et al., 2020; Mukhopadhyay et al., 2008; Sachse et al., 2007; Smith et al., 2010).

Our results with DN1a suggest that structural plasticity may occur more prevalently than previously appreciated. Measuring the ubiquity of structural plasticity has been limited by the ability to reproducibly locate and image sparse neurite branches. A collection of sparsely expressing split Gal4 lines has recently been made available (https://www.janelia.org/lab/rubin-lab/our-research/gal4-driver-lines/split-gal4-lines), which should allow for the assay of structural plasticity of a wide range of neuronal classes. Our pilot data with DN1as suggests that they may undergo activity-dependent plasticity (**Figure 4.3**), which has been seen previously with LNvs (Petsakou et al., 2015; Sivachenko et al., 2013). Chronic (6 hour) optogenetic activating and silencing protocols may therefore be a useful first-pass way to screen for the upper and lower end of possible morphological phenotypes. It would be informative to estimate how frequently structural plasticity can occur. With positive hits that show structural plasticity, it would be interesting to further investigate whether common molecular programs are used in different neuronal classes.

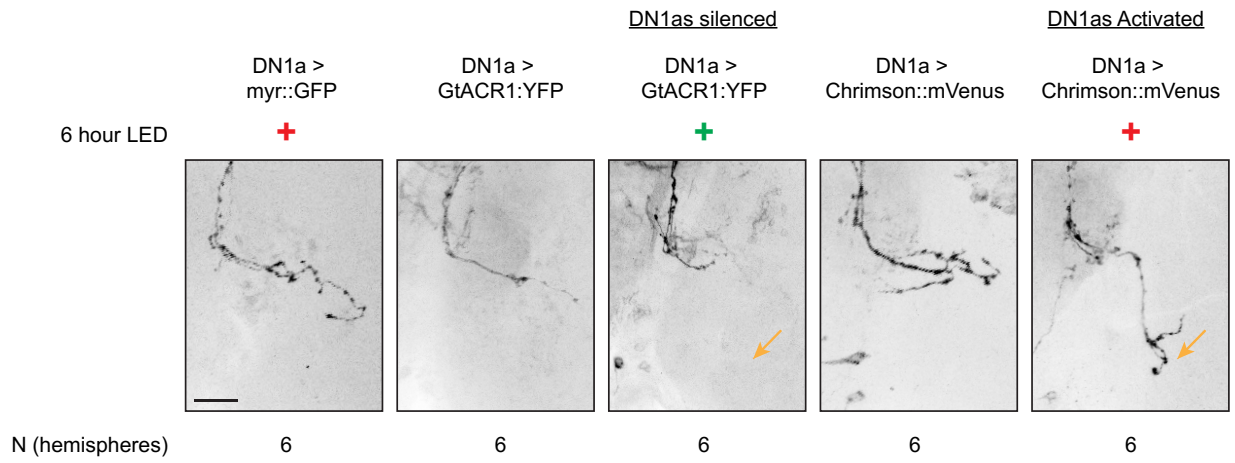

Figure 4.3. DN1a structural plasticity may be regulated by activity (pilot experiment)

Orange arrows indicate ventrolateral tract regions, for comparison between DN1a-silenced and DN1a-activated conditions.

Concluding thoughts

In this thesis, I have discussed our efforts to track a representation of time from molecules, to cells, to circuits, to behavior. Molecular cycles within clock neurons lead to the daily fluctuations of neuronal activity, which in turn influence ordered activities of subpopulations, leading to behavioral state transitions. My work builds upon decades of knowledge and is continually inspired by the ideas and imminent discoveries from the circadian field. The work presented here provides one potential mechanism by which changes to neurons might lead to meaningful modifications to circuits. My specific contributions towards understanding LNv-DN1a interactions raise the broader possibility that similar motifs are repeated throughout the *Drosophila* circadian network, or perhaps even in circuits underlying other slowly changing behavioral states.

References

Abruzzi, K.C., Zadina, A., Luo, W., Wiyanto, E., Rahman, R., Guo, F., Shafer, O., and Rosbash, M. (2017). RNA-seq analysis of Drosophila clock and non-clock neurons reveals neuron-specific cycling and novel candidate neuropeptides. PLoS Genet *13*, e1006613.

Agrawal, P., and Hardin, P.E. (2016). The Drosophila Receptor Protein Tyrosine Phosphatase LAR Is Required for Development of Circadian Pacemaker Neuron Processes That Support Rhythmic Activity in Constant Darkness But Not during Light/Dark Cycles. J Neurosci *36*, 3860-3870.

Akten, B., Jauch, E., Genova, G.K., Kim, E.Y., Edery, I., Raabe, T., and Jackson, F.R. (2003). A role for CK2 in the Drosophila circadian oscillator. Nat Neurosci *6*, 251-257.

Albus, H., Vansteensel, M.J., Michel, S., Block, G.D., and Meijer, J.H. (2005). A GABAergic mechanism is necessary for coupling dissociable ventral and dorsal regional oscillators within the circadian clock. Curr Biol *15*, 886-893.

Allada, R., White, N.E., So, W.V., Hall, J.C., and Rosbash, M. (1998). A mutant Drosophila homolog of mammalian Clock disrupts circadian rhythms and transcription of period and timeless. Cell *93*, 791-804.

Appelbaum, L., Wang, G., Yokogawa, T., Skariah, G.M., Smith, S.J., Mourrain, P., and Mignot, E. (2010). Circadian and homeostatic regulation of structural synaptic plasticity in hypocretin neurons. Neuron *68*, 87-98.

Aschoff, J., Fatranska, M., Giedke, H., Doerr, P., Stamm, D., and Wisser, H. (1971). Human circadian rhythms in continuous darkness: entrainment by social cues. Science *171*, 213-215.

Bae, K., Lee, C., Sidote, D., Chuang, K.Y., and Edery, I. (1998). Circadian regulation of a Drosophila homolog of the mammalian Clock gene: PER and TIM function as positive regulators. Mol Cell Biol *18*, 6142-6151.

Baik, L.S., Recinos, Y., Chevez, J.A., and Holmes, T.C. (2018). Circadian modulation of light-evoked avoidance/attraction behavior in Drosophila. PLoS One *13*, e0201927.

Baines, R.A., Uhler, J.P., Thompson, A., Sweeney, S.T., and Bate, M. (2001). Altered electrical properties in Drosophila neurons developing without synaptic transmission. J Neurosci *21*, 1523-1531.

Barber, A.F., Erion, R., Holmes, T.C., and Sehgal, A. (2016). Circadian and feeding cues integrate to drive rhythms of physiology in Drosophila insulin-producing cells. Genes Dev *30*, 2596-2606.

Bargiello, T.A., Jackson, F.R., and Young, M.W. (1984). Restoration of circadian behavioural rhythms by gene transfer in Drosophila. Nature *312*, 752-754.

Bargiello, T.A., and Young, M.W. (1984). Molecular genetics of a biological clock in Drosophila. Proc Natl Acad Sci U S A *81*, 2142-2146.

Bedrosian, T.A., Fonken, L.K., and Nelson, R.J. (2016). Endocrine Effects of Circadian Disruption. Annu Rev Physiol *78*, 109-131.

Benito, J., Houl, J.H., Roman, G.W., and Hardin, P.E. (2008). The blue-light photoreceptor CRYPTOCHROME is expressed in a subset of circadian oscillator neurons in the Drosophila CNS. J Biol Rhythms *23*, 296-307.

Berndt, A., Kottke, T., Breitkreuz, H., Dvorsky, R., Hennig, S., Alexander, M., and Wolf, E. (2007). A novel photoreaction mechanism for the circadian blue light photoreceptor Drosophila cryptochrome. J Biol Chem *282*, 13011-13021.

Bhadra, U., Thakkar, N., Das, P., and Pal Bhadra, M. (2017). Evolution of circadian rhythms: from bacteria to human. Sleep Med *35*, 49-61.

Blau, J., and Young, M.W. (1999). Cycling vrille expression is required for a functional Drosophila clock. Cell *99*, 661-671.

Boutros, C.L., Miner, L.E., Mazor, O., and Zhang, S.X. (2017). Measuring and Altering Mating Drive in Male Drosophila melanogaster. J Vis Exp.

Brancaccio, M., Maywood, E.S., Chesham, J.E., Loudon, A.S., and Hastings, M.H. (2013). A Gq-Ca2+ axis controls circuit-level encoding of circadian time in the suprachiasmatic nucleus. Neuron *78*, 714-728.

Buhl, E., Bradlaugh, A., Ogueta, M., Chen, K.F., Stanewsky, R., and Hodge, J.J. (2016). Quasimodo mediates daily and acute light effects on Drosophila clock neuron excitability. Proc Natl Acad Sci U S A *113*, 13486-13491.

Busza, A., Emery-Le, M., Rosbash, M., and Emery, P. (2004). Roles of the two Drosophila CRYPTOCHROME structural domains in circadian photoreception. Science *304*, 1503-1506.

Cao, G., and Nitabach, M.N. (2008). Circadian control of membrane excitability in Drosophila melanogaster lateral ventral clock neurons. J Neurosci *28*, 6493-6501.

Cao, G., Platisa, J., Pieribone, V.A., Raccuglia, D., Kunst, M., and Nitabach, M.N. (2013). Genetically targeted optical electrophysiology in intact neural circuits. Cell *154*, 904-913.

Cavanaugh, D.J., Geratowski, J.D., Wooltorton, J.R., Spaethling, J.M., Hector, C.E., Zheng, X., Johnson, E.C., Eberwine, J.H., and Sehgal, A. (2014). Identification of a circadian output circuit for rest:activity rhythms in Drosophila. Cell *157*, 689-701.

Cavey, M., Collins, B., Bertet, C., and Blau, J. (2016). Circadian rhythms in neuronal activity propagate through output circuits. Nat Neurosci *19*, 587-595.

Chatterjee, A., Lamaze, A., De, J., Mena, W., Chelot, E., Martin, B., Hardin, P., Kadener, S., Emery, P., and Rouyer, F. (2018). Reconfiguration of a Multi-oscillator Network by Light in the Drosophila Circadian Clock. Curr Biol *28*, 2007-2017 e2004.

Chen, T.W., Wardill, T.J., Sun, Y., Pulver, S.R., Renninger, S.L., Baohan, A., Schreiter, E.R., Kerr, R.A., Orger, M.B., Jayaraman, V.*, et al.* (2013). Ultrasensitive fluorescent proteins for imaging neuronal activity. Nature *499*, 295-300.

Chiu, J.C., Low, K.H., Pike, D.H., Yildirim, E., and Edery, I. (2010). Assaying locomotor activity to study circadian rhythms and sleep parameters in Drosophila. J Vis Exp.

Chiu, J.C., Vanselow, J.T., Kramer, A., and Edery, I. (2008). The phospho-occupancy of an atypical SLIMB-binding site on PERIOD that is phosphorylated by DOUBLETIME controls the pace of the clock. Genes Dev *22*, 1758-1772.

Choi, C., Fortin, J.P., McCarthy, E., Oksman, L., Kopin, A.S., and Nitabach, M.N. (2009). Cellular dissection of circadian peptide signals with genetically encoded membrane-tethered ligands. Curr Biol *19*, 1167-1175.

Choi, C., and Nitabach, M.N. (2013). Membrane-tethered ligands: tools for cell-autonomous pharmacological manipulation of biological circuits. Physiology (Bethesda) *28*, 164-171.

Citri, A., and Malenka, R.C. (2008). Synaptic plasticity: multiple forms, functions, and mechanisms. Neuropsychopharmacology *33*, 18-41.

Cohn, J.A., Cebul, E.R., Valperga, G., Brose, L., de Bono, M., Heiman, M.G., and Pierce, J.T. (2020). Long-term activity drives dendritic branch elaboration of a C. elegans sensory neuron. Dev Biol.

Collingridge, G.L., Isaac, J.T., and Wang, Y.T. (2004). Receptor trafficking and synaptic plasticity. Nat Rev Neurosci *5*, 952-962.

Collins, B., Kane, E.A., Reeves, D.C., Akabas, M.H., and Blau, J. (2012). Balance of activity between LN(v)s and glutamatergic dorsal clock neurons promotes robust circadian rhythms in Drosophila. Neuron *74*, 706-718.

Collins, B., Kaplan, H.S., Cavey, M., Lelito, K.R., Bahle, A.H., Zhu, Z., Macara, A.M., Roman, G., Shafer, O.T., and Blau, J. (2014). Differentially timed extracellular signals synchronize pacemaker neuron clocks. PLoS Biol *12*, e1001959.

Colwell, C.S. (2011). Linking neural activity and molecular oscillations in the SCN. Nat Rev Neurosci *12*, 553-569.

Cyran, S.A., Buchsbaum, A.M., Reddy, K.L., Lin, M.C., Glossop, N.R., Hardin, P.E., Young, M.W., Storti, R.V., and Blau, J. (2003). vrille, Pdp1, and dClock form a second feedback loop in the Drosophila circadian clock. Cell *112*, 329-341.

Darlington, T.K., Wager-Smith, K., Ceriani, M.F., Staknis, D., Gekakis, N., Steeves, T.D., Weitz, C.J., Takahashi, J.S., and Kay, S.A. (1998). Closing the circadian loop: CLOCK-induced transcription of its own inhibitors per and tim. Science *280*, 1599-1603.

Depetris-Chauvin, A., Berni, J., Aranovich, E.J., Muraro, N.I., Beckwith, E.J., and Ceriani, M.F. (2011). Adult-specific electrical silencing of pacemaker neurons uncouples molecular clock from circadian outputs. Curr Biol *21*, 1783-1793.

Diaz, M.M., Schlichting, M., Abruzzi, K.C., Long, X., and Rosbash, M. (2019). Allatostatin-C/AstC-R2 Is a Novel Pathway to Modulate the Circadian Activity Pattern in Drosophila. Curr Biol *29*, 13-22 e13.

Do, M.T.H. (2019). Melanopsin and the Intrinsically Photosensitive Retinal Ganglion Cells: Biophysics to Behavior. Neuron *104*, 205-226.

Dubowy, C., and Sehgal, A. (2017). Circadian Rhythms and Sleep in Drosophila melanogaster. Genetics *205*, 1373-1397.

Emery, P., So, W.V., Kaneko, M., Hall, J.C., and Rosbash, M. (1998). CRY, a Drosophila clock and light-regulated cryptochrome, is a major contributor to circadian rhythm resetting and photosensitivity. Cell *95*, 669-679.

Enoki, R., Kuroda, S., Ono, D., Hasan, M.T., Ueda, T., Honma, S., and Honma, K. (2012). Topological specificity and hierarchical network of the circadian calcium rhythm in the suprachiasmatic nucleus. Proc Natl Acad Sci U S A *109*, 21498-21503.

Farris, S.M., Robinson, G.E., and Fahrbach, S.E. (2001). Experience- and age-related outgrowth of intrinsic neurons in the mushroom bodies of the adult worker honeybee. J Neurosci *21*, 6395-6404.

Fernandez, M.P., Berni, J., and Ceriani, M.F. (2008). Circadian remodeling of neuronal circuits involved in rhythmic behavior. PLoS Biol *6*, e69.

Fernandez, M.P., Chu, J., Villella, A., Atkinson, N., Kay, S.A., and Ceriani, M.F. (2007). Impaired clock output by altered connectivity in the circadian network. Proc Natl Acad Sci U S A *104*, 5650-5655.

Fisher, Y.E., Lu, J., D'Alessandro, I., and Wilson, R.I. (2019). Sensorimotor experience remaps visual input to a heading-direction network. Nature *576*, 121-125.

Flourakis, M., and Allada, R. (2015). Patch-clamp electrophysiology in Drosophila circadian pacemaker neurons. Methods Enzymol *552*, 23-44.

Flourakis, M., Kula-Eversole, E., Hutchison, A.L., Han, T.H., Aranda, K., Moose, D.L., White, K.P., Dinner, A.R., Lear, B.C., Ren, D*., et al.* (2015). A Conserved Bicycle Model for Circadian Clock Control of Membrane Excitability. Cell *162*, 836-848.

Fogle, K.J., Baik, L.S., Houl, J.H., Tran, T.T., Roberts, L., Dahm, N.A., Cao, Y., Zhou, M., and Holmes, T.C. (2015). CRYPTOCHROME-mediated phototransduction by modulation of the potassium ion channel beta-subunit redox sensor. Proc Natl Acad Sci U S A *112*, 2245-2250.

Fogle, K.J., Parson, K.G., Dahm, N.A., and Holmes, T.C. (2011). CRYPTOCHROME is a blue-light sensor that regulates neuronal firing rate. Science *331*, 1409-1413.

Freeman, G.M., Jr., Krock, R.M., Aton, S.J., Thaben, P., and Herzog, E.D. (2013). GABA networks destabilize genetic oscillations in the circadian pacemaker. Neuron *78*, 799-806.

Frenkel, L., Muraro, N.I., Beltran Gonzalez, A.N., Marcora, M.S., Bernabo, G., Hermann-Luibl, C., Romero, J.I., Helfrich-Forster, C., Castano, E.M., Marino-Busjle, C.*, et al.* (2017). Organization of Circadian Behavior Relies on Glycinergic Transmission. Cell Rep *19*, 72-85.

Fujiwara, Y., Hermann-Luibl, C., Katsura, M., Sekiguchi, M., Ida, T., Helfrich-Forster, C., and Yoshii, T. (2018). The CCHamide1 Neuropeptide Expressed in the Anterior Dorsal Neuron 1 Conveys a Circadian Signal to the Ventral Lateral Neurons in Drosophila melanogaster. Front Physiol *9*, 1276.

Girardet, C., Blanchard, M.P., Ferracci, G., Leveque, C., Moreno, M., Francois-Bellan, A.M., Becquet, D., and Bosler, O. (2010). Daily changes in synaptic innervation of VIP neurons in the rat suprachiasmatic nucleus: contribution of glutamatergic afferents. Eur J Neurosci *31*, 359-370.

Gorostiza, E.A., Depetris-Chauvin, A., Frenkel, L., Pirez, N., and Ceriani, M.F. (2014). Circadian pacemaker neurons change synaptic contacts across the day. Curr Biol *24*, 2161-2167.

Gorska-Andrzejak, J., Chwastek, E.M., Walkowicz, L., and Witek, K. (2018). On Variations in the Level of PER in Glial Clocks of Drosophila Optic Lobe and Its Negative Regulation by PDF Signaling. Front Physiol *9*, 230.

Green, J., Adachi, A., Shah, K.K., Hirokawa, J.D., Magani, P.S., and Maimon, G. (2017). A neural circuit architecture for angular integration in Drosophila. Nature *546*, 101-106.

Gribkoff, V.K., Pieschl, R.L., and Dudek, F.E. (2003). GABA receptor-mediated inhibition of neuronal activity in rat SCN in vitro: pharmacology and influence of circadian phase. J Neurophysiol *90*, 1438-1448.

Grima, B., Chelot, E., Xia, R., and Rouyer, F. (2004). Morning and evening peaks of activity rely on different clock neurons of the Drosophila brain. Nature *431*, 869-873.

Gunawardhana, K.L., and Hardin, P.E. (2017). VRILLE Controls PDF Neuropeptide Accumulation and Arborization Rhythms in Small Ventrolateral Neurons to Drive Rhythmic Behavior in Drosophila. Curr Biol *27*, 3442-3453 e3444.

Guo, F., Cerullo, I., Chen, X., and Rosbash, M. (2014). PDF neuron firing phase-shifts key circadian activity neurons in Drosophila. Elife *3*.

Guo, F., Chen, X., and Rosbash, M. (2017). Temporal calcium profiling of specific circadian neurons in freely moving flies. Proc Natl Acad Sci U S A *114*, E8780-E8787.

Guo, F., Holla, M., Diaz, M.M., and Rosbash, M. (2018). A Circadian Output Circuit Controls Sleep-Wake Arousal in Drosophila. Neuron *100*, 624-635 e624.

Guo, F., Yu, J., Jung, H.J., Abruzzi, K.C., Luo, W., Griffith, L.C., and Rosbash, M. (2016). Circadian neuron feedback controls the Drosophila sleep--activity profile. Nature *536*, 292-297.

Hamasaka, Y., Rieger, D., Parmentier, M.L., Grau, Y., Helfrich-Forster, C., and Nassel, D.R. (2007). Glutamate and its metabotropic receptor in Drosophila clock neuron circuits. J Comp Neurol *505*, 32-45.

Hanai, S., Hamasaka, Y., and Ishida, N. (2008). Circadian entrainment to red light in Drosophila: requirement of Rhodopsin 1 and Rhodopsin 6. Neuroreport *19*, 1441-1444.

Hao, H., Allen, D.L., and Hardin, P.E. (1997). A circadian enhancer mediates PER-dependent mRNA cycling in Drosophila melanogaster. Mol Cell Biol *17*, 3687-3693.

Hardin, P.E. (2011). Molecular genetic analysis of circadian timekeeping in Drosophila. Adv Genet *74*, 141-173.

Harris, K.M., and Kater, S.B. (1994). Dendritic spines: cellular specializations imparting both stability and flexibility to synaptic function. Annu Rev Neurosci *17*, 341-371.

Hart, M.P., and Hobert, O. (2018). Neurexin controls plasticity of a mature, sexually dimorphic neuron. Nature *553*, 165-170.

Hastings, M.H., Maywood, E.S., and Brancaccio, M. (2018). Generation of circadian rhythms in the suprachiasmatic nucleus. Nat Rev Neurosci *19*, 453-469.

Helfrich-Forster, C. (1995). The period clock gene is expressed in central nervous system neurons which also produce a neuropeptide that reveals the projections of circadian pacemaker cells within the brain of Drosophila melanogaster. Proc Natl Acad Sci U S A *92*, 612-616.

Helfrich-Forster, C., Winter, C., Hofbauer, A., Hall, J.C., and Stanewsky, R. (2001). The circadian clock of fruit flies is blind after elimination of all known photoreceptors. Neuron *30*, 249-261.

Helfrich-Forster, C., Yoshii, T., Wulbeck, C., Grieshaber, E., Rieger, D., Bachleitner, W., Cusumano, P., and Rouyer, F. (2007). The lateral and dorsal neurons of Drosophila melanogaster: new insights about their morphology and function. Cold Spring Harb Symp Quant Biol *72*, 517-525.

Hendricks, J.C., Finn, S.M., Panckeri, K.A., Chavkin, J., Williams, J.A., Sehgal, A., and Pack, A.I. (2000). Rest in Drosophila is a sleep-like state. Neuron *25*, 129-138.

Herculano-Houzel, S., Mota, B., and Lent, R. (2006). Cellular scaling rules for rodent brains. Proc Natl Acad Sci U S A *103*, 12138-12143.

Herzog, E.D., Aton, S.J., Numano, R., Sakaki, Y., and Tei, H. (2004). Temporal precision in the mammalian circadian system: a reliable clock from less reliable neurons. J Biol Rhythms *19*, 35-46.

Hodge, J.J., and Stanewsky, R. (2008). Function of the Shaw potassium channel within the Drosophila circadian clock. PLoS One *3*, e2274.

Hong, J.H., Jeong, B., Min, C.H., and Lee, K.J. (2012). Circadian waves of cytosolic calcium concentration and long-range network connections in rat suprachiasmatic nucleus. Eur J Neurosci *35*, 1417-1425.

Houl, J.H., Ng, F., Taylor, P., and Hardin, P.E. (2008). CLOCK expression identifies developing circadian oscillator neurons in the brains of Drosophila embryos. BMC Neurosci *9*, 119.

Huber, R., Hill, S.L., Holladay, C., Biesiadecki, M., Tononi, G., and Cirelli, C. (2004). Sleep homeostasis in Drosophila melanogaster. Sleep *27*, 628-639.

Hunter-Ensor, M., Ousley, A., and Sehgal, A. (1996). Regulation of the Drosophila protein timeless suggests a mechanism for resetting the circadian clock by light. Cell *84*, 677-685.

Hyun, S., Lee, Y., Hong, S.T., Bang, S., Paik, D., Kang, J., Shin, J., Lee, J., Jeon, K., Hwang, S.*, et al.* (2005). Drosophila GPCR Han is a receptor for the circadian clock neuropeptide PDF. Neuron *48*, 267-278.

Im, S.H., Li, W., and Taghert, P.H. (2011). PDFR and CRY signaling converge in a subset of clock neurons to modulate the amplitude and phase of circadian behavior in Drosophila. PLoS One *6*, e18974.

Im, S.H., and Taghert, P.H. (2010). PDF receptor expression reveals direct interactions between circadian oscillators in Drosophila. J Comp Neurol *518*, 1925-1945.

Inoue, S., Yang, R., Tantry, A., Davis, C.H., Yang, T., Knoedler, J.R., Wei, Y., Adams, E.L., Thombare, S., Golf, S.R.*, et al.* (2019). Periodic Remodeling in a Neural Circuit Governs Timing of Female Sexual Behavior. Cell *179*, 1393-1408 e1316.

Itri, J.N., Michel, S., Vansteensel, M.J., Meijer, J.H., and Colwell, C.S. (2005). Fast delayed rectifier potassium current is required for circadian neural activity. Nat Neurosci *8*, 650-656.

Jenett, A., Rubin, G.M., Ngo, T.T., Shepherd, D., Murphy, C., Dionne, H., Pfeiffer, B.D., Cavallaro, A., Hall, D., Jeter, J.*, et al.* (2012). A GAL4-driver line resource for Drosophila neurobiology. Cell Rep *2*, 991-1001.

Kaneko, H., Head, L.M., Ling, J., Tang, X., Liu, Y., Hardin, P.E., Emery, P., and Hamada, F.N. (2012). Circadian rhythm of temperature preference and its neural control in Drosophila. Curr Biol *22*, 1851-1857.

Kaneko, M., and Hall, J.C. (2000). Neuroanatomy of cells expressing clock genes in Drosophila: transgenic manipulation of the period and timeless genes to mark the perikarya of circadian pacemaker neurons and their projections. J Comp Neurol *422*, 66-94.

Kaneko, M., Helfrich-Forster, C., and Hall, J.C. (1997). Spatial and temporal expression of the period and timeless genes in the developing nervous system of Drosophila: newly identified pacemaker candidates and novel features of clock gene product cycling. J Neurosci *17*, 6745-6760.

Kasugai, Y., Vogel, E., Hortnagl, H., Schonherr, S., Paradiso, E., Hauschild, M., Gobel, G., Milenkovic, I., Peterschmitt, Y., Tasan, R.*, et al.* (2019). Structural and Functional Remodeling of Amygdala GABAergic Synapses in Associative Fear Learning. Neuron *104*, 781-794 e784.

Kim, S.S., Hermundstad, A.M., Romani, S., Abbott, L.F., and Jayaraman, V. (2019). Generation of stable heading representations in diverse visual scenes. Nature *576*, 126-131.

Kim, S.S., Rouault, H., Druckmann, S., and Jayaraman, V. (2017). Ring attractor dynamics in the Drosophila central brain. Science *356*, 849-853.

King, A.N., Barber, A.F., Smith, A.E., Dreyer, A.P., Sitaraman, D., Nitabach, M.N., Cavanaugh, D.J., and Sehgal, A. (2017). A Peptidergic Circuit Links the Circadian Clock to Locomotor Activity. Curr Biol *27*, 1915-1927 e1915.

Klarsfeld, A., Leloup, J.-C., and Rouyer, F. (2003). Circadian rhythms of locomotor activity in Drosophila. Behavioural Processes *64*, 161-175.

Klose, M., Duvall, L., Li, W., Liang, X., Ren, C., Steinbach, J.H., and Taghert, P.H. (2016). Functional PDF Signaling in the Drosophila Circadian Neural Circuit Is Gated by Ral A-Dependent Modulation. Neuron *90*, 781-794.

Kloss, B., Price, J.L., Saez, L., Blau, J., Rothenfluh, A., Wesley, C.S., and Young, M.W. (1998). The Drosophila clock gene double-time encodes a protein closely related to human casein kinase Iepsilon. Cell *94*, 97-107.

Kloss, B., Rothenfluh, A., Young, M.W., and Saez, L. (2001). Phosphorylation of period is influenced by cycling physical associations of double-time, period, and timeless in the Drosophila clock. Neuron *30*, 699-706.

Ko, H.W., Jiang, J., and Edery, I. (2002). Role for Slimb in the degradation of Drosophila Period protein phosphorylated by Doubletime. Nature *420*, 673-678.

Koh, K., Zheng, X., and Sehgal, A. (2006). JETLAG resets the Drosophila circadian clock by promoting light-induced degradation of TIMELESS. Science *312*, 1809-1812.

Konopka, R.J., and Benzer, S. (1971). Clock mutants of Drosophila melanogaster. Proc Natl Acad Sci U S A *68*, 2112-2116.

Kula, E., Levitan, E.S., Pyza, E., and Rosbash, M. (2006). PDF cycling in the dorsal protocerebrum of the Drosophila brain is not necessary for circadian clock function. J Biol Rhythms *21*, 104-117.

Kula-Eversole, E., Nagoshi, E., Shang, Y., Rodriguez, J., Allada, R., and Rosbash, M. (2010). Surprising gene expression patterns within and between PDF-containing circadian neurons in Drosophila. Proc Natl Acad Sci U S A *107*, 13497-13502.

Kunst, M., Hughes, M.E., Raccuglia, D., Felix, M., Li, M., Barnett, G., Duah, J., and Nitabach, M.N. (2014). Calcitonin gene-related peptide neurons mediate sleep-specific circadian output in Drosophila. Curr Biol *24*, 2652-2664.

Lai, S.L., and Lee, T. (2006). Genetic mosaic with dual binary transcriptional systems in Drosophila. Nat Neurosci *9*, 703-709.

Lamaze, A., Kratschmer, P., Chen, K.F., Lowe, S., and Jepson, J.E.C. (2018). A Wake-Promoting Circadian Output Circuit in Drosophila. Curr Biol *28*, 3098-3105 e3093.

Lazopulo, S., Lazopulo, A., Baker, J.D., and Syed, S. (2019). Daytime colour preference in Drosophila depends on the circadian clock and TRP channels. Nature *574*, 108-111.

Lear, B.C., Lin, J.M., Keath, J.R., McGill, J.J., Raman, I.M., and Allada, R. (2005). The ion channel narrow abdomen is critical for neural output of the Drosophila circadian pacemaker. Neuron *48*, 965-976.

Lear, B.C., Zhang, L., and Allada, R. (2009). The neuropeptide PDF acts directly on evening pacemaker neurons to regulate multiple features of circadian behavior. PLoS Biol *7*, e1000154.

Lee, C., Bae, K., and Edery, I. (1998). The Drosophila CLOCK protein undergoes daily rhythms in abundance, phosphorylation, and interactions with the PER-TIM complex. Neuron *21*, 857-867.

Lee, C., Bae, K., and Edery, I. (1999). PER and TIM inhibit the DNA binding activity of a Drosophila CLOCK-CYC/dBMAL1 heterodimer without disrupting formation of the heterodimer: a basis for circadian transcription. Mol Cell Biol *19*, 5316-5325.

Li, M.T., Cao, L.H., Xiao, N., Tang, M., Deng, B., Yang, T., Yoshii, T., and Luo, D.G. (2018). Hub-organized parallel circuits of central circadian pacemaker neurons for visual photoentrainment in Drosophila. Nat Commun *9*, 4247.

Liang, X., Ho, M.C.W., Zhang, Y., Li, Y., Wu, M.N., Holy, T.E., and Taghert, P.H. (2019). Morning and Evening Circadian Pacemakers Independently Drive Premotor Centers via a Specific Dopamine Relay. Neuron *102*, 843-857 e844.

Liang, X., Holy, T.E., and Taghert, P.H. (2016). Synchronous Drosophila circadian pacemakers display nonsynchronous Ca(2)(+) rhythms in vivo. Science *351*, 976-981.

Liang, X., Holy, T.E., and Taghert, P.H. (2017). A Series of Suppressive Signals within the Drosophila Circadian Neural Circuit Generates Sequential Daily Outputs. Neuron *94*, 1173-1189 e1174.

Lima, S.Q., and Miesenbock, G. (2005). Remote control of behavior through genetically targeted photostimulation of neurons. Cell *121*, 141-152.

Lin, J.M., Kilman, V.L., Keegan, K., Paddock, B., Emery-Le, M., Rosbash, M., and Allada, R. (2002). A role for casein kinase 2alpha in the Drosophila circadian clock. Nature *420*, 816-820.

Lin, Y., Stormo, G.D., and Taghert, P.H. (2004). The neuropeptide pigment-dispersing factor coordinates pacemaker interactions in the Drosophila circadian system. J Neurosci *24*, 7951-7957.

Liu, Q., Tabuchi, M., Liu, S., Kodama, L., Horiuchi, W., Daniels, J., Chiu, L., Baldoni, D., and Wu, M.N. (2017). Branch-specific plasticity of a bifunctional dopamine circuit encodes protein hunger. Science *356*, 534-539.

Liu, S., Lamaze, A., Liu, Q., Tabuchi, M., Yang, Y., Fowler, M., Bharadwaj, R., Zhang, J., Bedont, J., Blackshaw, S.*, et al.* (2014). WIDE AWAKE mediates the circadian timing of sleep onset. Neuron *82*, 151-166.

Lu, B., Liu, W., Guo, F., and Guo, A. (2008). Circadian modulation of light-induced locomotion responses in Drosophila melanogaster. Genes Brain Behav *7*, 730-739.

Markow, T.A., and Manning, M. (1980). Mating success of photoreceptor mutants of Drosophila melanogaster. Behav Neural Biol *29*, 276-280.

Martinek, S., Inonog, S., Manoukian, A.S., and Young, M.W. (2001). A role for the segment polarity gene shaggy/GSK-3 in the Drosophila circadian clock. Cell *105*, 769-779.

Mauss, A.S., Busch, C., and Borst, A. (2017). Optogenetic Neuronal Silencing in Drosophila during Visual Processing. Sci Rep *7*, 13823.

Mehnert, K.I., and Cantera, R. (2011). Circadian rhythms in the morphology of neurons in Drosophila. Cell Tissue Res *344*, 381-389.

Meredith, A.L., Wiler, S.W., Miller, B.H., Takahashi, J.S., Fodor, A.A., Ruby, N.F., and Aldrich, R.W. (2006). BK calcium-activated potassium channels regulate circadian behavioral rhythms and pacemaker output. Nat Neurosci *9*, 1041-1049.

Mohammad, F., Stewart, J.C., Ott, S., Chlebikova, K., Chua, J.Y., Koh, T.W., Ho, J., and Claridge-Chang, A. (2017). Optogenetic inhibition of behavior with anion channelrhodopsins. Nat Methods *14*, 271-274.

Mohawk, J.A., Green, C.B., and Takahashi, J.S. (2012). Central and peripheral circadian clocks in mammals. Annu Rev Neurosci *35*, 445-462.

Moore, R.Y., and Speh, J.C. (1993). GABA is the principal neurotransmitter of the circadian system. Neurosci Lett *150*, 112-116.

Mrosovsky, N. (1999). Masking: history, definitions, and measurement. Chronobiol Int *16*, 415-429.

Mukhopadhyay, S., Lu, Y., Shaham, S., and Sengupta, P. (2008). Sensory signaling-dependent remodeling of olfactory cilia architecture in C. elegans. Dev Cell *14*, 762-774.

Muraro, N.I., Pirez, N., and Ceriani, M.F. (2013). The circadian system: plasticity at many levels. Neuroscience *247*, 280-293.

Myers, M.P., Wager-Smith, K., Rothenfluh-Hilfiker, A., and Young, M.W. (1996). Light-induced degradation of TIMELESS and entrainment of the Drosophila circadian clock. Science *271*, 1736-1740.

Narasimamurthy, R., and Virshup, D.M. (2017). Molecular Mechanisms Regulating Temperature Compensation of the Circadian Clock. Front Neurol *8*, 161.

Ni, J.D., Baik, L.S., Holmes, T.C., and Montell, C. (2017). A rhodopsin in the brain functions in circadian photoentrainment in Drosophila. Nature *545*, 340-344.

Ni, J.D., Gurav, A.S., Liu, W., Ogunmowo, T.H., Hackbart, H., Elsheikh, A., Verdegaal, A.A., and Montell, C. (2019). Differential regulation of the Drosophila sleep homeostat by circadian and arousal inputs. Elife *8*.

Ni, J.Q., Markstein, M., Binari, R., Pfeiffer, B., Liu, L.P., Villalta, C., Booker, M., Perkins, L., and Perrimon, N. (2008). Vector and parameters for targeted transgenic RNA interference in Drosophila melanogaster. Nat Methods *5*, 49-51.

Nicolai, L.J., Ramaekers, A., Raemaekers, T., Drozdzecki, A., Mauss, A.S., Yan, J., Landgraf, M., Annaert, W., and Hassan, B.A. (2010). Genetically encoded dendritic marker sheds light on neuronal connectivity in Drosophila. Proc Natl Acad Sci U S A *107*, 20553-20558.

Noguchi, T., Leise, T.L., Kingsbury, N.J., Diemer, T., Wang, L.L., Henson, M.A., and Welsh, D.K. (2017). Calcium Circadian Rhythmicity in the Suprachiasmatic Nucleus: Cell Autonomy and Network Modulation. eNeuro *4*.

Oh, Y., Yoon, S.E., Zhang, Q., Chae, H.S., Daubnerova, I., Shafer, O.T., Choe, J., and Kim, Y.J. (2014). A homeostatic sleep-stabilizing pathway in Drosophila composed of the sex peptide receptor and its ligand, the myoinhibitory peptide. PLoS Biol *12*, e1001974.

Ono, D., Honma, K.-i., Yanagawa, Y., Yamanaka, A., and Honma, S. (2019). GABA in the suprachiasmatic nucleus refines circadian output rhythms in mice. Communications Biology *2*.

Park, J.H., Helfrich-Forster, C., Lee, G., Liu, L., Rosbash, M., and Hall, J.C. (2000). Differential regulation of circadian pacemaker output by separate clock genes in Drosophila. Proc Natl Acad Sci U S A *97*, 3608-3613.

Patel, D. (2006). Shift work, light at night and risk of breast cancer. Occup Med (Lond) *56*, 433.

Patton, D.F., and Mistlberger, R.E. (2013). Circadian adaptations to meal timing: neuroendocrine mechanisms. Front Neurosci *7*, 185.

Pellman, B.A., and Kim, J.J. (2016). What Can Ethobehavioral Studies Tell Us about the Brain's Fear System? Trends Neurosci *39*, 420-431.

Peng, Y., Stoleru, D., Levine, J.D., Hall, J.C., and Rosbash, M. (2003). Drosophila free-running rhythms require intercellular communication. PLoS Biol *1*, E13.

Pennartz, C.M., de Jeu, M.T., Bos, N.P., Schaap, J., and Geurtsen, A.M. (2002). Diurnal modulation of pacemaker potentials and calcium current in the mammalian circadian clock. Nature *416*, 286-290.

Petsakou, A., Sapsis, T.P., and Blau, J. (2015). Circadian Rhythms in Rho1 Activity Regulate Neuronal Plasticity and Network Hierarchy. Cell *162*, 823-835.

Pfeiffer, B.D., Ngo, T.T., Hibbard, K.L., Murphy, C., Jenett, A., Truman, J.W., and Rubin, G.M. (2010). Refinement of tools for targeted gene expression in Drosophila. Genetics *186*, 735-755.

Pirez, N., Christmann, B.L., and Griffith, L.C. (2013). Daily rhythms in locomotor circuits in Drosophila involve PDF. J Neurophysiol *110*, 700-708.

Potdar, S., and Sheeba, V. (2018). Wakefulness Is Promoted during Day Time by PDFR Signalling to Dopaminergic Neurons in Drosophila melanogaster. eNeuro *5*.

Prakash, P., Nambiar, A., and Sheeba, V. (2017). Oscillating PDF in termini of circadian pacemaker neurons and synchronous molecular clocks in downstream neurons are not sufficient for sustenance of activity rhythms in constant darkness. PLoS One *12*, e0175073.

Price, J.L., Blau, J., Rothenfluh, A., Abodeely, M., Kloss, B., and Young, M.W. (1998). double-time is a novel Drosophila clock gene that regulates PERIOD protein accumulation. Cell *94*, 83-95.

Price, J.L., Dembinska, M.E., Young, M.W., and Rosbash, M. (1995). Suppression of PERIOD protein abundance and circadian cycling by the Drosophila clock mutation timeless. EMBO J *14*, 4044-4049.

Pyza, E., and Gorska-Andrzejak, J. (2008). External and internal inputs affecting plasticity of dendrites and axons of the fly's neurons. Acta Neurobiol Exp (Wars) *68*, 322-333.

Pyza, E., and Meinertzhagen, I.A. (1995). Monopolar cell axons in the first optic neuropil of the housefly, Musca domestica L., undergo daily fluctuations in diameter that have a circadian basis. J Neurosci *15*, 407-418.

Reddy, P., Zehring, W.A., Wheeler, D.A., Pirrotta, V., Hadfield, C., Hall, J.C., and Rosbash, M. (1984). Molecular analysis of the period locus in Drosophila melanogaster and identification of a transcript involved in biological rhythms. Cell *38*, 701-710.

Redlin, U., and Mrosovsky, N. (1999). Masking by light in hamsters with SCN lesions. J Comp Physiol A *184*, 439-448.

Renn, S.C., Park, J.H., Rosbash, M., Hall, J.C., and Taghert, P.H. (1999). A pdf neuropeptide gene mutation and ablation of PDF neurons each cause severe abnormalities of behavioral circadian rhythms in Drosophila. Cell *99*, 791-802.

Ribeiro, I.M.A., Drews, M., Bahl, A., Machacek, C., Borst, A., and Dickson, B.J. (2018). Visual Projection Neurons Mediating Directed Courtship in Drosophila. Cell *174*, 607-621 e618.

Rieger, D., Shafer, O.T., Tomioka, K., and Helfrich-Forster, C. (2006). Functional analysis of circadian pacemaker neurons in Drosophila melanogaster. J Neurosci *26*, 2531-2543.

Rieger, D., Stanewsky, R., and Helfrich-Forster, C. (2003). Cryptochrome, compound eyes, Hofbauer-Buchner eyelets, and ocelli play different roles in the entrainment and masking pathway of the locomotor activity rhythm in the fruit fly Drosophila melanogaster. J Biol Rhythms *18*, 377-391.

Rutila, J.E., Suri, V., Le, M., So, W.V., Rosbash, M., and Hall, J.C. (1998). CYCLE is a second bHLH-PAS clock protein essential for circadian rhythmicity and transcription of Drosophila period and timeless. Cell *93*, 805-814.

Ryder, E., Blows, F., Ashburner, M., Bautista-Llacer, R., Coulson, D., Drummond, J., Webster, J., Gubb, D., Gunton, N., Johnson, G.*, et al.* (2004). The DrosDel collection: a set of P-element insertions for generating custom chromosomal aberrations in Drosophila melanogaster. Genetics *167*, 797-813.

Sachse, S., Rueckert, E., Keller, A., Okada, R., Tanaka, N.K., Ito, K., and Vosshall, L.B. (2007). Activity-dependent plasticity in an olfactory circuit. Neuron *56*, 838-850.

Sawyer, L.A., Hennessy, J.M., Peixoto, A.A., Rosato, E., Parkinson, H., Costa, R., and Kyriacou, C.P. (1997). Natural variation in a Drosophila clock gene and temperature compensation. Science *278*, 2117-2120.

Schaap, J., Albus, H., VanderLeest, H.T., Eilers, P.H., Detari, L., and Meijer, J.H. (2003). Heterogeneity of rhythmic suprachiasmatic nucleus neurons: Implications for circadian waveform and photoperiodic encoding. Proc Natl Acad Sci U S A *100*, 15994-15999.

Schernhammer, E.S., Laden, F., Speizer, F.E., Willett, W.C., Hunter, D.J., Kawachi, I., and Colditz, G.A. (2001). Rotating night shifts and risk of breast cancer in women participating in the nurses' health study. J Natl Cancer Inst *93*, 1563-1568.

Schernhammer, E.S., Laden, F., Speizer, F.E., Willett, W.C., Hunter, D.J., Kawachi, I., Fuchs, C.S., and Colditz, G.A. (2003). Night-shift work and risk of colorectal cancer in the nurses' health study. J Natl Cancer Inst *95*, 825-828.

Schlichting, M., Diaz, M.M., Xin, J., and Rosbash, M. (2019a). Neuron-specific knockouts indicate the importance of network communication to Drosophila rhythmicity. Elife *8*.

Schlichting, M., Menegazzi, P., Rosbash, M., and Helfrich-Forster, C. (2019b). A Distinct Visual Pathway Mediates High-Intensity Light Adaptation of the Circadian Clock in Drosophila. J Neurosci *39*, 1621-1630.

Schmal, C., Herzog, E.D., and Herzel, H. (2018). Measuring Relative Coupling Strength in Circadian Systems. J Biol Rhythms *33*, 84-98.

Schultz, W. (2016). Dopamine reward prediction error coding. Dialogues Clin Neurosci *18*, 23-32.

Seelig, J.D., and Jayaraman, V. (2015). Neural dynamics for landmark orientation and angular path integration. Nature *521*, 186-191.

Sehadova, H., Glaser, F.T., Gentile, C., Simoni, A., Giesecke, A., Albert, J.T., and Stanewsky, R. (2009). Temperature entrainment of Drosophila's circadian clock involves the gene nocte and signaling from peripheral sensory tissues to the brain. Neuron *64*, 251-266.

Sehgal, A., Price, J.L., Man, B., and Young, M.W. (1994). Loss of circadian behavioral rhythms and per RNA oscillations in the Drosophila mutant timeless. Science *263*, 1603-1606.

Seluzicki, A., Flourakis, M., Kula-Eversole, E., Zhang, L., Kilman, V., and Allada, R. (2014). Dual PDF signaling pathways reset clocks via TIMELESS and acutely excite target neurons to control circadian behavior. PLoS Biol *12*, e1001810.

Shafer, O.T., Helfrich-Forster, C., Renn, S.C., and Taghert, P.H. (2006). Reevaluation of Drosophila melanogaster's neuronal circadian pacemakers reveals new neuronal classes. J Comp Neurol *498*, 180-193.

Shafer, O.T., Kim, D.J., Dunbar-Yaffe, R., Nikolaev, V.O., Lohse, M.J., and Taghert, P.H. (2008). Widespread receptivity to neuropeptide PDF throughout the neuronal circadian clock network of Drosophila revealed by real-time cyclic AMP imaging. Neuron *58*, 223-237.

Shafer, O.T., Rosbash, M., and Truman, J.W. (2002). Sequential nuclear accumulation of the clock proteins period and timeless in the pacemaker neurons of Drosophila melanogaster. J Neurosci *22*, 5946-5954.

Shafer, O.T., and Taghert, P.H. (2009). RNA-interference knockdown of Drosophila pigment dispersing factor in neuronal subsets: the anatomical basis of a neuropeptide's circadian functions. PLoS One *4*, e8298.

Shang, Y., Griffith, L.C., and Rosbash, M. (2008). Light-arousal and circadian photoreception circuits intersect at the large PDF cells of the Drosophila brain. Proc Natl Acad Sci U S A *105*, 19587-19594.

Shaw, P.J., Cirelli, C., Greenspan, R.J., and Tononi, G. (2000). Correlates of sleep and waking in Drosophila melanogaster. Science *287*, 1834-1837.

Sheeba, V., Fogle, K.J., Kaneko, M., Rashid, S., Chou, Y.T., Sharma, V.K., and Holmes, T.C. (2008a). Large ventral lateral neurons modulate arousal and sleep in Drosophila. Curr Biol *18*, 1537-1545.

Sheeba, V., Gu, H., Sharma, V.K., O'Dowd, D.K., and Holmes, T.C. (2008b). Circadian- and light-dependent regulation of resting membrane potential and spontaneous action potential firing of Drosophila circadian pacemaker neurons. J Neurophysiol *99*, 976-988.

Sheng, M., and Kim, M.J. (2002). Postsynaptic signaling and plasticity mechanisms. Science *298*, 776-780.

Simoni, A., Wolfgang, W., Topping, M.P., Kavlie, R.G., Stanewsky, R., and Albert, J.T. (2014). A mechanosensory pathway to the Drosophila circadian clock. Science *343*, 525-528.

Sivachenko, A., Li, Y., Abruzzi, K.C., and Rosbash, M. (2013). The transcription factor Mef2 links the Drosophila core clock to Fas2, neuronal morphology, and circadian behavior. Neuron *79*, 281-292.

Smith, C.J., Watson, J.D., Spencer, W.C., O'Brien, T., Cha, B., Albeg, A., Treinin, M., and Miller, D.M., 3rd (2010). Time-lapse imaging and cell-specific expression profiling reveal dynamic branching and molecular determinants of a multi-dendritic nociceptor in C. elegans. Dev Biol *345*, 18-33.

Song, B.J., and Rogulja, D. (2017). SnapShot: Circadian Clock. Cell *171*, 1468-1468 e1461.

Song, I., and Huganir, R.L. (2002). Regulation of AMPA receptors during synaptic plasticity. Trends Neurosci *25*, 578-588.

Stanewsky, R., Jamison, C.F., Plautz, J.D., Kay, S.A., and Hall, J.C. (1997). Multiple circadian-regulated elements contribute to cycling period gene expression in Drosophila. EMBO J *16*, 5006-5018.

Stanewsky, R., Kaneko, M., Emery, P., Beretta, B., Wager-Smith, K., Kay, S.A., Rosbash, M., and Hall, J.C. (1998). The cryb mutation identifies cryptochrome as a circadian photoreceptor in Drosophila. Cell *95*, 681-692.

Stephan, F.K., and Zucker, I. (1972). Circadian rhythms in drinking behavior and locomotor activity of rats are eliminated by hypothalamic lesions. Proc Natl Acad Sci U S A *69*, 1583-1586.

Stoleru, D., Nawathean, P., Fernandez, M.P., Menet, J.S., Ceriani, M.F., and Rosbash, M. (2007). The Drosophila circadian network is a seasonal timer. Cell *129*, 207-219.

Stoleru, D., Peng, Y., Agosto, J., and Rosbash, M. (2004). Coupled oscillators control morning and evening locomotor behaviour of Drosophila. Nature *431*, 862-868.

Stoleru, D., Peng, Y., Nawathean, P., and Rosbash, M. (2005). A resetting signal between Drosophila pacemakers synchronizes morning and evening activity. Nature *438*, 238-242.

Sun, Z.S., Albrecht, U., Zhuchenko, O., Bailey, J., Eichele, G., and Lee, C.C. (1997). RIGUI, a putative mammalian ortholog of the Drosophila period gene. Cell *90*, 1003-1011.

Suri, V., Qian, Z., Hall, J.C., and Rosbash, M. (1998). Evidence that the TIM light response is relevant to light-induced phase shifts in Drosophila melanogaster. Neuron *21*, 225-234.

Tabuchi, M., Monaco, J.D., Duan, G., Bell, B., Liu, S., Liu, Q., Zhang, K., and Wu, M.N. (2018). Clock-Generated Temporal Codes Determine Synaptic Plasticity to Control Sleep. Cell *175*, 1213-1227 e1218.

Takahashi, J.S. (2017). Transcriptional architecture of the mammalian circadian clock. Nat Rev Genet *18*, 164-179.

Takahashi, J.S., Hong, H.K., Ko, C.H., and McDearmon, E.L. (2008). The genetics of mammalian circadian order and disorder: implications for physiology and disease. Nat Rev Genet *9*, 764-775.

Talay, M., Richman, E.B., Snell, N.J., Hartmann, G.G., Fisher, J.D., Sorkac, A., Santoyo, J.F., Chou-Freed, C., Nair, N., Johnson, M.*, et al.* (2017). Transsynaptic Mapping of Second-Order Taste Neurons in Flies by trans-Tango. Neuron *96*, 783-795 e784.

Taube, J.S. (2007). The head direction signal: origins and sensory-motor integration. Annu Rev Neurosci *30*, 181-207.

Tayler, T.D., Pacheco, D.A., Hergarden, A.C., Murthy, M., and Anderson, D.J. (2012). A neuropeptide circuit that coordinates sperm transfer and copulation duration in Drosophila. Proc Natl Acad Sci U S A *109*, 20697-20702.

Tei, H., Okamura, H., Shigeyoshi, Y., Fukuhara, C., Ozawa, R., Hirose, M., and Sakaki, Y. (1997). Circadian oscillation of a mammalian homologue of the Drosophila period gene. Nature *389*, 512-516.

Turner-Evans, D., Wegener, S., Rouault, H., Franconville, R., Wolff, T., Seelig, J.D., Druckmann, S., and Jayaraman, V. (2017). Angular velocity integration in a fly heading circuit. Elife *6*.

VanVickle-Chavez, S.J., and Van Gelder, R.N. (2007). Action spectrum of Drosophila cryptochrome. J Biol Chem *282*, 10561-10566.

Vecsey, C.G., Pirez, N., and Griffith, L.C. (2014). The Drosophila neuropeptides PDF and sNPF have opposing electrophysiological and molecular effects on central neurons. J Neurophysiol *111*, 1033-1045.

Veenstra, J.A., and Ida, T. (2014). More Drosophila enteroendocrine peptides: Orcokinin B and the CCHamides 1 and 2. Cell Tissue Res *357*, 607-621.

Vitaterna, M.H., Takahashi, J.S., and Turek, F.W. (2001). Overview of circadian rhythms. Alcohol Res Health *25*, 85-93.

von der Ohe, C.G., Garner, C.C., Darian-Smith, C., and Heller, H.C. (2007). Synaptic protein dynamics in hibernation. J Neurosci *27*, 84-92.

Wagner, S., Castel, M., Gainer, H., and Yarom, Y. (1997). GABA in the mammalian suprachiasmatic nucleus and its role in diurnal rhythmicity. Nature *387*, 598-603.

Wang, Q., Abruzzi, K.C., Rosbash, M., and Rio, D.C. (2018). Striking circadian neuron diversity and cycling of Drosophila alternative splicing. Elife *7*.

Weber, P., Kula-Eversole, E., and Pyza, E. (2009). Circadian control of dendrite morphology in the visual system of Drosophila melanogaster. PLoS One *4*, e4290.

Welsh, D.K., Takahashi, J.S., and Kay, S.A. (2010). Suprachiasmatic nucleus: cell autonomy and network properties. Annu Rev Physiol *72*, 551-577.

Wheeler, D.A., Hamblen-Coyle, M.J., Dushay, M.S., and Hall, J.C. (1993). Behavior in light-dark cycles of Drosophila mutants that are arrhythmic, blind, or both. J Biol Rhythms *8*, 67-94.

Wright, K.P., Lowry, C.A., and Lebourgeois, M.K. (2012). Circadian and wakefulness-sleep modulation of cognition in humans. Front Mol Neurosci *5*, 50.

Wu, Y., Cao, G., and Nitabach, M.N. (2008). Electrical silencing of PDF neurons advances the phase of non-PDF clock neurons in Drosophila. J Biol Rhythms *23*, 117-128.

Yamaguchi, S., Isejima, H., Matsuo, T., Okura, R., Yagita, K., Kobayashi, M., and Okamura, H. (2003). Synchronization of cellular clocks in the suprachiasmatic nucleus. Science *302*, 1408-1412.

Yao, Z., Bennett, A.J., Clem, J.L., and Shafer, O.T. (2016). The Drosophila Clock Neuron Network Features Diverse Coupling Modes and Requires Network-wide Coherence for Robust Circadian Rhythms. Cell Rep *17*, 2873-2881.

Yao, Z., Macara, A.M., Lelito, K.R., Minosyan, T.Y., and Shafer, O.T. (2012). Analysis of functional neuronal connectivity in the Drosophila brain. J Neurophysiol *108*, 684-696.

Yao, Z., and Shafer, O.T. (2014). The Drosophila circadian clock is a variably coupled network of multiple peptidergic units. Science *343*, 1516-1520.

Yoshii, T., Hermann-Luibl, C., and Helfrich-Forster, C. (2016). Circadian light-input pathways in Drosophila. Commun Integr Biol *9*, e1102805.

Yoshii, T., Todo, T., Wulbeck, C., Stanewsky, R., and Helfrich-Forster, C. (2008). Cryptochrome is present in the compound eyes and a subset of Drosophila's clock neurons. J Comp Neurol *508*, 952-966.

Yoshii, T., Wulbeck, C., Sehadova, H., Veleri, S., Bichler, D., Stanewsky, R., and Helfrich-Forster, C. (2009). The neuropeptide pigment-dispersing factor adjusts period and phase of Drosophila's clock. J Neurosci *29*, 2597-2610.

Yu, W., Zheng, H., Houl, J.H., Dauwalder, B., and Hardin, P.E. (2006). PER-dependent rhythms in CLK phosphorylation and E-box binding regulate circadian transcription. Genes Dev *20*, 723-733.

Yu, W., Zheng, H., Price, J.L., and Hardin, P.E. (2009). DOUBLETIME plays a noncatalytic role to mediate CLOCK phosphorylation and repress CLOCK-dependent transcription within the Drosophila circadian clock. Mol Cell Biol *29*, 1452-1458.

Yuste, R., and Bonhoeffer, T. (2001). Morphological changes in dendritic spines associated with long-term synaptic plasticity. Annu Rev Neurosci *24*, 1071-1089.

Zehring, W.A., Wheeler, D.A., Reddy, P., Konopka, R.J., Kyriacou, C.P., Rosbash, M., and Hall, J.C. (1984). P-element transformation with period locus DNA restores rhythmicity to mutant, arrhythmic Drosophila melanogaster. Cell *39*, 369-376.

Zeng, H., Qian, Z., Myers, M.P., and Rosbash, M. (1996). A light-entrainment mechanism for the Drosophila circadian clock. Nature *380*, 129-135.

Zhang, L., Chung, B.Y., Lear, B.C., Kilman, V.L., Liu, Y., Mahesh, G., Meissner, R.A., Hardin, P.E., and Allada, R. (2010a). DN1(p) circadian neurons coordinate acute light and PDF inputs to produce robust daily behavior in Drosophila. Curr Biol *20*, 591-599.

Zhang, R., Lahens, N.F., Ballance, H.I., Hughes, M.E., and Hogenesch, J.B. (2014). A circadian gene expression atlas in mammals: implications for biology and medicine. Proc Natl Acad Sci U S A *111*, 16219-16224.

Zhang, S.X., Rogulja, D., and Crickmore, M.A. (2016). Dopaminergic Circuitry Underlying Mating Drive. Neuron *91*, 168-181.

Zhang, Y., Liu, Y., Bilodeau-Wentworth, D., Hardin, P.E., and Emery, P. (2010b). Light and temperature control the contribution of specific DN1 neurons to Drosophila circadian behavior. Curr Biol *20*, 600-605.

Zhang, Y.Q., Rodesch, C.K., and Broadie, K. (2002). Living synaptic vesicle marker: synaptotagmin-GFP. Genesis *34*, 142-145.

Zheng, Z., Lauritzen, J.S., Perlman, E., Robinson, C.G., Nichols, M., Milkie, D., Torrens, O., Price, J., Fisher, C.B., Sharifi, N.*, et al.* (2018). A Complete Electron Microscopy Volume of the Brain of Adult Drosophila melanogaster. Cell *174*, 730-743 e722.

Zielinski, T., Moore, A.M., Troup, E., Halliday, K.J., and Millar, A.J. (2014). Strengths and limitations of period estimation methods for circadian data. PLoS One *9*, e96462.

Zucker, R.S., and Regehr, W.G. (2002). Short-term synaptic plasticity. Annu Rev Physiol *64*, 355-405.

Appendix

Supplemental Tables

Supplementary Table 1. Genotypes and sample sizes.

Figure	Label	Genotype	N	Statistics
Figure 2.1				
2.1a, Left and Middle (24 hour LD and DD activity)	Wild-type	*w^+, iso31*	125	
2.1a, Right	Wild-type	*w^+, iso31*	62 (2pm), 63 (2am)	
2.1b	Wild-type	*w^+, iso31*	63 (8am), 69 (2pm, Day, same flies as Figure 2.1a), 67 (8pm), 63 (2am, Night, same flies as Figure 2.1a)	
2.1c	Wild-type	*w^+, iso31*	63 (8am, same flies as 1b), 25 (8:30am), 14 (9am), 17 (9:30am), 51 (10am), 17, (10:30am), 60 (11am), 26 (12pm), 47 (1pm), 62 (2pm, same flies as 1b), 72 (3pm), 50 (4pm), 24 (4:30pm), 39 (5pm), 81 (6pm), 108 (7pm), 38 (7:30pm), 87 (8pm), 73 (8:30pm), 72 (9pm), 33 (9:30pm), 53 (10pm), 17	

			(10:30pm), 30 (11pm), 17 (11:30pm), 42 (12am), 17 (1am), 63 (2am, same flies as 1a and B), 62 (3am), 52 (4am), 25 (5am), 62 (6am), 31 (7am), 11 (7:30am)	
Figure 2.2				
2.2a,b		*w+, iso31*	62 (2pm), 63 (2am). Same flies as 1a and B.	One-way ANOVA $F(3,496)=77.85$, $p<0.0001$, with Tukey's multiple comparisons test. LD Day vs DD day: $p<0.0001$. DD Day vs DD night: $p<0.0353$.
2.2c		*w+, iso31*	33 (2pm), 58 (2am). Subsample of sleeping flies from Figure 2.1a and 2.1b.	
2.2d, left		*w+, iso31*	62 (2pm), 63 (2am). Same flies as Figure 2.1a and 2.1b	
2.2d, right		*w+, iso31*	Requantificatio n of flies from Figure 2.1c.	
2.2e,f	Wild-type females	*w+, iso31*	31 (2pm), 35 (2am)	Unpaired t test $t(64)=8.248$, $p=<0.0001$.
2.2g		*w+, iso31*	30 (2pm)	
Figure 2.3				
2.3e, left	Tim > GFP	w-; Tim(UAS)-Gal4, Repo-Gal80 / UAS-myr::GFP; UAS-Dicer2 / +	Representative sample of at least ten flies	

2.3e, right	Clock	w^-; Tim(UAS)-Gal4, Repo-Gal80 / UAS-myr::GFP; UAS-Dicer2 / +	Representative sample of at least ten flies	
2.3f, red	Tim > Clock-RNAi	w^-; Tim(UAS)-Gal4, Repo-Gal80 / UAS-Clock-RNAi; UAS-Dicer2 / UAS-Dicer2	56 (8am), 31 (11am), 67 (2pm), 34 (5pm), 54 (8pm), 29 (11pm), 61 (2am) , 34 (5am) 51 (7am)	
2.3f, purple	Tim > Period-RNAi	w^-; Tim(UAS)-Gal4, Repo-Gal80 / UAS-Dicer2; UAS-Period-RNAi / UAS-Dicer2	48 (8am), 31 (11am) 58 (2pm), 12 (5pm), 60 (8pm), 20 (11pm), 61 (2am), 45 (5am), 34 (7am)	
2.3f, black			28 (8am), 28 (11am) 77 (2pm), 29 (5pm), 23 (8pm), 44 (11pm), 75 (2am), 55 (5am), 28 (7am)	
2.3f, grey			43 (8am), 46 (11am) 49 (2pm), 27 (5pm), 19 (8pm), 49 (11pm), 74 (2am), 32 (5am), 27 (7am)	
2.3g, black	UAS-Clock-RNAi	w^+; UAS-Clock-RNAi/+; UAS-Dicer2 / +	88 (2pm), 74 (2am)	Two-way ANOVA $F(2,440)=100.4$, interaction $p<0.0001$, with Tukey's multiple comparisons test. 2pm: UAS-control vs GFP control: $p=0.0977$. UAS control vs experimental:
2.3g, grey	Tim > GFP	w^-; Tim(UAS)-Gal4, Repo-Gal80 / UAS-myr::GFP or UAS-mCD8::GFP; UAS-Dicer2 / +	77 (2pm), 75 (2am)	

2.3g, red	Tim > Clock-RNAi	w-; Tim(UAS)-Gal4, Repo-Gal80 / UAS-Clock-RNAi; UAS-Dicer2 / UAS-Dicer2	67 (2pm, same flies as 1c), 61 (2am, same flies as 1c)	p<0.0001. GFP control vs experimental p<0.0001. 2am: UAS-control vs GFP control: p=0.8602. UAS control vs experimental: p<0.0001. GFP control vs experimental p<0.0001.
Figure 2.4				
2.4a left	UAS-Clock-RNAi	w^+; UAS-Clock-RNAi/+; UAS-Dicer2 / +	32	
2.4a middle	Tim > GFP	w^-; Tim(UAS)-Gal4, Repo-Gal80 / UAS-myr::GFP; UAS-Dicer2 / +	33	
2.4a right	Tim > Clock-RNAi	w^-; Tim(UAS)-Gal4, Repo-Gal80 / UAS-Clock-RNAi; UAS-Dicer2 / UAS-Dicer2	35	
2.4b, left image	UAS-Clock-RNAi	w^+; UAS-Clock-RNAi / +; UAS-Dicer2 / +	Representative samples (ZT6) of at least ten flies	
2.4b, middle image	Tim > Clock-RNAi	w-; Tim(UAS)-Gal4, Repo-Gal80 / UAS-Clock-RNAi; UAS-Dicer2 / UAS-Dicer2	Representative samples (ZT6) of at least ten flies	
2.4b, right panel, grey		w^+; UAS-Clock-RNAi / +; UAS-Dicer2 / +	11	Unpaired t test t(18)=6.464, p=<0.0001.
2.4b, right panel, red		w-; Tim(UAS)-Gal4, Repo-Gal80 / UAS-Clock-RNAi; UAS-Dicer2 / UAS-Dicer2	9	
2.4c, left image	UAS-Period-RNAi	w^+; UAS-Dicer2 / +; UAS-Period-RNAi / +	Representative samples (ZT1) of at least ten flies	
2.4c, middle image	Tim > Period-RNAi	w^-; Tim(UAS)-Gal4, Repo-Gal80 / UAS-Dicer2; UAS-Period-RNAi / UAS-Dicer2	Representative samples (ZT1) of at least ten flies	

2.4c, right panel, grey		w^+; UAS-Dicer2 / +; UAS-Period-RNAi / +	11	Unpaired t test t(21)=10.91, p=<0.0001.
2.4c, right panel, purple		w^-; Tim(UAS)-Gal4, Repo-Gal80 / UAS-Dicer2; UAS-Period-RNAi / UAS-Dicer2	12	
2.4d, top	Wild-type	*w^+, iso31*	46	
2.4d, bottom	*w^+per^S*	*w^+per^S*	15	
2.4e, grey	Wild-type	*w^+, iso31*	Same control flies as Figure 2.1c.	
2.4e, red	*w^+per^S*	*w^+per^S*	9am (16), 14 (1pm), 16 (5pm), 13 (8pm), 13 (9pm), 14 (11pm)	
Figure 2.5				
2.5a, brain	LNv > GFP	w^-; Pdf-Gal4 / UAS-myr::GFP; Pdf-Gal4 / +	Representative sample (2pm), of at least ten flies	
2.5a, VNC	LNv > GFP	w^-; Pdf-Gal4 / UAS-myr::GFP; + / +	Representative sample (2pm), of at least five flies	
2.5b	LNv > GFP	w^-; Pdf-Gal4 / UAS-myr::GFP; Pdf-Gal4 / +	Representative sample (2pm), of at least ten flies	
2.5c, black	UAS-GtACR1	w^+; +/+; UAS-GtACR1::eYFP / +	58 (2pm), 70 (2am)	Two-way ANOVA F(2,365)=30.28, interaction p<0.0001, with Tukey's multiple comparisons test. 2pm: UAS-control vs GFP control: p=0.7016. UAS control vs experimental:
2.5c, grey	LNv > GFP	w^-; Pdf-Gal4 / UAS-myr::GFP; Pdf-Gal4 / +	52 (2pm), 68 (2am)	
2.5c, blue	LNv > GtACR1	w^-; Pdf-Gal4 / +; Pdf-Gal4 / UAS-GtACR1::eYFP / +	62 (2pm), 61 (2am)	

				p<0.0001. GFP control vs experimental p<0.0001. 2am: UAS-control vs GFP control: p=0.9928. UAS control vs experimental: p=0.6758. GFP control vs experimental: p=0.9411.
2.5d		*w^+, iso31*	Representative sample (2pm), of at least ten flies	
2.5e, black	UAS-PDF-RNAi	w^-; UAS-Dicer2; UAS-PDF-RNAi	52 (2pm), 49 (2am)	Two-way ANOVA F(2,325)=33.52, interaction p<0.0001, with Tukey's multiple comparisons test. 2pm: UAS-control vs Gal4 control: p=0.4789. UAS control vs experimental: p<0.0001. Gal4 control vs experimental p<0.0001. 2am: UAS-control vs Gal4 control: p<0.0001. UAS control vs experimental: p=0.8602. Gal4 control vs experimental: p=0.0051.
2.5e, grey	LNv-Gal4	UAS-Dicer2 / y; Pdf-Gal4 / +; Pdf-Gal4 / +	43 (2pm), 68 (2am)	
2.5e, blue	LNv > PDF-RNAi	UAS-Dicer2 / y; Pdf-Gal4 / UAS-Dicer2; Pdf-Gal4 / PDF-RNAi	59 (2pm), 60 (2am)	
2.5f, black	*w^{1118}*	*w^{1118}*	72 (2pm), 74 (2am)	Two-way ANOVA F(2,404)=35.99, interaction p<0.0001, with Tukey's multiple comparisons test. 2pm: *han^{3369}* mutant vs *han^{5304}* mutant p=0.0228. WT control vs *han^{3369}* mutant: p=0.0020. WT control vs *han^{5304}* mutant: p<0.0001. 2am: *han^{3369}* mutant vs *han^{5304}* mutant p=0.0228. WT control vs *han^{3369}* mutant: p<0.0001. WT control vs *han^{5304}* mutant: p=0.0056.
2.5f, blue	*han^{3369}*	*han^{3369}*	63 (2pm), 71 (2am)	
2.5f, purple	*han^{5304}*	*han^{5304}*	65 (2pm), 65 (2am)	

Figure 2.6				
2.6a, orange	Small LNv (681) > GFP	w^-; JRC_SS00681 split-Gal4 hemidriver / +; JRC_SS00681 split-Gal4 hemidriver; UAS-myr::GFP	Representative sample of at least five flies	
2.6a, purple	Large LNv (645) > GFP	w^-; JRC_SS00645 split-Gal4 hemidriver / +; JRC_SS00645 split-Gal4 hemidriver; UAS-myr::GFP	Representative sample of at least five flies	
2.6b, left and right panels, black	UAS-PDF-RNAi	w^-; UAS-Dicer2; UAS-PDF-RNAi	30 (same flies in left and right panels)	
2.6b, left panel, grey	Small LNv (681) > GFP	w^-; JRC_SS00681 split-Gal4 hemidriver / +; JRC_SS00681 split-Gal4 hemidriver; UAS-myr::GFP	66	
2.6b, left panel, orange	Small LNv (681) > PDF-RNAi	w^-; JRC_SS00681 split-Gal4 hemidriver / UAS-Dicer2; JRC_SS00681 split-Gal4 hemidriver; UAS-PDF-RNAi	45	
2.6b, right panel, grey	Large LNv (645) > GFP	w^-; JRC_SS00645 split-Gal4 hemidriver / +; JRC_SS00645 split-Gal4 hemidriver; UAS-myr::GFP	46	
2.6b, right panel, purple	Large LNv (645) > PDF-RNAi	w^-; JRC_SS00645 split-Gal4 hemidriver / UAS-Dicer2; JRC_SS00645 split-Gal4 hemidriver; UAS-PDF-RNAi	44	

2.6c, left panel	UAS-PDF-RNAi	w^-; UAS-Dicer2; UAS-PDF-RNAi	Representative sample of ten flies	
2.6c, middle panel	Small LNv (681) > PDF-RNAi	w^-; JRC_SS00681 split-Gal4 hemidriver / UAS-Dicer2; JRC_SS00681 split-Gal4 hemidriver; UAS-PDF-RNAi	Representative sample of ten flies	
2.6c, right panel	Large LNv (645) > PDF-RNAi	w^-; JRC_SS00645 split-Gal4 hemidriver / UAS-Dicer2; JRC_SS00645 split-Gal4 hemidriver; UAS-PDF-RNAi	Representative sample of ten flies	
2.6d, first column (black)	UAS-PDF-RNAi	w^-; UAS-Dicer2; UAS-PDF-RNAi	30 (Quantification of Fig. 2.6b)	One-Way ANOVA $F(7,334)=14.56$, with Tukey's multiple comparisons test. 2pm: UAS control vs 681>PDF-RNAi: $p<0.0001$. UAS control vs R6>PDF-RNAi: $p=0.0463$. UAS control vs 645>PDF-RNAi: $p=0.9186$. UAS control vs C929>PDF-RNAi: $p=0.1092$. UAS control vs 645>GFP $p=0.0226$. UAS control vs 681>PDF-RNAi: $p=0.1901$. UAS control vs R6>GFP: $p>0.9999$. 645>GFP vs 645>PDF-RNAi: $p=0.9282$. 645>PDF-RNAi vs C929>PDF-RNAi: $p=0.7739$. 645>PDF-RNAi vs 681>PDF-RNAi: $p<0.0001$. 645>PDF-RNAi vs R6>PDF-RNAi: $p=0.0095$. C929>PDF-RNAi vs R6>PDF-RNAi: $p=0.0002$. 681>GFP vs 681>PDF-RNAi: $p<0.0001$.
2.6d, second column (Grey)	GFP control (645-Gal4)	w^-; JRC_SS00645 split-Gal4 hemidriver / +; JRC_SS00645 split-Gal4 hemidriver; UAS-myr::GFP	46 (Quantification of Fig. 2.6b)	
2.6d, third column (purple)	Large LNv > PDF-RNAi (645-Gal4)	w^-; JRC_SS00645 split-Gal4 hemidriver / UAS-Dicer2; JRC_SS00645 split-Gal4 hemidriver; UAS-PDF-RNAi	44 (Quantification of Fig. 2.6b)	
2.6d, fourth column (purple)	Large LNv > PDF-RNAi (C929-Gal4)	w^-; C929-Gal4 / UAS-Dicer2; UAS-PDF-RNAi / +	15	
2.6d, fifth column (grey)	GFP control (R6-Gal4)	UAS-Dicer2 / y; R6-Gal4/UAS-myr::GFP; UAS-Dicer2 / +	26	

2.6d, sixth column (orange)	Small LNv > PDF-RNAi (R6-Gal4)	UAS-Dicer2 / y; R6-Gal4/UAS-Dicer2; UAS-PDF-RNAi	14	681>GFP vs R6>PDF-RNAi: p=0.0002. 681>GFP vs R6>GFP: p=0.0002. 681>PDF-RNAi vs R6>PDF-RNAi: p=0.9999. R6>Myr vs R6>PDF-RNAi p=0.0875.
2.6d, seventh column (grey)	GFP control (681-Gal4)	w^-; JRC_SS00681 split-Gal4 hemidriver / +; JRC_SS00681 split-Gal4 hemidriver; UAS-myr::GFP	66 (Quantification of Fig. 2.6b)	
2.6d, eighth column (orange)	Small LNv > PDF-RNAi (681-Gal4)	w^-; JRC_SS00681 split-Gal4 hemidriver / UAS-Dicer2; JRC_SS00681 split-Gal4 hemidriver; UAS-PDF-RNAi	45 (Quantification of Fig. 2.6b)	
2.6e, black		w^-; UAS-Dicer2; UAS-PDF-RNAi	10 (Quantification of Fig. 2.6c)	ZT6: Two-way ANOVA $F(2,55)=59.78$, interaction $p<0.0001$, with Tukey's multiple comparisons test. Small LNv axons: UAS control vs lLNv>PDF-RNAi: p=0.9995. UAS control vs sLNv>PDF-RNAi: p<0.0001. sLNv>PDF-RNAi vs lLNv-PDF-RNAi: p<0.0001. large LNv axons: UAS control vs lLNv>PDF-RNAi: p<0.0001. UAS control vs sLNv>PDF-RNAi: p=0.3529. sLNv>PDF-RNAi vs lLNv-PDF-RNAi: p<0.0001.
2.6e, orange		w^-; JRC_SS00681 split-Gal4 hemidriver / UAS-Dicer2; JRC_SS00681 split-Gal4 hemidriver; UAS-PDF-RNAi	10 (Quantification of Fig. 2.6c)	
2.6e, purple		w^-; JRC_SS00645 split-Gal4 hemidriver / UAS-Dicer2; JRC_SS00645 split-Gal4 hemidriver; UAS-PDF-RNAi	10 (Quantification of Fig. 2.6c)	
Figure 2.7				
2.7a, black	Wild-type	*w^+, iso31*	92 (2pm)	
2.7a, blue	*$pdfr^{han}$*; UAS-Pdfr	*han^{3369}* / y; UAS-Pdfr-16 / +; Attp2 / + and *han^{5304}* / y; UAS-Pdfr-16 /+ ; Attp2 / +	154 (2pm). 78 (*han^{3369}*/y;UAS-Pdfr-16/+;+/+). 76 (*han^{5304}*/y;UAS	

			-Pdfr-16/+;+/+).	
2.7a, grey	*pdfr*^{han}; candidate-Gal4 > Pdfr	*han*^{3369} / y; Candidate-Gal4 > UAS-Pdfr-16 and *han*^{5304} / y; Candidate-Gal4 > UAS-Pdfr-16	274 candidate Gal4 lines	
2.7b, green	*pdfr*^{han}; R23E05-Gal4 > Pdfr	*han*^{3369} / y; teashirt-Gal80 / UAS-Pdfr-16; R23E05-Gal4 / + and *pdfr*^{han5304} / y; teashirt-Gal80/UAS-Pdfr-16; R23E05-Gal4 / +	56 (2pm)	
2.7b , blue	*han*^{3369}; UAS-Pdfr	*han*^{3369} / y; UAS-Pdfr-16 / +; Attp2 / +	78 (2pm), 45 (2am)	Two-way ANOVA F(2,347)=14.10, interaction p<0.0001, with Tukey's multiple comparisons test. 2pm: R23E05 rescue vs DN1a rescue: p=0.9993. Mutant vs R23E05 recue: p<0.0001. Mutant vs DN1a rescue: p<0.0001. 2am: R23E05 rescue vs DN1a rescue: p=0.8009. Mutant vs R23E05 recue: p=0.9999. Mutant vs DN1a rescue: p=0.7312.
2.7b , dark green	*han*^{3369}; R23E05-Gal4 > Pdfr	*han*^{3369} / y; UAS-Pdfr-16 / +; R23E05-Gal4 / +	71 (2pm), 67 (2am)	
2.7b , green	*han*^{3369}; DN1a-Gal4 > Pdfr	*han*^{3369} / y; teashirt-Ga80 / UAS-Pdfr-16; R23E05-Gal4 / +	52 (2pm), 60 (2am)	
2.7c	DN1a > GFP	w^{-}; teashirt-Gal80 / UAS-myr::GFP; R23E05-Gal4 / +	Representative sample (2am), of at least ten flies	
2.7d, left	DN1a > GFP with Clock antibody	w^{-}; teashirt-Gal80 / UAS-myr::GFP; R23E05-Gal4 / +	Representative sample (2pm), of at least ten flies	
2.7d, right	DN1a > GFP with Period antibody	w^{-}; teashirt-Gal80 / UAS-myr::GFP; R23E05-Gal4 / +	Representative sample (9am), of at least ten flies	
2.7e, black	UAS-GtACR1	w^{+}; +/+; UAS-GtACR1::eYFP / +	87 (2pm), 95 (2am)	Two-way ANOVA F(2,540)=100.4, interaction

2.7e, grey	DN1a > GFP	w^-; teashirt-Gal80 / UAS-myr::GFP; R23E05-Gal4 / +	64 (2pm), 103 (2am)	p = 0.0002, with Tukey's multiple comparisons test. 2pm: UAS-control vs GFP control: p=0.6804. UAS control vs experimental: p>0.9999. GFP control vs experimental: p=0.6590. 2am: UAS-control vs GFP control: p>0.9999. UAS control vs experimental: p=0.0003. GFP control vs experimental p=0.0001.
2.7e, green	DN1a > GtACR1	w^-; teashirt-Gal80/+; R23E05-Gal4/UAS-GtACR1::eYFP	85 (2pm), 112 (2am)	
2.7g, black	UAS-t-PDF	w^+; +/+; 10x UAS-tethered-PDF	62 (2pm), 88 (2am)	Two-way ANOVA F(2,331)=7.990, interaction p=0.0004, with Tukey's multiple comparisons test. 2pm: UAS-control vs GFP control: p=0.0111. UAS control vs experimental: p=0.2058. GFP control vs experimental p=0.8725. 2am: UAS-control vs GFP control: p=0.9846. UAS control vs experimental: p<0.0001. GFP control vs experimental: p=0.0001.
2.7g, grey	DN1a > GFP	w^-; teashirt-Gal80 / UAS-myr::GFP; R23E05-Gal4/+	41 (2pm), 43 (2am)	
2.7g, green	DN1a > t-PDF	w^-; teashirt-Gal80 / +; R23E05-Gal4 / 10x UAS tethered-PDF	48 (2pm), 55 (2am)	
Figure 2.8				
2.8a, blue	*han*^{5304}; UAS-Pdfr	*han*^{5304} / y; UAS-Pdfr-16 /+ ; Attp2 / +	76 (2pm), 55 (2am)	Two-way ANOVA F(2,383)=34.21, interaction p<0.0001, with Tukey's multiple comparisons test. 2pm: R23E05 rescue vs DN1a rescue: p<0.0001. Mutant vs R23E05 recue: p<0.0001. Mutant vs DN1a rescue: p<0.0001. 2am: R23E05 rescue vs DN1a rescue: p=0.9898. Mutant vs R23E05 recue: p=0.5132. Mutant vs DN1a rescue: p=0.9348.
2.8a, dark green	*han*^{5304}; R23E05-Gal4 > Pdfr	*han*^{5304} / y; UAS-Pdfr-16 / + ; R23E05-Gal4 / +	68 (2pm), 77 (2am)	
2.8a , green	*han*^{5304};DN 1a-Gal4 > Pdfr	*han*^{5304} / y; teashirt-Ga80/UAS-Pdfr-16; R23E05-Gal4 / +	68 (2pm), 45 (2am)	
2.8b	R23E05 > RedStinger	w^-; UAS-RedStinger / +; R23E05-Gal4 / +	Representative sample of at least ten flies	

2.8c	DN1a > myr::GFP	w^-; teashirt-Gal80 / UAS-myr::GFP; R23E05-Gal4/+	Representative sample of at least five flies	
2.8d	DN1a > Denmark, Syt::GFP	w^-; teashirt-Gal80 / repo-Gal80; UAS-Denmark, UAS-Syt::GP; R23E05-Gal4/+	Representative sample of at least ten flies	
2.8e, top	R23E05 > myr::GFP	w^-; UAS-myr::GFP / +; R23E05-Gal4 / +	Representative sample of at least ten flies	
2.8e, bottom	R23E05 > myr::GFP, tsh-Gal80	w^-; teashirt-Gal80 / UAS-myr::GFP; R23E05-Gal4/+	Representative sample of at least ten flies	
Figure 2.9				
2.9a, first column (black)	UAS-Clock-RNAi	w+;UAS-Clock-RNAi/+; UAS-Dicer2 / +	74 (2am, same flies as Figure 2.3b).	One-way ANOVA $F(8,739)=2.557$, $p=0.0094$, with Tukey's post hoc test. UAS-GtACR1 (from LNv experiments) vs: LNv>GFP, p=0.8765. LNv>GtACR1, p>0.9999. UAS-GtACR1 (from DN1a experiments), p=0.5163. DN1a>GFP, p=0.9487. DN1a>GtACR1, p>0.9999. Tim>Clk-RNAi, p=0.8894. UAS-Clk-RNAi, p>0.9999. Tim>GFP, p=0.9983. LNv>GFP vs: LNv>GtACR1, p=0.9431. UAS-GtACR1 (from DN1a experiments), p>0.9999. DN1a>GFP, p>0.9999. DN1a>GtACR1, p=0.7552. Tim>Clk-RNAi, p=0.1099. UAS-Clk-RNAi, p=0.8358 Tim>GFP, p=0.4054. LNv>GtACR1 vs: UAS-GtACR1 (from DN1a experiments), p=0.6823. DN1a>GFP, p=0.9837. DN1a>GtACR1, p>0.9999. Tim>Clk-RNAi, p=0.8443. UAS-Clk-RNAi, p>0.9999.. Tim>GFP, p=0.9948.
2.9a, second column (grey)	Tim > GFP	w-; Tim(UAS)-Gal4, Repo-Gal80 / UAS-myr::GFP; UAS-Dicer2 / +	75 (2am, same flies as Figure 2.3b).	
2.9a, third column (red)	Tim > Clock-RNAi	w-; Tim(UAS)-Gal4, Repo-Gal80 / UAS-Clock-RNAi; UAS-Dicer2 / UAS-Dicer2	61 (2am, same flies as Figure 2.3b).	
2.9a, fourth column (black)	UAS-GtACR1	w^+; +/+; UAS-GtACR1::eYFP / +	70 (2am) . Same flies as Figure 2.5c.	
2.9a, fifth column (grey)	LNv > GFP	w^-; Pdf-Gal4 / UAS-myr::GFP; Pdf-Gal4 / +	68 (2am) . Same flies as Figure 2.5c.	
2.9a, sixth column (blue)	LNv > GtACR1	w^-; Pdf-Gal4 / +; Pdf-Gal4 / UAS-GtACR1::eYFP / +	61 (2am) . Same flies as Figure 2.5c.	
2.9a, seventh column (black)	UAS-GtACR1	w^+; +/+; UAS-GtACR1::eYFP / +	95 (2am). Same flies as Figure 2.7e.	
2.9a, eighth column (grey)	DN1a > GFP	w^-; teashirt-Gal80 / UAS-myr::GFP; R23E05-Gal4 / +	103 (2am). Same flies as Figure 2.7e.	
2.9a, ninth column (grey)	DN1a > GtACR1	w^-; teashirt-Gal80/+; R23E05-Gal4/UAS-GtACR1::eYFP	112 (2am). Same flies as Figure 2.7e.	

				UAS-GtACR1 (from DN1a experiments) vs: DN1a>GtACR1, p=0.2866. DN1a>GFP, p=0.9922 Tim>Clk-RNAi, p=0.0139. UAS-Clk-RNAi, p=0.4602. Tim>GFP, p=0.0965. DN1a>GFP vs: DN1a>GtACR1, p=0.8597. Tim>Clk-RNAi, p=0.1327. UAS-Clk-RNAi, p=0.9212. Tim>GFP, p=0.4974. DN1a>GtACR1 vs: Tim>Clk-RNAi, p=0.8524. UAS-Clk-RNAi, p>0.9999. Tim>GFP, p=0.9981. Tim>Clk-RNAi vs: UAS-Clk-RNAi, p=0.9356. Tim>GFP, p=0.9983. UAS-Clk-RNAi vs Tim>GFP, p=0.9996.
2.9b, left, black	UAS-GtACR1	w^+; +/+; UAS-GtACR1::eYFP / +	26	One-way ANOVA F(8,739)=16.15, p<0.0001, with Tukey's post hoc test. UAS-GtACR1 (from LNv experiments) vs: LNv>GFP, p<0.0001. LNv>GtACR1, p=0.9951. UAS-GtACR1 (from DN1a experiments), p>0.9999. DN1a>GFP, p>0.9999 . DN1a>GtACR1, p=0.0176. Tim>Clk-RNAi, p<0.0001. UAS-Clk-RNAi, p=0.9424. Tim>GFP, p=0.6718. LNv>GFP vs: LNv>GtACR1, p=0.0034. UAS-GtACR1 (from DN1a experiments), p<0.0001. DN1a>GFP, p<0.0001. DN1a>GtACR1, p<0.0001. Tim>Clk-RNAi, p<0.0001. UAS-Clk-RNAi, p<0.0001.
2.9b, left, grey	LNv > GFP	w^-; Pdf-Gal4/UAS-myr::GFP; Pdf-Gal4 / +	23	
2.9b, left, blue	LNv > GtACR1	w^-; Pdf-Gal4 / +; Pdf-Gal4 / GtACR1::eYFP	23	
2.9b, left, grey	DN1a > GFP	w^-; teashirt-Gal80 / UAS-myr::GFP; R23E05-Gal4 / +	28	
2.9b, left, green	DN1a > GtACR1	w^-; teashirt-Gal80/+; R23E05-Gal4/UAS-GtACR1::eYFP	26	
2.9b, right, black	UAS-GtACR1	w^+; +/+; UAS-GtACR1::eYFP / +	70 (2am) . Same flies as Figure 2.5c.	
2.9b, right, grey	LNv > GFP	w^-; Pdf-Gal4 / UAS-myr::GFP; Pdf-Gal4 / +	68 (2am) . Same flies as Figure 2.5c.	
2.9b, right, blue	LNv > GtACR1	w^-; Pdf-Gal4 / +; Pdf-Gal4 / UAS-GtACR1::eYFP / +	61 (2am) . Same flies as Figure 2.5c.	

2.9b, right, black	UAS-GtACR1	w^+; +/+; UAS-GtACR1::eYFP / +	95 (2am). Same flies as Figure 2.7e.	Tim>GFP, p<0.0001. LNv>GtACR1 vs: UAS-GtACR1 (from DN1a experiments), p=0.9629. DN1a>GFP, p=0.9983. DN1a>GtACR1, p=0.0008. Tim>Clk-RNAi, p<0.0001. UAS-Clk-RNAi, p=0.5040. Tim>GFP, p=0.1798. UAS-GtACR1 (from DN1a experiments) vs: DN1a>GFP, p=0.0160 Tim>Clk-RNAi, p<0.0001. UAS-Clk-RNAi, p=0.9757. Tim>GFP, p=0.7553. DN1a>GFP vs: DN1a>GtACR1, p=0.0016. Tim>Clk-RNAi, p=0.8214. Tim>GFP, p=0.4081. DN1a>GtACR1 vs: Tim>Clk-RNAi, p=0.2890. UAS-Clk-RNAi, p=0.5668. Tim>GFP, p=0.8594. Tim>Clk-RNAi vs: UAS-Clk-RNAi, p=0.0042. Tim>GFP, p=0.0153. UAS-Clk-RNAi vs Tim>GFP, p>0.9999.
2.9b, right, grey	DN1a > GFP	w^-; teashirt-Gal80 / UAS-myr::GFP; R23E05-Gal4 / +	103 (2am). Same flies as Figure 2.7e.	
2.9b, right, green	DN1a > GtACR1	w^-; teashirt-Gal80/+; R23E05-Gal4/UAS-GtACR1::eYFP	112 (2am). Same flies as Figure 2.7e.	
2.9c, first column (brown)	GMR-hid	w^+; GMR-hid[10]	8	One-way ANOVA $F(3,28)=14.47$, p<0.0001, with Tukey's post hoc test. GMR-hid vs: UAS-Clk-RNAi, p<0.0001. Tim>GFP, p<0.0001. Tim>Clk-RNAi, p=0.0008. UAS-GtACR1, p<0.0001. LNv>GFP, p<0.0001. LNv>GtACR1, p<0.0001. DN1a>GFP, p<0.0001. DN1a>GtACR1, p<0.0001. UAS-Clk-RNAi vs: Tim>GFP, p=0.9999.
2.9c, second column (black)	UAS-Clock-RNAi	w+;UAS-Clock-RNAi/+; UAS-Dicer2 / +	8	
2.9c, third column (grey)	Tim > GFP	w-; Tim(UAS)-Gal4, Repo-Gal80 / UAS-myr::GFP; UAS-Dicer2 / +	8	
2.9c, fourth colun (red)	Tim > Clock-RNAi	w-; Tim(UAS)-Gal4, Repo-Gal80 / UAS-Clock-RNAi; UAS-Dicer2 / UAS-Dicer2	8	

2.9c, fifth column (black)	UAS control	w^+; +/+; UAS-GtACR1::eYFP / +	8	Tim>Clk-RNAi, p=0.9878. UAS-GtACR1, p=0.7868. LNv>GFP, p>0.9999. LNv>Gtacr1, p=0.9992. DN1a>GFP, p>0.9999. DN1a>GtACR1, p=0.9973. Tim>Clock-RNAi vs: UAS-GtACR1, p =0.2117. LNv>GFP, p=0.9956. DN1a>GFP, p =0.9884. DN1a>GtACR1, p=0.7247. UAS-GtACR1 vs: LNv>GFP, p=0.7055. LNv>GtACR1, p=0.9864. DN1a>GFP, p=0.7830. DN1a>GtACR1: p=0.9944. LNv>GFP vs: LNv>GtACR1, p=0.9970. DN1a>GFP, p>0.9999. DN1a>GtACR1, p=0.9919. LNv>GtACR1 vs: DN1a>GFP: p=0.9992. DN1a>GtACr1: p>0.9990. DN1a>GFP vs DN1a>GtACR1: p>0.9972.
2.9c, sixth column (grey)	GFP control	w^-; Pdf-Gal4 / UAS-myr::GFP; Pdf-Gal4 / +	8	
2.9c, seventh column (red)	LNv > GtACR1	w^-; Pdf-Gal4 / +; Pdf-Gal4 / UAS-GtACR1::eYFP / +	8	
2.9c, eighth column (grey)	GFP control	w^-; teashirt-Gal80 / UAS-myr::GFP; R23E05-Gal4 / +	8	
2.9c, ninth column (green)	DN1a > GtACR1	w^-; teashirt-Gal80/+; R23E05-Gal4/UAS-GtACR1::eYFP	8	
Figure3.1				
3.1a	LNv > GFP; DN1a > GFP	w^-; teashirt-Gal80, PDF-LexA LexAop-myr::TdTomato; R23E05-Gal4/UAS-myr::GFP	Representative sample (2am), of at least ten flies	
3.1b, left	LNv > Denmark; R23E05 > syt::GFP	w^-; Pdf-Gal4 / UAS-DenMark; R23E05-LexA / LexAop-syt::GDP::HA	Representative sample (2am), of at least ten flies	
3.1b, right	R23E05 > Denmark; LNv > syt::GFP	w^-; PDF-LexA / UAS-DenMark; R23E05-Gal4 / LexAop-syt::GDP::HA	Representative sample (2pm), of at least ten flies	

3.1c, left	LNv > GFP, *trans*-Tango	w^-; UAS-myr::GFP.QUAS-mtdTomato-3xHA; Pdf-Gal4 / *trans*-Tango; Pdf-Gal4/+	Representative sample of at least ten flies	
3.1c, right	DN1a > GFP, *trans*-Tango	w^-; UAS-myr::GFP.QUAS-mtdTomato-3xHA; teashirt-Gal80 / *trans*-Tango; R23E05-Gal4 / +	Representative sample of at least ten flies	
3.1d, grey	LNv > $P2X_2$; R23E05 > GCaMP (saline)	w^-; PDF-LexA / UAS-op-GCaMP6s; R23E05-Gal4 / LexAop-$P2X_2$	13 (2am)	2am Minimum: One-way ANOVA $F(2,34)=9.721$, $p=0.0005$, with Tukey's multiple comparisons test. 2am minimum: No $P2X_2$ control vs saline control: $p=0.9903$. No $P2X_2$ control vs experimental: $p=0.0020$. Saline control vs experimental $p=0.0011$. 2am Maximum: One-way ANOVA $F(2,34)=0.1978$, $p=0.8214$, with no multiple comparisons.
3.1d, black	LNv > R23E05 > GCaMP	w^-; PDF-LexA / UAS-op-GCaMP6s; R23E05-Gal4 / +	12 (2am)	
3.1d, green	LNv > $P2X_2$; R23E05 > GCaMP	w^-; PDF-LexA / UAS-op-GCaMP6s; R23E05-Gal4 / LexAop-$P2X_2$	12 (2am)	
3.1e, grey	R23E05 > $P2X_2$; LNv > GCaMP (saline)	w^-; Pdf-Gal4 / UAS-op-GCaMP6s; R23E05-LexA / LexAop-$P2X_2$	13 (2pm)	2pm Minimum: One-way ANOVA $F(2,38)=6.646$, $p=0.0033$, with Tukey's multiple comparisons test. 2pm minimum: No $P2X_2$ control vs saline control: $p=0.8549$. No $P2X_2$ control vs experimental: $p=0.0050$. saline control vs experimental $p=0.0175$. 2pm Maximum: One-way ANOVA $F(2,38)=2.345$, $p=0.1095$, with no multiple comparisons.
3.1e, black	R23E05 > LNv > GCaMP	w^-; Pdf-Gal4 / UAS-op-GCaMP6s; R23E05-LexA / +	13 (2pm)	
3.1e, blue	R23E05 > $P2X_2$; LNv > GCaMP	w^-; Pdf-Gal4 / UAS-op-GCaMP6s; R23E05-LexA / LexAop-$P2X_2$	14 (2pm)	
Figure 3.2				
3.2a	R23E05-LexA > LexAop-Myr::GFP	w^-; +/+; R23E05-LexA / 13xLexAop2-IVS-Myr::GFP	Representative sample of at least five flies	
3.2b		w^-; teashirt-Gal80, PDF-LexA LexAop-	Single confocal stack from Figure 3.1a	

		myr::TdTomato; R23E05-Gal4/UAS-myr::GFP		
3.2b		w^-; UAS-myr::GFP.QUAS-mtdTomato-3xHA; teashirt-Gal80 / *trans*-Tango; R23E05-Gal4 / +	Single confocal stack from Figure 3.1c	
3.2b		w^-; UAS-myr::GFP.QUAS-mtdTomato-3xHA; teashirt-Gal80 / *trans*-Tango; R23E05-Gal4 / +	Single confocal stack from Figure 3.1c	
3.2b		w^-; UAS-myr::GFP.QUAS-mtdTomato-3xHA; Pdf-Gal4 / *trans*-Tango; Pdf-Gal4/+	Single confocal stack from Figure 3.1c	
3.2c, middle	LNv-LexA; R23E05 > GCaMP	w^-; PDF-LexA / UAS-op-GCaMP6s; R23E05-Gal4 / LexAop-P2X$_2$	Representative sample (2am).	
3.2c, right	LNv-LexA; R23E05 > GCaMP	w^-; PDF-LexA / UAS-op-GCaMP6s; R23E05-Gal4 / +	Representative baseline activity (2am).	
3.2d, left	LNv > P2X2; R23E05 > GCaMP (saline)	w^-; PDF-LexA / UAS-op-GCaMP6s; R23E05-Gal4 / LexAop-P2X$_2$	13 (2am). Individual trials from Figure 3.1d.	
3.2d, middle	LNv-LexA; R23E05 > GCaMP	w^-; PDF-LexA / UAS-op-GCaMP6s; R23E05-Gal4 / +	12 (2am). Individual trials from Figure 3.1d.	
3.2d, right	LNv > P2X2; R23E05 > GCaMP	w^-; PDF-LexA / UAS-op-GcaMP6s; R23E05-Gal4 / LexAop-P2X$_2$	12 (2am). Individual trials from Figure 3.1d.	
3.2e, middle	R23E05-LexA; LNv > GCaMP	w^-; Pdf-Gal4 / UAS-op-GCaMP6s; R23E05-LexA / +	Representative sample (2pm).	

3.2e, right	R23E05-LexA LNv > GCaMP	w^-; Pdf-Gal4 / UAS-op-GCaMP6s; R23E05-LexA / +	Representative baseline activity (2pm).	
3.2f, left	R23E05-LexA; LNv > GCaMP	w^-; Pdf-Gal4 / UAS-op-GCaMP6s; R23E05-LexA / +	13 (2pm). Individual trials from Figure 3.1e.	
3.2f, middle	R23E05 > P2X2; LNv > GCaMP (saline)	w^-; Pdf-Gal4 / UAS-op-GCaMP6s; R23E05-LexA / LexAop-P2X2	13 (2pm). Individual trials from Figure 3.1e.	
3.2e, right	R23E05 > P2X2; LNv > GCaMP	w^-; Pdf-Gal4 / UAS-op-GCaMP6s; R23E05-LexA / LexAop-$P2X_2$	14 (2pm). Individual trials from Figure 3.1e.	
3.2g, left	PDF-LexA > LexAop-Myr::GFP	w^-; PDFLexA / +; 13xLexAop2-IVS-Myr::GFP / +	Representative sample of nine flies	
3.2g, middle	R23E05-LexA > LexAop-Myr::GFP	w^-; +/+; R23E05-LexA / 13xLexAop2-IVS-Myr::GFP / +	Representative sample of ten flies	
3.2g, right, blue		w^-; PDFLexA / +; 13xLexAop2-IVS-Myr::GFP / +	9	Unpaired t-test t(17)=10.34, p<0.0001.
3.2g, right, green		w^-; +/+; R23E05-LexA / 13xLexAop2-IVS-Myr::GFP / +	10	
Figure 3.3				
3.3a	R23E05 > myr::GFP	w^-; / UAS-myr::GFP; R23E05-Gal4 / +	Representative sample of at least ten flies	
3.3b, top, black	UAS-CCHa1-RNAi	w^+; UAS-CCHa1-RNAi / +; +/+	42 (2pm), 44 (2am)	Two-way ANOVA F(2,289)=6.517, interaction p=0.0017, with Tukey's multiple comparisons test. 2pm: UAS-control vs GFP control: p=0.0005. UAS control vs experimental: p=0.0384. GFP control vs experimental p<0.0001.
3.3b, top, grey	R23E05 > GFP	w^-; UAS-Dicer2 / UAS-myr::GFP; R23E05-Gal4 / +	55 (2pm), 48 (2am)	
3.3b, top, green	R23E05 > CCHa1-RNAi	w^-; UAS-Dicer2 / UAS- CCHa1; R23E05-Gal4 / +	51 (2pm), 55 (2am)	

				2am: UAS-control vs FP control: p=0.9599. UAS control vs experimental: p=0.2008. GFP control vs experimental: p=0.6900.
3.3b, bottom, black	UAS-CCHa1R-RNAi	w^+; UAS-CCHa1R-RNAi / +; +/+	49 (2pm), 61 (2am)	Two-way ANOVA $F(2,311)=0.4671$, interaction p=0.6272, no multiple comparisons test.
3.3b, bottom, grey	LNv > GFP	UAS-Dicer2 / y; Pdf-Gal4 / UAS-myr::GFP; Pdf-Gal4 / +	58 (2pm), 63 (2am)	
3.3b, blue	LNV > CCHa1R-RNAi	UAS-Dicer2 / y; Pdf-Gal4 / UAS-CCHa1R-RNAi; Pdf-Gal4 / +	41 (2pm), 45 (2am)	
3.3c, black	UAS-mGluRA-RNAi	w^+; +/+; UAS-mGluRA-RNAi	61 (2pm), 44 (2am)	Two-way ANOVA $F(2,324)=13.51$, interaction p<0.0001, with Tukey's multiple comparisons test. 2pm: UAS-control vs GFP control: p=0.6464. UAS control vs experimental: p=0.2398. GFP control vs experimental: p=0.0034. 2am: UAS-control vs GFP control: p=0.9606. UAS control vs experimental: p=0.0031. GFP control vs experimental: p=0.0348.
3.3c, grey	LNv > GFP	w^-; Pdf-Gal4 / UAS-mCD8::GFP; Pdf-Gal4 / +	65 (2pm), 51 (2am)	
3.3c, blue	LNV > mGluRA-RNAi	w^-; Pdf-Gal4 / +; Pdf-Gal4 / UAS-mGluRA-RNAi	53 (2pm), 56 (2am)	
Figure 3.4				
3.4a, left panel, top images	LNv > GFP	w^-; Pdf-Gal4 / + ; UAS-myr::GFP / +	Representative samples (2pm, 2am) of at least ten flies	
3.4a, left panel, bottom images	DN1a > GFP	w^-; teashirt-Gal80 / UAS-myr::GFP; R23E05-Gal4 / +	Representative samples (2pm, 2am) of at least ten flies	
3.4a, middle panel		w^-; Pdf-Gal4 / + ; UAS-myr::GFP / +	40 hemispheres (2pm), 34 hemispheres (2am)	Unpaired t test $t(72)=4.200$, p<0.0001.

3.4a, right panel		w^-; teashirt-Gal80 / UAS-myr::GFP; R23E05-Gal4 / +	133 hemispheres (2pm), 174 hemispheres (2am).	Two-way ANOVA $F(1,610)=9.709$, interaction $p=0.0019$, with Tukey's multiple comparisons test. 2pm VL tract vs 2am VL tract: $p<0.0001$. 2pm VM tract vs 2am VM tract: $p=0.9930$.
3.4b, left panel, top images	LNv > myr::GFP; brp::Cherry	w^-; Pdf-Gal4 / UAS-myr::GFP; Pdf-Gal4/UAS-brp-D3::mCherry	Representative samples (2pm, 2am) of at least ten flies	
3.4b, left panel, bottom images	DN1a > myr::GFP; brp::Cherry	w^-; teashirt-Gal80 / UAS-myr::GFP; R23E05-Gal4 / UAS-brp-D3::mCherry	Representative samples (2pm, 2am) of at least ten flies	
3.4b, middle panel		w^-; Pdf-Gal4 / UAS-myr::GFP; Pdf-Gal4 / UAS-brp-D3::mCherry	10 hemispheres (2pm), 20 hemispheres (2am)	Unpaired t test $t(28)=5.254$, $p<0.0001$.
3.4b, right panel		w^-; teashirt-Gal80 / UAS-myr::GFP; R23E05-Gal4 / UAS-brp-D3::mCherry	18 hemispheres (2pm), 18 hemispheres (2am)	Two-way ANOVA $F(1,62)=6.417$, interaction $p=0.0138$, with Tukey's multiple comparisons test. 2pm VL tract vs 2am VL tract: p-0.0395. 2pm VM tract vs 2am VM tract: $p=0.8316$.
3.4c	LNv > GFP, Brp	w^-; Pdf-Gal4 / UAS-myr::GFP; Pdf-Gal4 / UAS-brp-D3::mCherry	30 (same flies as Figure 4A, pooled 2pm and 2am)	Pearson correlation $r=0.83$, $p<0.0001$.
3.4d	DN1a > GFP, Brp	w^-; teashirt-Gal80 / UAS-myr::GFP; R23E05-Gal4 / UAS-brp-D3::mCherry	57 (same flies as Figure 4B, pooled 2pm and 2am)	Pearson correlation $r=0.46$, $p=0.0004$.
3.4e, top images	per^{01}; LNv > GFP	per^{01}; Pdf-Gal4 / +; Pdf-Gal4 / UAS-myr::GFP	Representative samples (2pm, 2am) of at least ten flies	
3.4e, bottom images	per^{01}; R23E05 > GFP	per^{01}; teashirt-Gal80 / + ;	Representative samples (2pm,	

		R23E05-Gal4 / UAS-myr::GFP	2am) of at least ten flies	
3.4e, middle panel		*per*^{01}; Pdf-Gal4 / +; Pdf-Gal4 / UAS-myr::GFP	37 hemispheres (2pm), 30 hemispheres (2am)	Unpaired t test t(67)=1.822, p=0.0730.
3.4e, right panel		*per*^{01}; teashirt-Gal80 / + ; R23E05-Gal4 / UAS-myr::GFP	59 hemispheres (2pm), 43 hemispheres (2am)	Two-way ANOVA F(1,200)=1.619, interaction p=0.2048, with no multiple comparisons.
Figure 3.5				
3.5a, top row	LNv > GFP	w$^-$; Pdf-Gal4 / + ; UAS-myr::GFP / +	Representative samples (2pm, 2am) of at least ten flies	
3.5a, bottom left image	LNv > GFP, Rho1	w$^-$; Pdf-Gal4 / +; UAS-myr::GFP / UAS-Rho1.Sph	Representative samples (2pm) of at least ten flies	
3.5a , bottom right image	LNv > GFP, Rho1-RNAi	w -; Pdf-Gal4 / UAS-Rho1-dsRNA; UAS-myr::GFP / UAS-Dicer2	Representative samples (2am) of at least ten flies	
3.5a , blue circles		w$^-$; Pdf-Gal4 / +; UAS-myr::GFP / +	67 hemispheres (2pm), 34 hemispheres (2am)	One-way ANOVA F(3,165)=8.681, p<0.0001, with Tukey's multiple comparisons test. 2pm control vs 2am control: p=0.0048. 2pm control vs LNv>Rho1: p=0.0019. 2am control vs 2am LNv>Rho1-RNAi: p=0.0029.
3.5a , blue upward triangle (Rho1 OE)		w$^-$; Pdf-Gal4 / +; UAS-myr::GFP / UAS-Rho1.Sph	45 hemispheres (2pm)	
3.5a , blue downward triangle (Rho1-RNAi)		w$^-$; Pdf-Gal4 / UAS-Rho1-dsRNA; UAS-myr::GFP / UAS-Dicer2	22 hemispheres (2am)	
3.5b, top row	R23E05 > GFP	w$^-$; UAS-myr::GFP / +; R23E05-Gal4 / +	Representative samples (2pm) of at least ten flies	
3.5b, bottom left image	R23E05 > GFP, Rho1-RNAi	w$^-$; UAS-myr::GFP / UAS-Rho1-dsRNA; R23E05-Gal4 / +	Representative samples (2pm) of at least ten flies	

3.5b, bottom right image	R23E05 > GFP, Rho1	w^-; UAS-myr::GFP / +; R23E05-Gal4 / UAS-Rho1.Sph	Representative samples (2am) of at least ten flies	
3.5b, green circles		w^-; UAS-myr::GFP / + ; R23E05-Gal4 / +	33 hemispheres (2pm), 37 hemispheres (2am)	One-way ANOVA $F(7,280)=12.98$, $p<0.0001$, with Tukey's multiple comparisons test. VL: 2pm control vs 2am control: p=0.0160. 2pm control vs DN1a>Rho1: p=0.0002. 2am control vs 2am DN1a>Rho1: p<0.0001. VM: 2pm control vs 2am control: p>0.9999. 2pm control vs DN1a>Rho1: p>0.9999. 2am control vs 2am DN1a>Rho1: p>0.9999.
3.5b, downward triangle (Rho1-RNAi)		w^-; UAS-myr::GFP / UAS-Rho1-dsRNA; R23E05-Gal4 / +	32 hemispheres (2pm)	
3.5b, upward triangle (Rho1 OE)		w^-; UAS-myr::GFP / +; R23E05-Gal4 / UAS-Rho1.Sph	40 hemispheres (2am)	
3.5c, black	UAS-Rho1	w^+; +/+; UAS-Rho1.Sph / +	71 (2pm), 2am (68)	Two-way ANOVA $F(3,546)=10.25$, interaction $p<0.0001$, with Tukey's multiple comparisons test. 2pm: UAS-control vs LNv>GFP control: p=0.8420. UAS control vs LNv>Rho1: p=0.001. UAS control vs DN1a>Rho1: p>0.9999. LNv>GFP control vs LNv>Rho1: p<0.0001. LNv>GFP control vs DN1a>Rho1: p=0.7598. LNv>Rho1 vs DN1a>Rho1: p=0.0006. 2am: UAS-control vs DN1a>GFP control: p=0.3743. UAS control vs LNv>Rho1: p=0.9269. UAS control vs DN1a>Rho1: p=0.0094. LNv>GFP control vs LNv>Rho1: p=0.9981.
3.5c, grey (2pm)	GFP Control, left	w^-; Pdf-Gal4 / UAS-myr::GFP; Pdf-Gal4 / +	57	
3.5c, grey (2am)	GFP Control, right	w^-; teashirt-Gal80 / UAS-myr::GFP; R23E05-Gal4/+	73	
3.5c , blue	Rho1 OE in LNvs	w^-; Pdf-Gal4 / + ; Pdf-Gal4 / UAS-Rho1.Sph	97 (2pm), 42 (2am)	

3.5c , green	Rho1 OE in DN1as	w^-; teashirt-Gal80 / +; R23E05-Gal4 / UAS-Rho1.Sph	64 (2pm), 82 (2am)	DN1a>GFP control vs DN1a>Rho1: p<0.0001. LNv>Rho1 vs DN1a>Rho1: p=0.0005.
Figure 3.6				
3.6a	UAS-Rho1	w^+; +/+; UAS-Rho1.Sph / +	24	
3.6a	LNv > GFP	w^-; Pdf-Gal4 / UAS-myr::GFP; Pdf-Gal4 / +	24	
3.6a	LNv > Kir2.1	w^-; Pdf-Gal4 / UAS-Kir2.1; Pdf-Gal4 / +	17	
3.6a	LNv > Rho1	w^-; Pdf-Gal4 / + ; Pdf-Gal4 / UAS-Rho1.Sph	22	
3.6a	DN1a > GFP	w^-; teashirt-Gal80 / UAS-myr::GFP; R23E05-Gal4/+	24	
3.6a	DN1a > Rho1	w^-; teashirt-Gal80 / +; R23E05-Gal4 / UAS-Rho1.Sph	21	
Figure 4.1				
4.1a	Wild-type	*w^+, iso31*	44 (same animals as Table S2, aside from 2 deceased animals).	
4.1b	Wild-type	*w^+, iso31*	46 (same flies as Table S2)	
4.1c,d	Wild-type	*w^+, iso31*	29 (6am), 29 (8am), 32 (10am), 26 (6pm), 27 (8pm), 26 (20pm)	
Figure 4.3				
4.3a	DN1a > myr::GFP	w^-; teashirt-Gal80/+; R23E05-Gal4/UAS-GtACR1::eYFP	6 hemispheres	
4.3a	DN1a > GtACR1:: YFP	w^-; teashirt-Gal80/+; R23E05-Gal4/UAS-GtACR1::eYFP	6 hemispheres	

4.3a	DN1a > GtACR1::YFP	w⁻; teashirt-Gal80/+; R23E05-Gal4/UAS-GtACR1::eYFP	6 hemispheres	
4.3a	DN1a > Chrimson::mVenus	w⁻; teashirt-Gal80/UAS-Chrimson::mVenus; R23E05-Gal4/+	6 hemispheres	
4.3a	DN1a > Chrimson::mVenus	w⁻; teashirt-Gal80/UAS-Chrimson::mVenus; R23E05-Gal4/+	6 hemispheres	

Supplementary Table 2. Circadian rhythmicity during the first four days in darkness

Genotype	N	% Rhythmic after 4 days in darkness	Tau (S.E.M.)	Power (S.E.M.)
w^+, iso31	46	100	23.9 (0.12)	71.9 (1.7)
UAS-Clock-RNAi	23	100	23.8 (0.12)	74 (2.44)
Tim > GFP	24	100	23.6 (0.1)	86.3 2.33)
Tim > Clock-RNAi	22	9.1	17.8 (0.75)	22.7 (2.55)
UAS-Period-RNAi	23	100	24.7 (0.13)	71.9 (1.7)
Tim > Period-RNAi	24	0	****	****
w^+per^s	19	94.7	18.9 (0.05)	69.8 (4.82)
UAS-GtACR1	20	95	23.6 (0.06)	68.2 (4.91)
LNv > GFP	24	100	24.3 (0.16)	71 (2.47)
LNv > GtACR1	21	52.4	23.8 (0.31)	53.8 (5.3)
UAS-Kir2.1	20	94.4	23.7(0.15)	74.7 (3.52)
LNv > Kir2.1	17	70.6	23 (0.13)	66.7 (5.71)
DN1a > GFP	25	84	23.8 (0.11)	56 (4.59)
DN1a > GtACR1	19	78.9	23.9 (0.23)	37.8 (3.49)
han^{3369}; UAS-PDFR16	14	57.1	23.4 (0.48)	52.9 (7.09)
han^{5304}; UAS-PDFR16	17	70.6	23.1 (0.21)	46.2 (5.56)
han^{3369}; DN1a > PDFR16	10	90	23.4 (0.15)	66 (7.86)
han^{5304}; DN1a > PDFR16	17	100	22.9 (0.12)	84.1 (3.82)
UAS-tethered PDF	22	95.5	23.5 (0)	87.5 (3.79)
DN1a > tethered PDF	21	100	23.5 (0.02)	87.8 (3)
UAS-Rho1	24	95.8	23.7 (0.09)	72.2 (3.26)
LNv > Rho1	22	90.9	24.8 (0.28)	52 (2.74)
DN1a > Rho1	21	95.2	23.5 (0.07)	71.5.4 (3.95)
UAS-Rho1-RNAi	24	95.8	23.9 (0.13)	73.8 (3.56)
LNv > GFP (with Dicer2)	22	100	24 (0.16)	70.1 (2.43)

LNv > Rho1-RNAi (with Dicer2)	15	66.7	23.6 (0.16)	55 (6.19)
R23E05 > GFP (with Dicer2)	24	100	23.5 (0)	81.8 (4.79)
R23E05 > Rho1-RNAi (with Dicer2)	25	72	23.9 (0.17)	60.2 (6.29)

Supplementary Table 3. Selected results from PDFR screen, related to Figure 2.4A

Gal4 Line	Change in locomotor activity	Expression pattern	Expression in DN1a
All hits (activity decreased by light. Δ below 0.)			
R23E05-Gal4	-18.0	This paper	Yes
R23E05-Gal4 + tsh Gal80 (data not shown in 2D)	-16.0	This paper	Yes
Trojan VGLUT-Gal4	-17.3	Glutamatergic	Unknown
VGLUT-Gal4 (data not shown in 2D because redundancy with Trojan VGLUT-Gal4)	-35.9	Glutamatergic	Unknown
DDC-Gal4	-15.5	Serotonergic and dopaminergic	Unknown
Gad-Gal4	-14.6	GABAergic	Unknown
R78H08-Gal4	-13.9	Available on FlyLight	Unknown
R94G04-Gal4	-10.9	Available on FlyLight	Unknown
R94C05-Gal4	-10.8	Available on FlyLight	Unknown
VGAT-Gal4	-8.9	GABAergic	Unknown
207324VT-Gal4	-6.1	Putative PDFR expressing	Unknown
TM5c-Gal4 (Ortc1a-Gal4::DBD; Vglut-Gal4::AD)	-5.1	Glutamatergic neurons in optic lobe	Unknown
200573VT-Gal4	-4.6	DN1a, some DN1p (canonical LNv target), some LNd (canonical LNv target)	Yes
Mai179-Gal4; PDF-Gal80	-4.6	DN1a, LNds (canonical LNv target)	Yes
C929-Gal4	-4.5	Peptidergic neurons, including l-LNvs	Unknown
R85C03-Gal4	-4.2	Available on FlyLight	Unknown
R17C09-Gal4	-3.5	Available on FlyLight	Unknown
C217-Gal4	-3.0	Available on FlyLight	Unknown
R38E07-Gal4	5.8	Available on FlyLight	Unknown
Elav-Gal4	-2.0	Pan-neuronal	Unknown
200112VT-Gal4	-1.6	Putative PDFR-expressing	Unknown

R13B08-Gal4	-1.6	Available on FlyLight	Unknown
NPF-Gal4	-1.1	Neuropeptide F-expressing	Unknown
R22E12-Gal4	-1.1	Available on FlyLight	Unknown
R51B02-Gal4	-0.7	Available on FlyLight	Unknown
Canonical LNv-targets, broad neurotransmitter lines and regions controlling locomotor activity.			
R18H11-Gal4	3.1	DN1a and DN1p (canonical s-LNv target)	Yes
Cry-Gal4-Gal4	6.6	DN1a, LNvs, some DN1ps (canonical LNv target), some LNds (canonical LNv target)	Yes
R6-Gal4-Gal4	9.9	s-LNv (Canonical l-LNv target)	Unknown
Kurs58-Gal4-Gal4	10.1	Pars intercerebralis	Unknown
Tim(UAS)-Gal4	11.9	All clock	Yes
Doublesex-Gal4	15.2	Sexually dimorphic	Unknown
Tph2-Gal4-Gal4	17.8	Serotonergic	Unknown
R23E10-Gal4	18.3	Fan shaped body	Unknown
Pdf-Gal4-Gal4	19.3	LNvs	Unknown
TH-Gal4-Gal4	23.2	Dopaminergic n	Unknown
GMR-Gal4-Gal4	23.8	Photoreceptors	Unknown
Clk4.1-Gal4-Gal4	25.2	DN1p (canonical LNv target)	Unknown
R69F08-Gal4	27.4	Ellipsoid body (canonical LNv target)	Unknown
Clk9m-Gal4	29.7	DN2 and LNvs	Unknown
OK107-Gal4	33.1	Mushroom body	Unknown
Cha-Gal4	35.8	Cholinergic	Unknown
Ilp2-Gal4	43	Insulin producing	Unknown

Supplementary Table 4. Origin of fly stocks and reagents

Antibodies		
chicken anti-GFP	Aves	GFP-1020, **RRID:AB_10000240**
mouse anti-Bruchpilot	DHSB (Developmental Studies Hybridoma Bank)	nc82, **RRID:AB_2314866**
mouse anti-PDF	DHSB	PDF C7, **RRID:AB_760350**
rabbit anti-DsRed	Clontech	632496, **RRID:AB_10013483**
Guinea pig anti-Clock	Gift from Paul Hardin	
Alexa Fluor 488 donkey anti-mouse	Thermo Fisher Scientific	**A-21202, RRID:AB_141607**
Alexa Fluor 568 donkey anti-rabbit	Thermo Fisher Scientific	A-10042, **RRID:AB_2534017**
Alexa Fluor 647 donkey anti-mouse	Thermo Fisher Scientific	A-31571, **RRID:AB_162542**
Alexa Fluor 488 donkey anti-chicken	Jackson ImmunoResearch	703-545-155, **RRID:AB_2340375**
Alexa Fluor 488 donkey anti-guinea pig	Jackson ImmunoResearch	706-545-148, **RRID:AB_2340472**
Alexa Fluor Cy3 donkey anti-guinea pig	Jackson ImmunoResearch	706-165-148, **RRID:AB_2340460**
Guinea pig anti-Period	Gift from Amita Sehgal	
Alexa Fluor 647 donkey anti-guinea pig	Jackson ImmunoResearch	706-605-148, **RRID:AB_2340476**
Rabbit anti-CCHa1	This lab (sequence from Veenstra et al., 2014).	
Bacterial and Virus Strains		

One Shot® ccdB Survival™ Competent Cells	Thermo Fisher Scientific	C751003
Biological Samples		
Chemicals, Peptides, and Recombinant Proteins		
ATP disodium salt hydrate	Sigma-Aldrich	A2383
All-trans-retinal	Sigma-Aldrich	R2500
Critical Commercial Assays		
Gateway® LR Clonase® II Enzyme Mix	Thermo Fisher Scientific	11791020
Gateway® BP Clonase® II Enzyme Mix	Thermo Fisher Scientific	11789020
Deposited Data		
Experimental Models: Cell Lines		
Experimental Models: Organisms/Strains		
D. melanogaster: iso31	Ryder et al., Genetics, 2004	
D. melanogaster: Canton S	Barry Dickson (via Michael Crickmore)	
D. melanogaster: UAS-myr::GFP (attP2)	BDSC (Bloomington Drosophila Stock Center) 32197 (via Matt Pecot)	
D. melanogaster: UAS-myr::GFP (attP40)	BDSC 32198	
D. melanogaster: Tim(UAS)-Gal4	Blau and Young, Cell, 1999 (Flybase:FBtp0011839)	
D. melanogaster: UAS-Dicer2 (X)	BDSC 24646	
D. melanogaster: UAS-Dicer2 (2)	BDSC 24650	
D. melanogaster: UAS-Dicer2 (3)	BDSC 24651	
D. melanogaster: repo-Gal80	Awasaki et al., J. Neurosci, 2008 (Flybase: FBtp0067904)	
D. melanogaster: UAS-Clock RNAi	Vienna Drosophila Resource Center VDRC (VDRC)	107576KK

D. melanogaster: UAS-Period RNAi	Fly Stocks of National Institutes of Genetics (via Michael Young)	2647R-1
D. melanogaster: $w^{+}per^{S}$	Jeffrey Price	
D. melanogaster: yw; PDF-Gal4; PDF-Gal4 (LNv-Gal4)	Justin Blau	
D. melanogaster: UAS-GtACR1::eYFP	Adam Claridge-Chang (via Michael Crickmore)	
D. melanogaster: UAS-ChR2-XXM	Robert Kittel (via Michael Crickmore)	
D. melanogaster: R23E05-Gal4	BDSC	BDSC_49029
D. melanogaster: UAS-ChR2-XXL	BDSC	BDSC_58374
D. melanogaster: trans-Tango	BDSC	BDSC_77124
D. melanogaster: $pdfr^{Han3369}$	Laboratory of Paul Taghert	
D. melanogaster: $pdfr^{Han5304}$	Laboratory of Paul Taghert	
D. melanogaster: UAS-Pdfr-16	Laboratory of Paul Taghert	
D. melanogaster: UAS-Denmark	BDSC	BDSC_33062
D. melanogaster: PDF-LexA	Shang et al., PNAS, 2008 (Flybase: FBtp0093323)	
D. melanogaster: LexAop-myr::tdTom	Laboratory of Matt Pecot (Chen et al., 2014)	
D. melanogaster: LexAop-syt::GDP::HA	BDSC	BDSC_62142
D. melanogaster: UAS-opGCaMP6s	Laboratory of David Anderson (via Michael Crickmore)	
D. melanogaster: UAS-tdTomato	BDSC 36327	
D. melanogaster: LexAop-P2X2	Laboratory of Orie Shafer (via Rachel Wilson)	
D. melanogaster: UAS-brp-D3::mCherry	Christiansen et al., J. Neurosci, 2011 (Flybase: FBtp0069949)	
D. melanogaster: per^{01}	Konopka and Benzer, PNAS, 1971 (Flybase: FBal0013649)	
D. melanogaster: UAS-Rho1.Sph	BDSC	BDSC_7334
D. melanogaster: UAS-Rho1-RNAi	BDSC	BDSC_9909

D. melanogaster: R6-Gal4	Helfrich-Forster et al., J. Comp. Neurol., 2007 (Flybase FBti0016844)	
D. melanogaster: JRC_SS00645	Laboratory of Gerry Rubin	
D. melanogaster: C929-Gal4	BDSC	BDSC_9909
D. melanogaster: JRC_SS00681	Laboratory of Gerry Rubin	
D. melanogaster: UAS- PDF-RNAi	VDRC	4380
D. melanogaster: UAS-10x UAS t-PDF	Laboratory of Michael Nitabach	
D. melanogaster: R23E05-Gal4	BDSC	BDSC_49029
D. melanogaster: R23E05-LexA	This paper	
D. melanogaster: R23E05-Gal80	This paper	
D. melanogaster: UAS-RedStinger	BDSC	BDSC_8546
D. melanogaster: PDF-Gal80	Stoleru et al., Nature, 2004 (Flybase: Fbtp0019042)	
D. melanogaster: LexAop-myr::GFP	BDSC (via Matt Pecot)	BDSC_32209
D. melanogaster: Vglut-Gal4 (OK371)	BDSC	BDSC_26160
D. melanogaster: GMR-hid[10]	Laboratory of Andreas Bergmann	
D. melanogaster: UAS-mGluRA-RNAi	BDSC	BDSC_34872
D. melanogaster: UAS-CCHA1-RNAi	VDRC	104794KK
D. melanogaster: UAS-CCHA1R-RNAi	VDRC	103055KK
D. melanogaster: UAS-mCD8::GFP	Laboratory of Michael Crickmore	
D. melanogaster: UAS-Kir2.1	Laboratory of Michael Crickmore	
Oligonucleotides		
R23E05 Forward	gtcccgatttcgtcgaaggattcaa	Integrated DNA Technologies
R23E05 Reverse	gctaaccggatgacggtaccaggag	Integrated DNA Technologies
Recombinant DNA		
pBPLexa:P65UW	Addgene	26231
pBPGal80uw-6	Addgene	26236
Software and Algorithms		
FIJI	Schindelin et al., 2012	https://fiji.sc/, RRID: SCR_002285

Loocomotor quantification and plotting package (MATLAB)	This paper	https://github.com/CrickmoreRoguljaLabs/WakeAnalysis
TurbReg (Plugin for FIJI)	Thévenaz et al., 1998	https://imagej.net/TurboReg
GraphPad Prism		http://www.graphpad.com/, RRID:SCR_002798
Other		
DAPI Fluoromount-G	SouthernBiotech	0100-20
KPL 10X Dulbeco's PBS	SeraCare	5460-0030
Microscope coverslips	Electron Microscopy Sciences	72230-01
Microscope coverslips	VWR	48393-251
Microscope glass slides Super Frost Plus	VWR	48311-703
Microscope glass slides	Electron Microscopy Sciences	64321-10
Normal donkey serum	Jackson ImmunoResearch	017-000-121
PFA (16%)	Electron Microscopy Sciences	15710
Prolong Gold antifade reagent	Invitrogen	1942345
Schneidner's medium	Gibco	21720-001
Potato flakes	Carolina Bio Supply	Formula 4-24 Instant *Drosophila* Medium, Blue
Nunclon cell culture dishes	Thermo Fisher Scientific	150318
Ethanol	Koptec	V1001
Triton X-100	Amresco	M143-1L
KPL 10X Dulbeco's PBS		5460-0030
Drosophila activity Monitors	Trikinetics	DAM2
DigiTherm CircKinetics incubators	Tritech Research	DT2-CIRC-TK
Arduino Uno Rev3	Arduino	A000066
Drosophila incubator	Percival	DR-41VL
Troemner vortexer with VMP Mounting Plate installed	Trikinetics	TVOR-120
530 nm green LEDs	Luxeon Rebel	LXML-PM01-0100
BuckPuck	LuxDrive	03021-D-E-700
Power meter	Thorlabs	PM100D

Light Meter	Extech	LT300
Spectrometer	Thorlabs	CCS200
Light pad	Artograph	LightPad 930
Video camera	Canon	Vixia HRF800
donkey serum	Jackson ImmunoResearch	017-000-121

Supplemental Videos

Supplementary Video 1. Circadian light reactivity in wild-type flies.

Light pulse presented to wild-type (*w*$^{+}$*iso31*) flies. Flies are in glass tubes with food on one end (outer end of the frame), and a cotton plug on the other (inner end of the frame). Lights turn on 13 seconds into the video. Flies in left and right columns are entrained to opposite cycles. On the left side, lights turn on in the middle of subjective day. On the right side, lights turn on in the middle of subjective night. Video is sped up 30x.

Supplementary Video 2. Overlapping projections of LNvs (blue) and DN1as (green). 3D reconstruction of confocal stacks using Imaris, shown with and without nc82 (grey). Same image as Figure 3.1A.

Supplementary Video 3. LNv axons (blue) adjacent to DN1a dendrites (green). 3D reconstruction of confocal stacks using Imaris, shown with and without nc82 (grey). Same image as Figure 3.1B, left.

Supplementary Video 4. DN1a axons (green) adjacent to LNv dendrites (blue). 3D reconstruction of confocal stacks using Imaris, shown with and without nc82 (grey). Same image as Figure 3.1B, right.